A Mining Research Contract Report
SEPTEMBER 1985

Geologic Factors Affecting Vibration from Surface Mine Blasting

FINAL REPORT
Contract H0222009
Vibra-Tech Engineers, Incorporated

Bureau of Mines Open File Report 33-86

Bureau of Mines
UNITED STATES DEPARTMENT OF INTERIOR

The views and conclusions contained in this document are those of the authors and should not be interpreted as necessarily representing the official policies or recommendations of the Interior Department's Bureau of Mines or of the U. S. Government.

FOREWORD

This report was prepared by Vibra-Tech Engineers, Inc., under USBM Contract number H0222009. The contract was initiated under the Mining Research Conservation and Development Program. It was administered under the technical direction of Twin Cities Research Center, with Mr. Dennis V. D'Andrea acting as Technical Project Officer. R.J. Simonich was the contract administrator for the Bureau of Mines. This report is a summary of the work recently completed as a part of this contract during the period October 1983 to April 1985. This report was submitted by the authors in September 1985.

Additional material, including some 3000 pages of plots and figures and high-speed films of the blasts, have been filed with the Twin Cities Research Center. These data have not been included in the formal report in the interest of manageability but can be examined, upon request, at either the Twin Cities Research Center or Vibra-Tech Engineers.

We would like to acknowledge the assistance, material, and facilities that were graciously provided by Genstar Stone Products Co. and General Crushed Stone Co. Special thanks are due to Price Hurt, Carroll Geldmacher, and Theron Myers of Genstar; and James Carr, Anthony DeMasi, Gene Webster, and James Fryer of General Crushed Stone. We would also like to acknowledge the assistance and material provided by E.I. DuPont deNemours & Co. (Inc.) and specifically thank Dr. Alday Andrews, Paul Jones, and William Gehnert for their assistance. We would like to acknowledge the able assistance from Vibra-Tech and Martin Marietta personnel, including Stuart Brashear, Dennis Clark, Joseph Lozosky,

William Rose, Douglas Rudenko, and Mohammad Sharifinassab; the tireless typing of the manuscript by Laurie A. Perry; and the skillful editing by Aylene Kovensky. Finally, we would like to acknowledge helpful discussions with Dennis D'Andrea and Mark Stagg of the Twin Cities Research Center.

TABLE OF CONTENTS

LIST OF FIGURES

LIST OF FIGURES
(continued)

LIST OF FIGURES
(continued)

LIST OF FIGURES
(continued)

LIST OF FIGURES
(continued)

LIST OF TABLES

LIST OF TABLES
(continued)

1 INTRODUCTION

The Bureau of Mines has supported blasting-related research, covering many different aspects of the subject, since the early 1950s. A primary topic of concern has been blast-induced ground vibration and its effect on structures surrounding a mining operation. In this report the results of a Bureau-supported research contract to investigate the effect of geology on blast-induced low-frequency ground vibration will be described.

The scope of the investigation was broader in two major respects than the title of the report indicates. First, the determination that certain geological structures will enhance low-frequency ground vibration does not aid a mine operator in designing blasts to address the problem; therefore, we investigated methods to predict and control ground vibration. Second, those methods should not be detrimental to productivity but, ideally, should enhance it. To this end, we have also investigated the effect of vibration control methods on fragmentation. These topics will also be discussed.

Siskind, et al. (1980, Bureau of Mines RI 8507) indicated that ground-vibration-induced damage is related to the peak particle velocity (PPV) and to the frequency of vibration. The traditional method for attempting to control ground vibration is to decrease the amount of explosive used per delay, in order to reduce the PPV. As we will discuss in some detail later, several studies have shown that the frequency of blast-induced ground vibration is related to the delay sequence used. We have modified delay sequences to affect the frequency of the resultant ground vibration as well as the PPV. We have also determined an effect of delay on fragmentation to determine how changes in delay affect productivity.

This report is divided into sections on background, methodology, experimental procedures, analytical procedures, results and discussion, discussion of related issues, and conclusions. In the Background section we will discuss previous work on the effect of geology and delay on ground vibration, as well as some pertinent earthquake seismology studies; previous work on fragmentation mechanisms; and the effect of delay on fragmentation. In the Methodology section, we will discuss the approach we chose to investigate these problems. In particular, we will discuss several hypotheses that we formulated and subsequently tested. In the Experimental Procedures section, the actual test methods, a series of well-controlled single- and multiple-hole blasts at two quarries, will be presented. The processing methods used for the data collected will be discussed in the Analytical Procedures. The Results and Discussion sections will contain a discussion of the data obtained for ground vibration, fragmentation, and strain-pulse propagation individually, as well as verification of the hypotheses proposed. Discussion of Related Issues will include the effect of fragmentation on ground vibration, the effect of initiator inaccuracy on predictability of ground vibration and fragmentation, and how the various parts of the study fit together.

2 BACKGROUND

We will concentrate on the effect of geology on low-frequency ground vibration, deriving much of our information from the seismological literature. We also will discuss the effect of delay on blast-induced ground vibration, since we believe that varying the delay strongly influences the resultant frequency and amplitude of ground vibration. We will not discuss productivity studies in substantial detail, only to the extent necessary to understand the approach used.

2.1 LOW-FREQUENCY GROUND VIBRATION

2.1.1 Geological Causes

Amplification of ground vibration by geological features has received more attention in earthquake seismology than in blasting. Critical facility siting and estimates of potential earthquake hazards are strongly dependent upon the maximum likely vibration levels. Typically, the predictions are based on maximum magnitude estimates and attenuation relationships. The maximum magnitude is determined primarily by the size of the fault plane that can be assumed to slip during an earthquake, and by previous seismic history. Attenuation is assumed to be strictly distance dependent, and does not involve local geological effects.

Recently, this view has been called into question, where it has been shown that at sites on thick soil layers close to the earthquake source, magnitudes calculated from the obtained vibration are much greater than that which would be predicted from the attenuation relations and more distant seismic records. The mechanism inferred for this phenomenon is multiply-reflected shear waves. Sediment-filled valleys strongly amplify

waves at earthquake seismology "high frequencies," in the range from 2 to 20 Hertz, which are low frequencies in blasting seismology.

Borcherdt (1970) discussed the effect of local geology on ground motion produced by nuclear blasting and earthquakes. Significant differences in the amplitude and duration of ground motion were observed between locations having thick soil layers and those having little or none. For example, sites with a thick layer of soil overlying bedrock produced ground motions ten times greater than sites of minimum soil thickness. The magnitude of the motion increased as the thickness of the soil layer increased; however, the effect on frequency was not discussed. Sites where neighboring residential structures are located on thick soil layers would be subject to potentially higher vibration amplitudes of longer duration.

The amplification of body waves by low-velocity surface layers was reported by Murphy, et al. (1971). They found that the frequency and magnitude of the ground motion produced by underground nuclear blasting could be significantly affected by near-surface geological conditions at the recording site.

Earthquake-resistant structural design techniques consider the effects of local geology on site response to incoming seismic energy (Rosenblueth, 1980; Dowrick, 1977). Such geologic features as the depth and horizontal extent of soil overlying bedrock, the slope of bedding planes, the topography of both bedrock and soil deposits, and the water content of soils have been cited as influencing the site response.

National security interests, such as the vulnerability of missile silos to nuclear blast effects, have also been considered. The security

of such structures, if sited in alluvial valleys, could be jeopardized by the enhancement of ground vibration (Murphy and Bennett, 1980; Murphy, 1979).

According to Kubosov (1976), ground vibration from earthquakes may also be amplified by a lake bed. Other similar studies include: Dravinski, 1982; King and Brune, 1981; and Joyner, et al., 1981.

2.1.2 The Gupta Model

Although similar results have been observed in blasting seismology studies, the relation between the overburden and the resultant amplification of low-frequency vibration has generally not been explicitly demonstrated. However, Gupta (1961) has generated a model to predict the effect of a low-velocity layer on ground vibration and tested it in a few simple situations.

Seismic waves incident on the lower boundary of a surface low-velocity layer, such as soil, may be multiply reflected within that layer. Once the seismic energy has been transmitted to the layer, reflections within the layer may be trapped if there is a strong velocity contrast at the boundary. This is called a waveguide effect. O'Brien (1957) has indicated that the resultant waves are mutiply-reflected refractions. For the wave to be amplified, there must be constructive interference of the reflections within the layer with the newly arriving energy.

Figure 1 schematically shows the situation for this waveguide effect. A layer of thickness H with a p-wave velocity V_1 overlays a semi-infinite

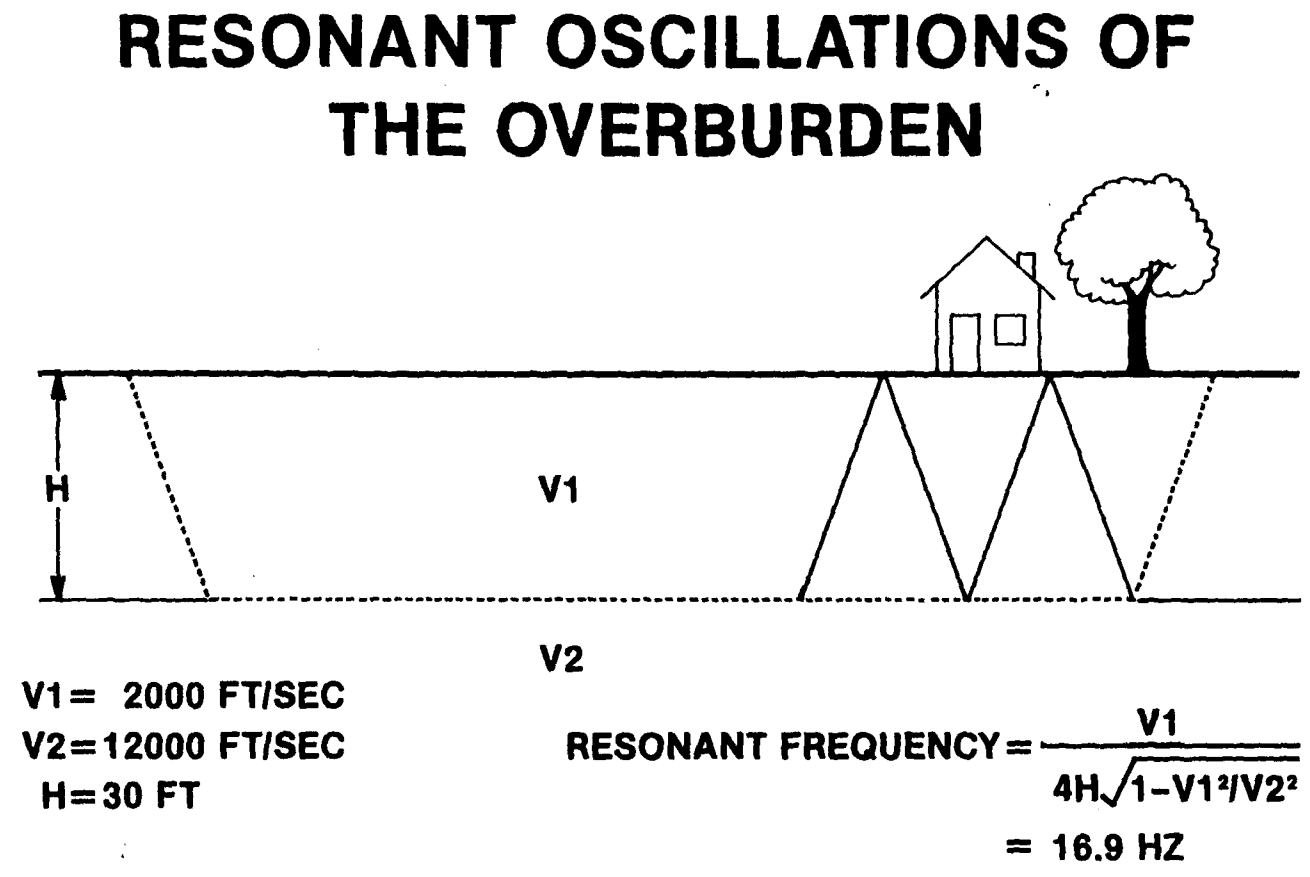

Figure 1. Schematic diagram of the Gupta model

layer with a higher velocity V_2. Waves multiply-reflected will constructively interfere if the travel times of the wave paths differ by an integral multiple of the period of the wave. Since there is a phase difference of 180° at the free surface, for a critical angle of incidence (θ), the period may be calculated trigonometrically by:

$$mT - \tfrac{T}{2} = \frac{2H \sec(\theta)}{V_1} - \frac{2H \tan(\theta)}{V_2}$$

where m is a positive integer corresponding to the mode.

This equation may be solved for T:

$$T = \frac{4H}{(2m-1)V_1} (1 - V_1^2/V_2^2)^{1/2}$$

If $V_1 \ll V_2$, T may be approximated by:

$$T = \frac{4H}{(2m - 1) V_1}$$

and, if only the fundamental mode is considered:

$$T = \frac{4H}{V_1} .$$

Given the thickness and the seismic velocity of the overburden, this final equation may be applied to assess whether a low-frequency ground vibration problem due to resonant oscillations of the overburden may be expected at a mine site. On this basis, new sites that have a potential vibration problem may be rejected.

Because existing sites may already have a documented low-frequency vibration problem, and other considerations may outweigh potential ground

vibration problems at new sites, possible methods to control low-frequency ground vibration must be considered. One possible method, modifying vibration by changing the blast delay sequence, will be discussed here.

2.1.3 Delay Effects

A major advance in the control of ground vibration was the introduction of the millisecond delay initiator in the 1940s. Although intended primarily to improve fragmentation, delay initiators also had the beneficial effects of decreasing ground vibration, airblast, and flyrock. With millisecond delays, it was possible to reduce the vibration significantly from the levels usually generated by instantaneously detonated shots. The maximum expected level was determined by a scaled-distance criterion, in which the distance to a neighboring structure from a blast and the pounds per delay were both considered. The use of the scaled-distance criterion and its applications have been discussed in detail in Bureau of Mines Report of Investigations 8507 (Siskind, et al., 1980).

Plots of peak particle velocity versus scaled distance, as in Siskind, et al., show considerable scatter. In many cases, an operator must design blasts quite conservatively in terms of pounds per delay to assure a reasonable confidence in resultant vibration levels. As noted above, even when an operator has blasted within acceptable limits, he sometimes receives complaints. Some of the difficulty is due to the frequency of the ground vibration, as discussed by Medearis (1979) and Siskind, et al. Three factors contribute to this effect.

First, the low-rise residential structures often found near mining operations resonate in response to certain ground vibration frequencies. Typically, resonant frequencies in the 5- to 12-Hertz range (1 Hertz = 1 cycle/sec) are found in the racking mode for these structures and in the 12- to 22-Hertz range in the midwall mode (see Fig. 2). Ground vibrations with these frequencies will be amplified by the structures, and even small vibrations may be amplified to unacceptable levels. Response spectral analysis may be used to show this effect.

Second, the local geology surrounding mining operations affects the ground vibration, as discussed above. In quarrying, for example, economic operations generally can be carried out only if the overburden thickness is less than about 80 feet, because the overburden must be stripped in order to mine. For a typical overburden wave-velocity of 1800 ft/sec and thickness of 50 ft, the resonant frequency calculated for multiply-reflected waves would be 9 Hertz, which is within the resonant frequency range for residential structures.

Finally, delay intervals in the millisecond delay series correspond to low frequencies: a 50-ms delay corresponds to 20 Hertz. Several studies have investigated how the phasing due to delay affects ground vibration from blasting.

Fish (1951) showed that the resultant vibration from small test blasts could be modified by destructive interference. At that time, millisecond delays were sufficiently inaccurate that the major concern was to avoid constructive interference. Langefors and Kihlstrom (1978) used the scatter in initiator firing times to assess how well constructive interference could be avoided.

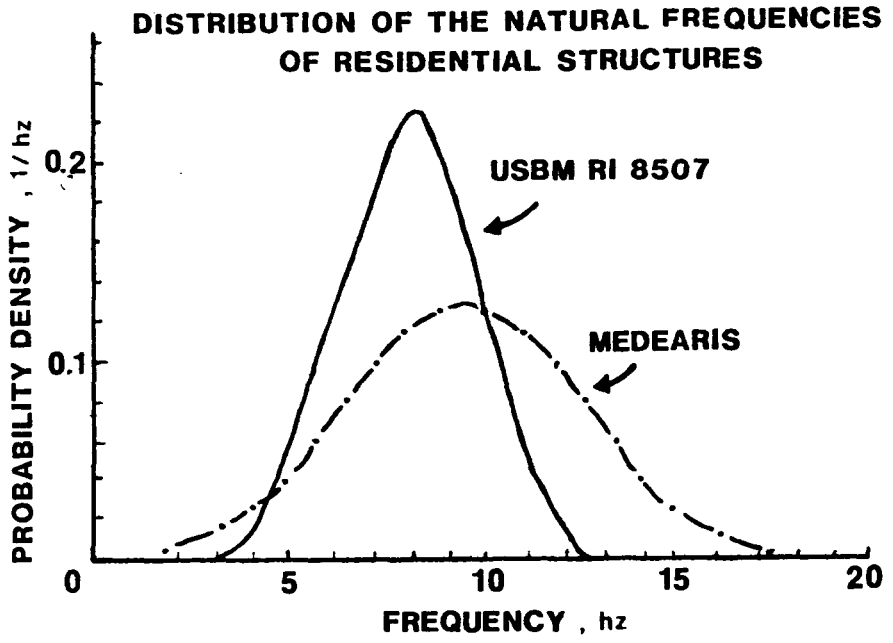

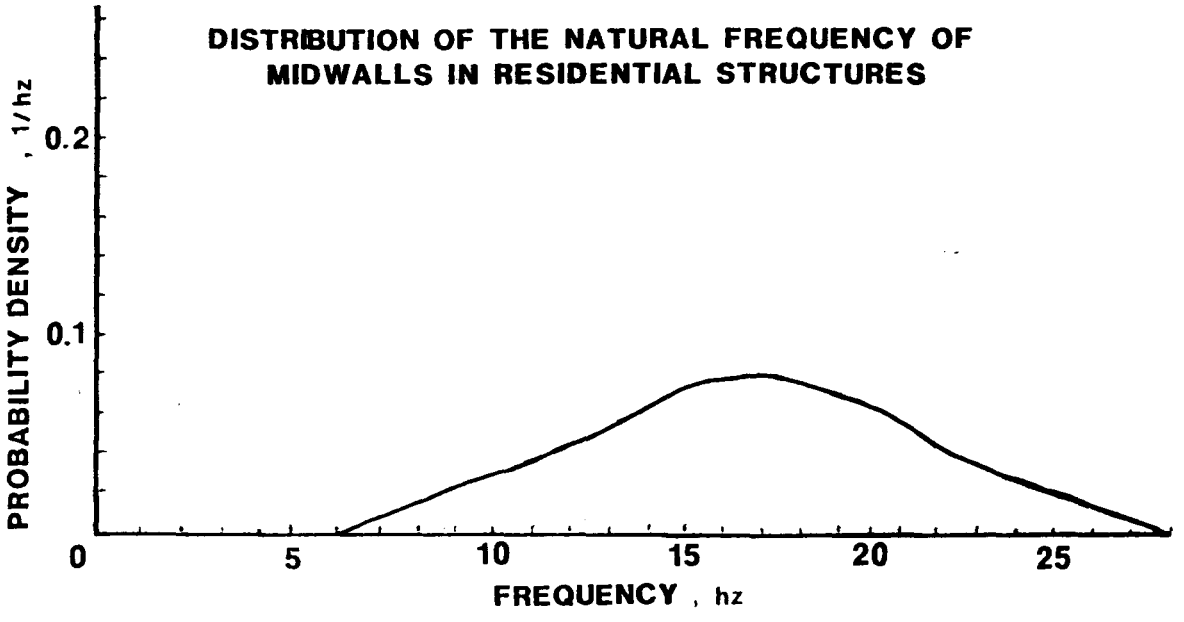

Figure 2. Natural frequencies of residential structures and midwalls

The effect of delay on the resultant frequency of ground vibration has been documented by Frantti (1963), Pollack (1963), and Greenhalgh (1980). In the latter study, the frequency related to the delay period was observed at a distance of 170 kilometers! Wiss and Linehan (1978) also indicated that delays on the order of 50 ms could sometimes be observed in the seismic records. Shoop and Daemen (1983) indicated that delay intervals used in mine blasts could also be observed in the seismic records. Anderson, et al. (1982) reported a method of modifying the frequency of ground vibration by changing blast design, such that the resultant frequencies were above the resonant frequencies of residential structures. The method was found effective at a problem location, but was neither site-specific nor very flexible. Andrews (1981) showed that a resonant frequency in the local geology could be minimized by appropriate delays such that the vibrations were out of phase.

Means of controlling ground vibration must be considered in the context of the total mine operation. In particular, methods to control ground vibration should not adversely affect the fragmentation resulting from the blasting. We will discuss some of the previous work done on the mechanisms of fragmentation in general and focus on the effect of delay on fragmentation, as it has been investigated. First though, we will discuss the strain waves generated by the explosive column because they are the link between fragmentation and ground vibration.

2.2 STRAIN WAVES GENERATED BY EXPLOSIVES

These waves are relevant to this study in two ways. First, they are the seismic source for ground vibration. Second, they participate in

the initial break-up of the rock mass, although the exact mechanisms for inducing rock failure are a matter of some controversy at present. We studied these strain pulses to understand 1) how they may be affected by delay, 2) the nature of the seismic source, and 3) the basics of the interaction of rock with the explosive. We will discuss some of the existing knowledge about blast-induced strain waves in rock.

Model studies have shown that, under dynamic loading conditions, flawed material behaves substantially differently from unflawed material (e.g., Fourney, et al., 1983). In high-speed photographs of the fragmentation of a birefringent polymer, fractures are seen to emanate from the point of interaction of a strain wave with a discontinuity. The tensile tail of the p-wave is observed to be absorbed in creating a cage of finely comminuted material immediately surrounding the borehole. No significant tensile pulse is therefore available for fracturing within the rock mass. The fractures are hypothesized to be related to the shear component of the p-waves and to the s-waves themselves.

The interaction of strain waves with discontinuities has been inferred in high-speed films of full-scale quarry blasts (Winzer, et al., 1979), where the first observable crack openings were related to the predicted arrival time of p-waves at the free face, which was significantly earlier than the time for any of the explosive-produced gases to reach the free face. Computer models of the fragmentation process, which incorporate discontinuities in the model medium (Dienes, 1982, Adams, 1983), generate fragmentation patterns that correlate better with fragmentation profiles observed in cratering experiments than models that assume the medium to be homogeneous.

The form and nature of the strain waves must be determined before assessing their effect on the fragmentation process. Analytical solutions to the problem have become progressively more sophisticated over the years, from the initial work of Sharpe (1942), through the models of Heelan (1953), Jordan (1962), and Favreau (1969). Plewman and Starfield (1965) devised a numerical approach wherein the cylindrical explosive column is modeled as a linear series of spherical charges detonated with delays corresponding to the detonation velocity of the explosive. The resultant waveform is then a repeated summation of the strain waves generated by a spherical charge, appropriately lagged, and attenuated according to path-length differences.

Field studies to determine the response of rock to explosive loading were carried out by the Bureau in an extensive series of studies in the 1950s and 60s. Starfield and Pugliese (1968) compared strain-gage records obtained in these studies with the numerical model of Plewman and Starfield, and found generally good agreement. The model did not simulate the s-wave from the explosive column nor any reflections. All testing was done on the quarry floor, so that reflections from a vertical free face were not present, limited movement of material was available, and the material had received limited damage from preceding blasts.

During a typical free-face blast, complicated strain histories in the affected rock may arise due to several causes. First, strain waves generated by the explosive column will have a broad pulse-width due to the finite detonation velocity of the explosive. This is evident from the work discussed above. Second, the rock through which the waves will propagate will have discontinuities due to jointing, layering, and damage from previous blasts; these discontinuities may attenuate strain waves

and serve as sources of internal reflection (Hudson, 1981; Kikuchi, 1981). Third, the fracturing process itself may generate strain waves (Rice, 1980; Achenbach, et al., 1983) which cascade such that those generated from multiple fractures may influence each other's propagation. Finally, either a p- or an s-wave will reflect both p- and s-waves from the free face; the angles of reflection and magnitudes of the reflected waves will be functions of the angle of incidence and the wave velocities of the rock (Rinehart, 1975; Aki and Richards, 1980).

2.3 FRAGMENTATION

Although several mechanisms for rock fragmentation have been proposed, we will concentrate on strain wave interaction with discontinuities, because these serve as a basis for some of our hypotheses. Consequently, we will review some of the pertinent research.

2.3.1 Structural Effects

Barker, et al. (1979), Fourney and Barker (1979), Fourney, et al. (1979), and Holloway, et al. (1980), at the University of Maryland, conducted dynamic fragmentation studies in Homalite-100 models, both unflawed or with flaws simulating the different types of macroflaws (e.g., joints, bedding planes, larger fractures), found in a typical mine bench, and made the following conclusions: In unflawed models, radial cracks dominate fragmentation. Typically, only 6-12 radial cracks propagate from the borehole. Stress waves reflected from the free faces of the model interact with the outgoing radial cracks, causing branching and arrest. Fragmentation of the models closely resembles the fragmentation of rock plates of similar size made from

Westerly granite or Solenhofen limestone. In flawed models, new fractures are initiated at flaws that simulate joint or bedding planes by resolved shear stress associated with the s-wave and compressive portion of the p wave. Fragment size is smaller overall; the smallest size is achieved with shorter delay times than in unflawed models.

Larger-scale studies conducted by Winzer and Ritter (1979) and by Winzer, et al. (1979) in large blocks of Chambersburg limestone established the following: New fractures form at the free face in about twice the time it takes for the p-wave to traverse the burden distance. Old fractures either are the loci of new fractures or are themselves reinitiated early in the event; they continue to be active for several tens of milliseconds after detonation of the explosive. Fragmentation continues in blocks of rock following detachment from the main rock mass, similar to fracture propagation observed in detached fragments of Homalite-100. The fracture pattern on the free face is well developed prior to the expected time of arrival of radial cracks from the borehole. Gas venting occurs through already open cracks relatively late in the event, indicating that most of the fractures observed on the free face are not gas pressurized.

High-speed motion pictures of full production-scale blasts showed that fractures in the blasted faces initiate and propagate from joint and bedding planes, suggesting the same operating mechanism(s) as those observed in Homalite-100 models simulating these large-scale flaws. Initiator firing times deviated considerably from nominal firing times given by manufacturers, up to and including reversals. Such firing time errors were correlated with production of oversize, fly-rock, backbreak, and tight muck piles.

2.3.2. Delay Effects

Winzer and Ritter (1984) discussed the effect of delay and explosive distribution on fragmentation in small-scale bench and block tests. In summary, the block and bench data show two general features. First, the mean fragment size usually is determined by the pre-existing fracture spacing of the rock mass. Second, the delay serves to skew the fragment size distribution about this mean. In granite blocks, significant reduction in size (80% passing) was obtained with increasing delay, up to 1.5 ms (1 ms/ft between holes). The fragment size distribution continues to change, however, by a continuous reduction in the amount of the larger fraction with increased delay, and a corresponding increase in the amount of the smaller fraction. Thus, the average size in these tests appears to be controlled by rock type, flaw distribution, and distribution of explosive within the rock mass.

In two-hole production-scale tests, optimum fragmentation was achieved at 2 ms/ft (20-ms delay, 10-ft spacing) (Winzer et al., 1983; Anderson, et al., 1984). Optimum fragmentation for the less massive portion of the face was achieved at about 4 ms/ft between holes, which is longer than indicated by the block and bench tests. However, different rock types are involved and the scale is sufficiently different that mass effects and gross structural differences might have influenced the results considerably. These values are in substantial agreement with optimum relief values obtained using stemming vent velocity and vertical motion (Winzer, et al., 1979).

The fragmentation data also clearly show that too long delays degrade fragmentation. At and beyond 40-ms delay (or 4 ms/ft) between holes in a row or on the burden, fragmentation in massive and fragmented portions

of the rock deteriorates. Although strictly valid only for this rock and the configuration described, these results give an upper-limit guideline for blast design and suggest that the long-delay blasting patterns have definite limits.

Fracture density appears to exert some control on the delay needed for optimum fragmentation. In comparison with more heavily fractured rock, massive rock shows more rapid changes in fragment size distribution with delay, and the finest fragmentation occurs at shorter delay times. At delays above 4 ms/ft (between holes), fragmentation deteriorates in both massive and fractured rock. No explanation for these observations or for the differences in fragmentation with delay for massive and fractured rock was provided, although the differences are likely related to stress history, attenuation, differences in crack initiation and propagation, and mass effects.

Bergmann et al. (1972) found that in small blocks there was no appreciable change in fragmentation with increasing delay, although there was a slight improvement. The differences in their results from the other work may be due to the scale of the model, or perhaps because the tests were conducted in intact blocks with little pre-test damage.

The studies discussed here were either scale-model blasts or two-hole bench blasts. The results indicating an optimum delay time were generally consistent; applicability to full-scale production blasting remains to be demonstrated.

2.4 SUMMARY

Previous work has indicated that near-surface geology, particularly the presence of low-velocity layers, can induce low-frequency ground

vibration. A model by Gupta (1961) specifically predicts the predominant frequency generated by a surface layer of a given velocity. However, in many cases, knowledge of a potential problem is not sufficient for a mine operator. A potential means of control is the changing of delay patterns to destructively interfere successive hole waveforms. Previous work has indicated that changing delay may also influence fragmentation. We will now discuss the approach we have used to determine how to resolve these various issues.

3 METHODOLOGY

The basic problem we are addressing is how to control low-frequency ground vibration while maintaining or improving production efficiency. To approach this problem, we have formulated several hypotheses which must have the following characteristics:

- Testability
- Reasónability, based upon existing knowledge
- Relevance to the problems at hand.

Once the initial hypotheses have been chosen, a testing scheme must be devised. As much as possible, only one variable should be changed at a time, and changes in those variables that could not be kept constant should be noted. Assumptions made in the test procedure must be clearly set forth, with deviations and the implications of those deviations clearly noted.

As discussed in the Introduction, we have chosen to investigate the effects of delay timing on ground vibration and fragmentation. The hypotheses related to vibration and fragmentation will be discussed separately.

3.1 GROUND VIBRATION

We have formulated three basic hypotheses with respect to the effect of delay on ground vibration.

Single-hole free-face blasts with constant blast-design parameters will generate reproducible waveforms at a given seismometer location.

A corollary of this hypothesis is as follows:

The major factor determining the ground vibration from a single-hole blast is the geology between the source and the receiver location.

This hypothesis and corollary assume that variability in the source parameters has minor influence on the resultant ground vibration at the frequencies of interest.

> The ground vibration from a production shot consisting of a sequence of delayed explosive charges may be determined by appropriate time-lagged linear superposition of the ground vibration from a single-hole blast.

This hypothesis assumes that the source from each hole in a production blast is identical to that of the single hole and that spatial distribution of the boreholes and modification of the source region and near-source path due to blasting of previous holes does not affect the resultant vibrations. We considered a third hypothesis, related to deviations from ideal behavior:

> Deviations of ground vibrations from the predictions are attributable, in part, to two factors: first, the resultant vibration is affected by the spatial distribution of the explosive boreholes; and second, the vibration is modified by the amount of deformation to the rock in the source region.

3.2 FRAGMENTATION

As discussed earlier, Winzer, et al. (1983) indicated that face fragmentation determined from high-speed films of small bench and block blasts is indicative of the fragmentation determined by sieving the entire muckpile and is affected by delay. We initially hypothesized:

> In a given location, there is a particular delay between holes in a row that will produce optimum fragmentation.

The standard we have chosen for "optimum fragmentation" is the finest fragment size obtainable at 50% passing a screen. At times longer or

shorter than that delay time, the fragmentation will degrade. This hypothesis is consistent with the work discussed in the Background section.

We have also assumed that the face fragmentation will not be substantially affected by between-row delays. This is an assumption, rather than a hypothesis, because we cannot test it directly without assuming that all other variables are constant. This assumption must be made in order to modify delay schemes that will change ground vibration while obtaining the optimum fragmentation.

The test series at each location was designed to test the hypotheses both for fragmentation and for ground vibration. Single-hole shots were detonated to determine the reproducibility of the ground vibration waveforms and fragmentation, i.e., to test the first hypothesis. Production shots were designed to determine the effect of between-hole delay on fragmentation and vibration. The between-row relief was varied to obtain ground vibration with maximum constructive and destructive interference at low frequencies. We have not explicitly addressed the effect of spatial distribution of the boreholes. A discussion of this effect has been given by Linehan and Wiss (1979). The effect of fragmentation on deviations from predictions will be discussed at the end of the report.

4 EXPERIMENTAL PROCEDURES

In this section we will review the experiments and the equipment used to test the hypotheses discussed in the previous section. The discussion will be limited to where and how the data were collected, along with the general test design; processing techniques will be discussed in section 5, along with the methods used to choose delay times.

4.1 SITE SELECTION

Five sites were selected on the basis of Vibra-Tech's records as having a history of low-frequency ground vibration. The sites were visted, and informal agreements were obtained with the supervisory personnel at those sites for conducting test series there. Videotape documentation of the sites, and potential benches for working were made. A presentation was made to the Twin Cities Bureau personnel of the data for all the sites; two sites were recommended by the investigators, and these recommendations were approved by the Bureau.

Two test sites were selected on the basis of the following criteria:

- Low-frequency ground vibrations generated from previous blasting operations as indicated from seismograph history
- Enthusiastic, cooperative quarry management
- Suitable working bench with sufficient room to do all the test blasts yet not interfere with normal quarry production schedules
- One site having a massive rock type; the second site having a fractured or thin-bedded rock type

- One site using large diameter blast holes; the second site using smaller diameter blast holes
- Location close to both Vibra-Tech and Martin Marietta Labs to minimize travel costs.

The sites selected were Genstar Stone Product's Marriottsville Quarry, located 9 miles west of Baltimore, Maryland, and The General Crushed Stone Company's Downingtown Quarry, located approximately 20 miles west of Philadelphia, Pennsylvania.

Response spectrum analysis of the vibrations from production blasting at each of these operations has shown the presence of low-frequency ground vibration. Although the operating bench at each quarry is sufficiently distant from neighboring properties that low-frequency vibration is far below damaging levels, the geologic conditions that generate low-frequency ground motion do appear to be present.

The management at both quarries was enthusiastic about the project and arranged their yearly production schedules to keep the same working bench available for all the test blasts.

The Marriottsville quarry uses 6-in.-diameter holes to blast a massive rock, whereas the Downingtown quarry uses 8-in.-diameter holes in a thinly-bedded rock.

Both quarries are within reasonable traveling distances, Marriottsville being less than 20 miles from Martin Marietta Laboratories, and Downingtown located almost exactly midway between Vibra-Tech and Martin Marietta.

4.1.1 Marriottsville

Genstar Stone Product's Marriottsville Quarry is located approximately 9 miles west of the City of Baltimore in Baltimore County, Maryland. It

is on the northwest flank of the Woodstock Gneiss Dome just north of the Carroll County-Baltimore County line.

The quarry produces aggregate from the Cockeysville Formation, the major carbonate rock of the central Maryland Piedmont (Figs. 3 and 4). The Cockeysville Formation at Marriottsville is a massive calcite marble, dipping approximately 50° to the west.

The marble occupies a broad lowland between the ridge-producing Setters Quartzite to the east, which partially underlies the marble, and the hills of the Wissahickon Schist on the west, which partially overlies the marble. A small stream, Falls Run, flows south along the eastern edge of the quarry, along Marriottsville Road, just west of the contact between the Cockeysville Formation and the Setters Quartzite.

Two geologic conditions at Marriottsville should be favorable to the generation of low-frequency ground vibrations. The first is the presence of recent alluvium (gravel, sands, silts, and clays) along the Falls Run flood plain. This unconsolidated material, overlying the residual weathered soils of the Cockeysville, could produce thick, low-velocity overburden material. The second condition is the deeply weathered Wissahickon Formation where thick sections of saprolite are present. Saprolite, which is distintegrated and somewhat decomposed rock that lies in its original place, has a low seismic wave velocity, often indistinguishable from soil. In seismic refraction surveys carried out by Vibra-Tech in the Central Maryland Piedmont, saprolite depths of 30 to 40 ft in the Wissahickon schist-Baltimore gneiss complex have frequently been measured.

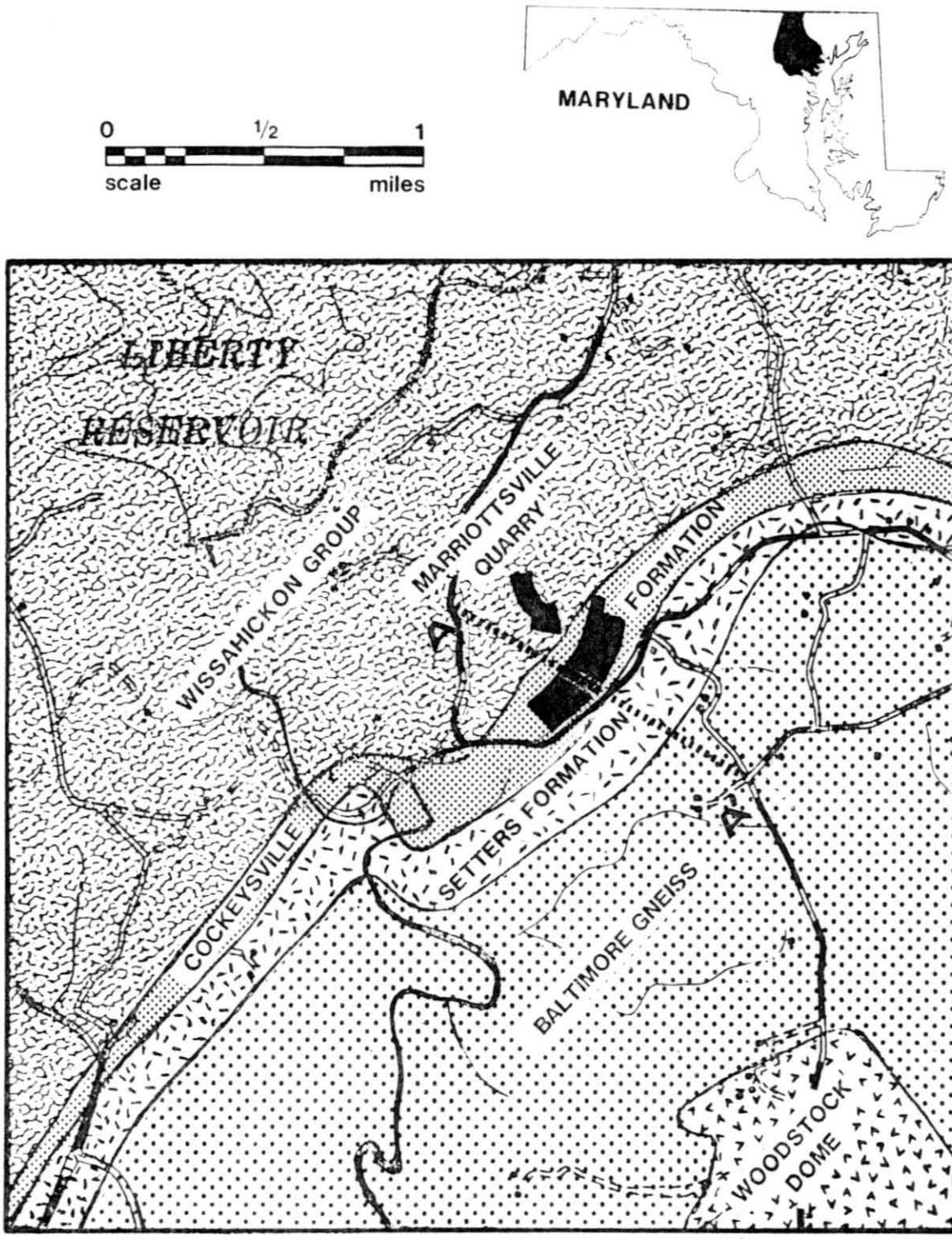

Figure 3. Geologic map of the Marriottsville quarry.

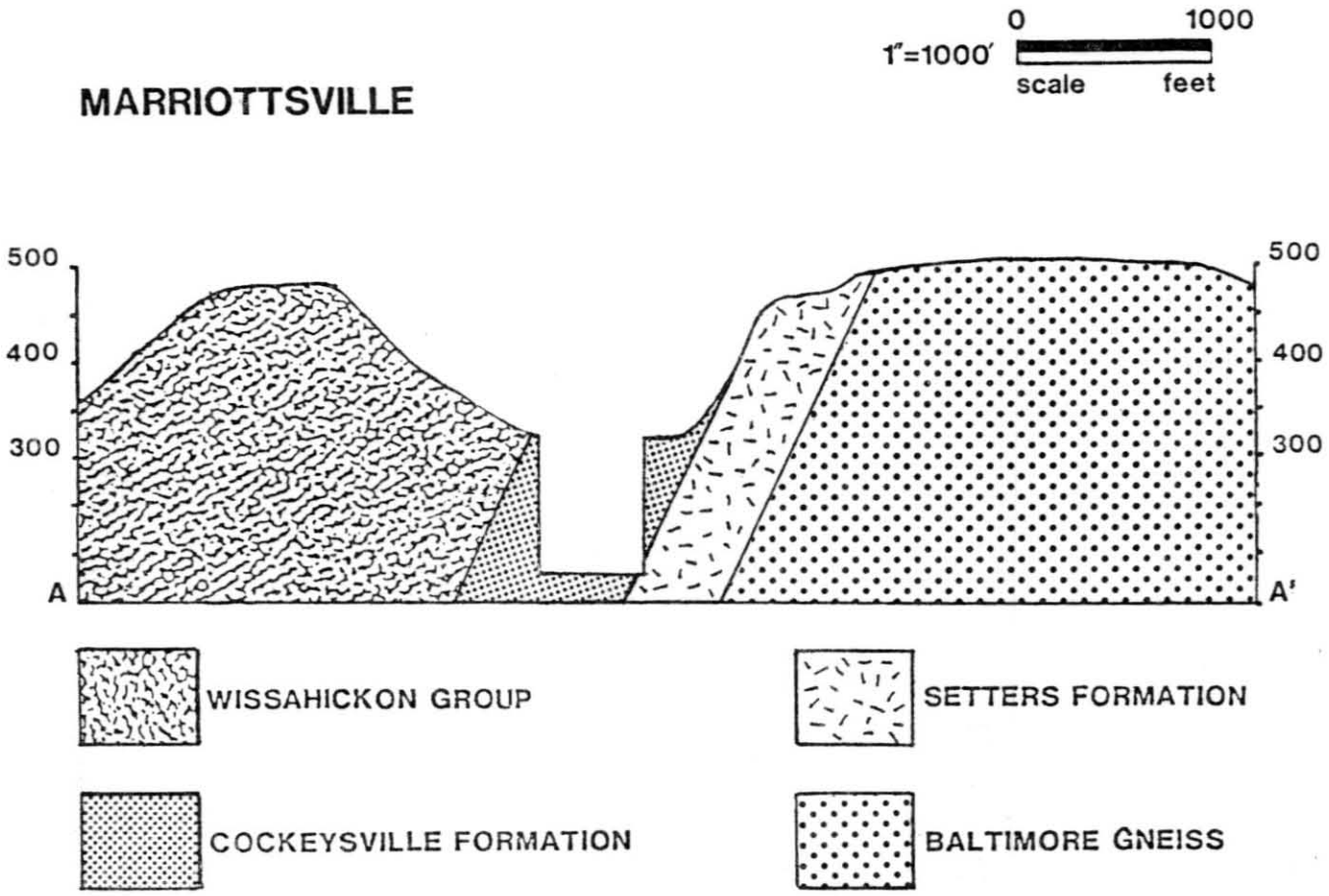

Figure 4. Geologic cross section of the Marriottsville quarry.

4.1.2 Downingtown

The General Crushed Stone Company's Downingtown Quarry lies in the rolling lowlands of the Chester Valley in southeastern Pennsylvania. The quarry produces aggregate from the Ledger Dolomite on the southern limit of an east-west syncline (Figs. 5 and 6).

The Ledger Dolomite consists of thin-bedded to massive dolomite of the Cambrian Age. The test blasting was done in nearly vertically dipping, thinly bedded stone, which became more thinly bedded and more deeply weathered going from south to north. North of the pit the Conestoga Formation, which in the Chester Valley is an impure limestone containing an upper micaceous limestone, a middle phyllite, and lower alternating beds of limestone and dolomite is exposed and dates from the Ordovician Age. The soil mantle thickness overlying the Conestoga can be up to 50 ft.

Results of Vibra-Tech's seismic refraction investigations in the Chester Valley have indicated that subsurface conditions associated with this particular geologic sequence are favorable for generating low-frequency ground vibrations. The deeply weathered micaceous limestone and phyllite of the Conestoga Formation produce not only a thick soil mantle, but relatively low seismic wave velocities in the underlying bedrock.

4.2 SITE CHARACTERIZATION

Seismic refraction surveys were carried out to obtain subsurface geologic information on factors that control the seismic energy propagation. In particular, the surveys were intended to determine the compressional wave velocities in the soil overburden and underlying bedrock. The

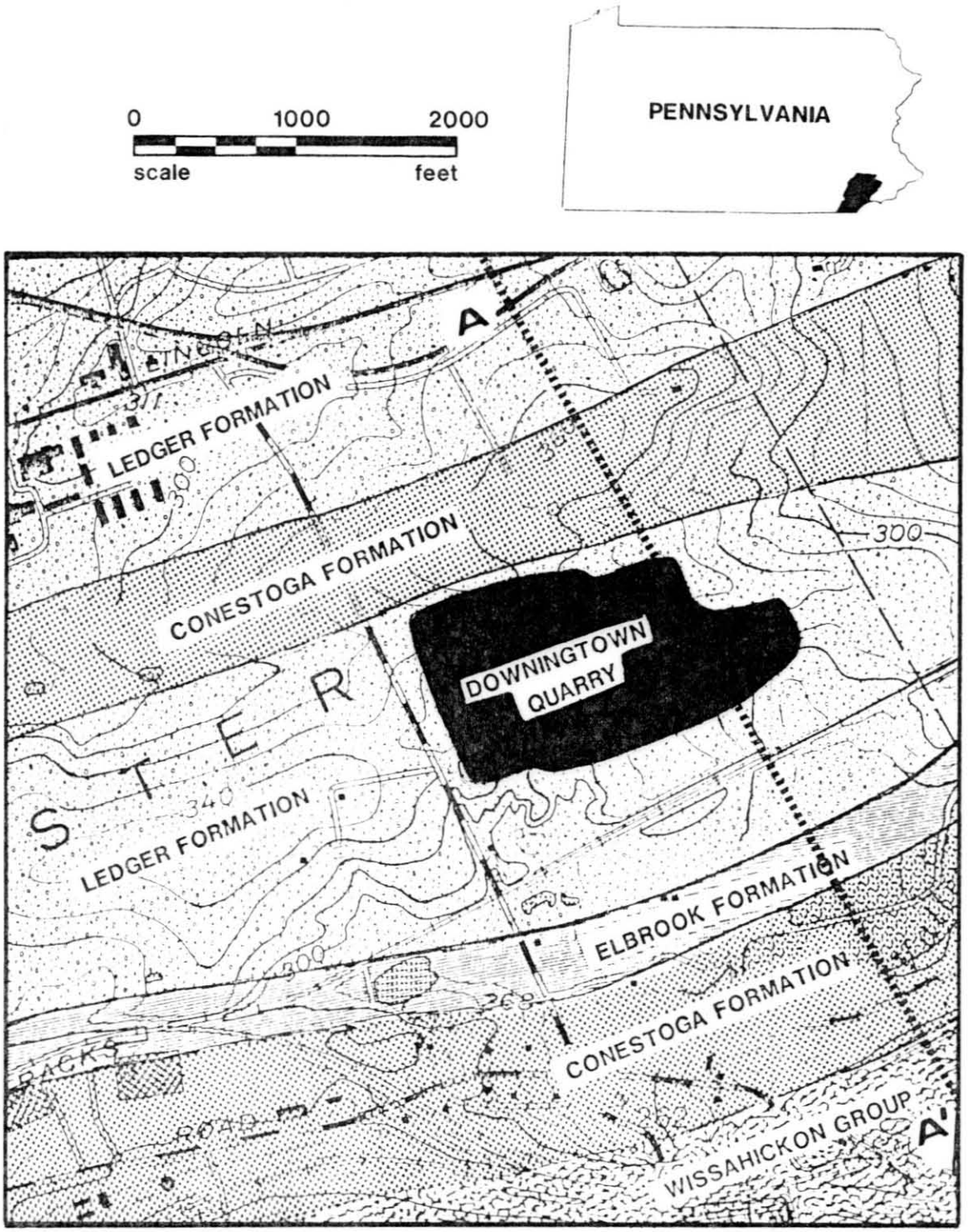

Figure 5. Geologic map of the Downingtown quarry.

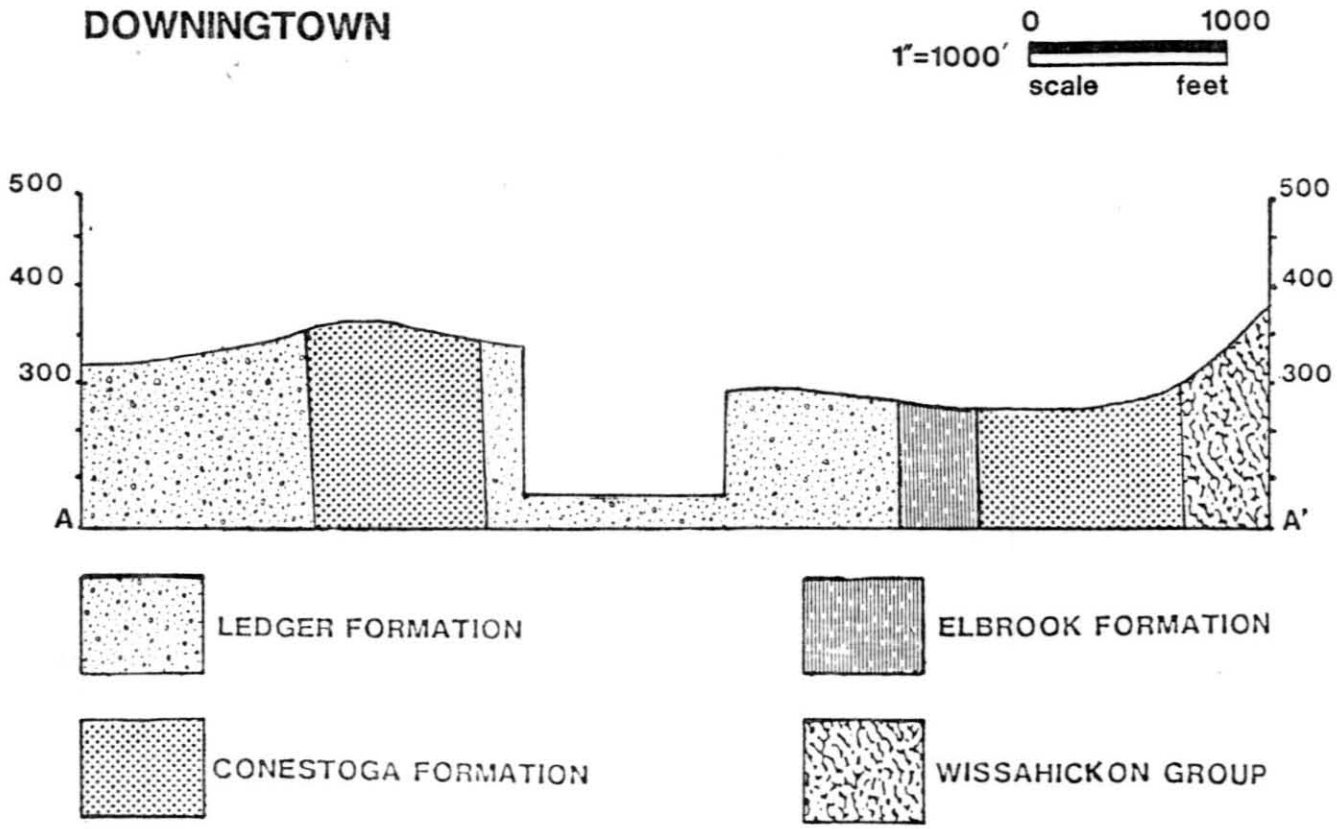

Figure 6. Geologic cross-section of the Downingtown quarry.

influence of soil thickness as well as other low-velocity materials in amplifying seismic energy was discussed in the Background section.

The seismic profiling done at Marriottsville covered approximately 4000 linear ft and at Downingtown, 6500 linear ft. The locations of the seismic survey lines for both sites, along with far-field seismograph locations, are shown in Figs. 7 and 8. Some physical obstacles, such as public highways, quarry structures, and farm crops, placed some limitations as to where the seismic lines could be located. Ambient vibrations around each quarry produced by heavy equipment moving, crusher operations, and general traffic necessitated conducting the refraction survey during late afternoon and early evening after the quarry production operations had ceased.

Standard shallow seismic refraction methods were used for the field survey. A Dresser Industries RS-4 seismograph system* with a series of 12-geophone spreads along the entire survey line was used to collect the field data. Geophone spacings varied from 20 to 30 ft, depending on the depth to the soil/rock interface. Small explosive charges were used as the seismic energy source.

In addition to the seismic subsurface mapping in the seismometer location areas, measurements were taken to obtain compressional and shear wave velocities of the rock on the test benches at both Marriottsville and Downingtown.

4.3 TEST DESIGN

4.3.1 General

At each quarry, two single-hole shots were followed by five eight-hole production blasts. All shots at each quarry were made on the same face,

*Reference to specific brands, equipment, or trade names in this report is made to facilitate understanding and does not imply endorsement by the Bureau of Mines.

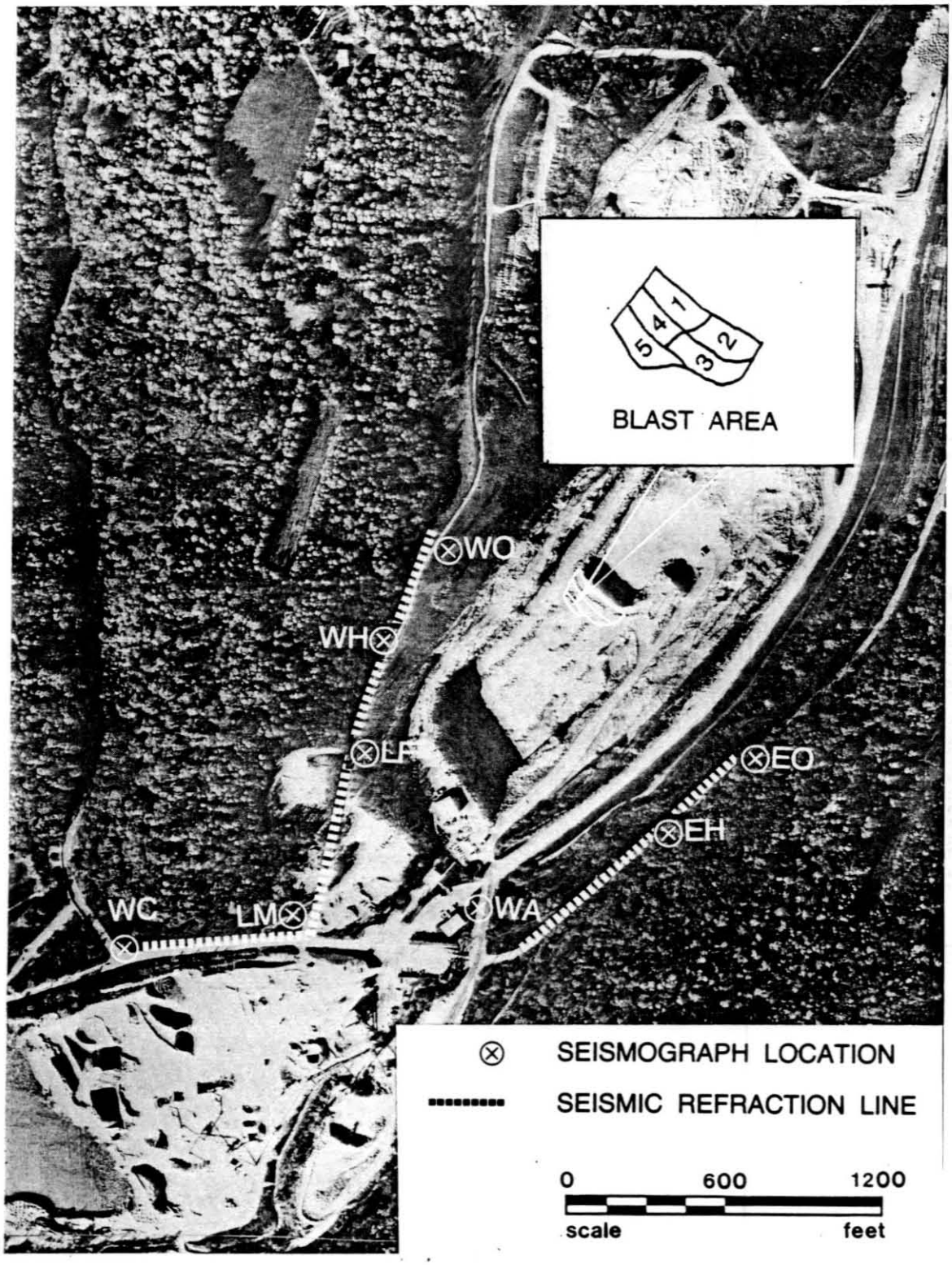

Figure 7. Far-field seismographs and seismic refraction survey line locations -- Marriottsville quarry.

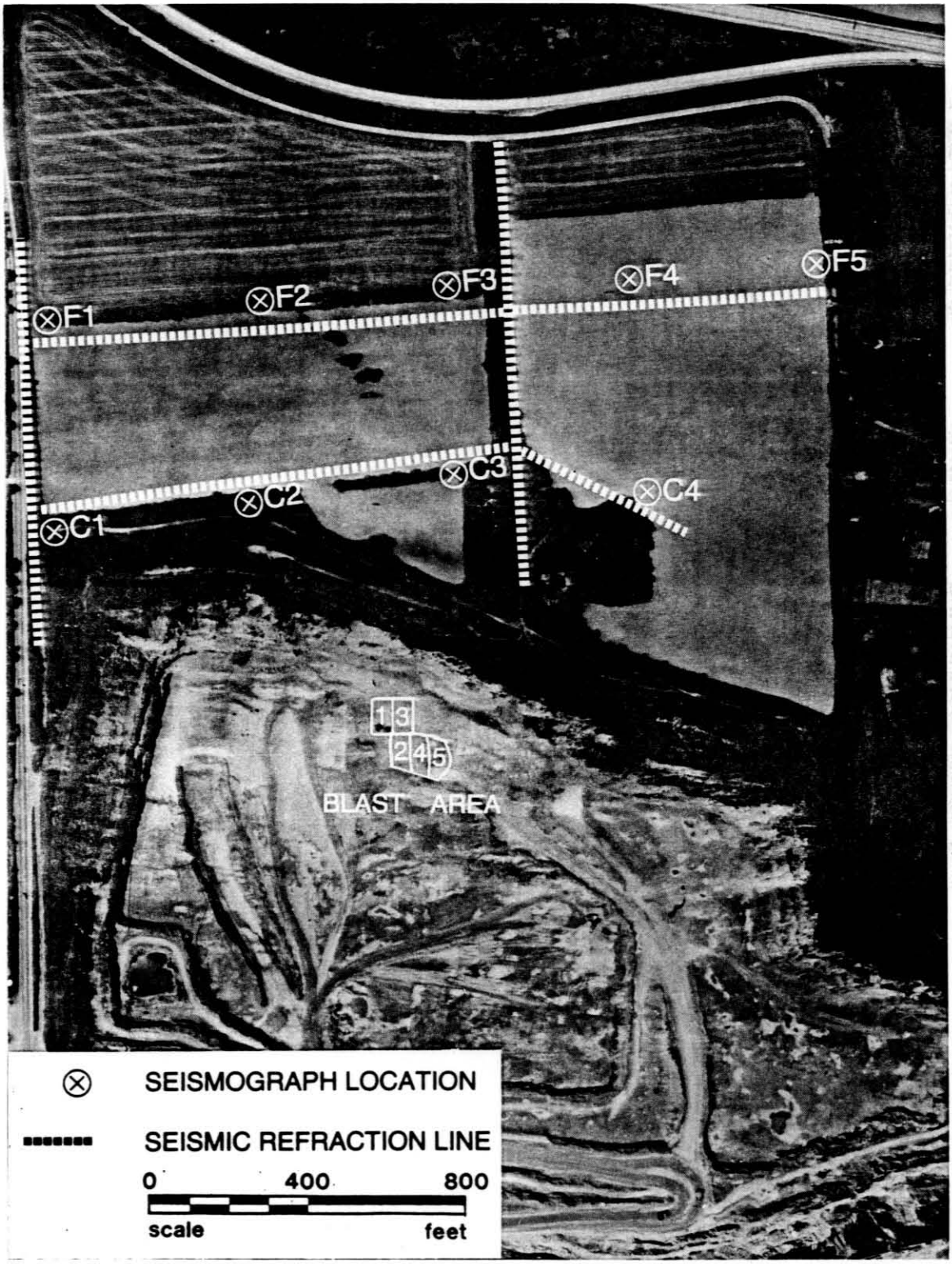

Figure 8. Far-field seismographs and seismic refraction survey line locations -- Downingtown quarry.

with approximately the same explosive loading, stemming, and other pertinent blast parameters, to minimize variation between tests. The only design changes were the delay intervals between holes and between rows on production blasts. The explosive used at both sites was Tovex Extra®, from E.I. DuPont deNemours Company, a non-cap-sensitive water gel slurry packaged in polyethylene, having a weight of 30 lb in 6-in. diameter cartridges and a rated detonation velocity of 19,000 to 20,000 ft/s.

Each shot was monitored with a single high-speed camera focused on the face to assess fragmentation. An additional high-speed camera was located to the rear to determine timing and burden motion for each shot. Two six-component strain gages were grouted at a depth of 25 ft in boreholes adjacent to single-hole tests and within and behind the production tests. Four three-axis seismometers were used to record ground vibration on the bench being shot. The seismometer and strain gage outputs were recorded on a common-time-base FM analog tape recorder. At sites either around the test perimeter (Marriottsville) or to one side (Downingtown), eight to ten seismographs were used to record vibration. A schematic diagram of instrumentation layout is shown in Fig. 9.

Hercules Vibrodet #8 (SSS) seismic initiators, which have a function time of about 30 μs, were used in conjunction with an REO System 5000 programmable sequential blasting machine. Use of secondary backup initiators, either Atlas Rockmasters or DuPont M.S. millisecond-delay caps ensured that the individual blast holes detonated. Two cast primers were used in each hole, a 2-lb primer 5 ft above the base of the explosive column and a 1-lb primer 5 ft below the stemming column.

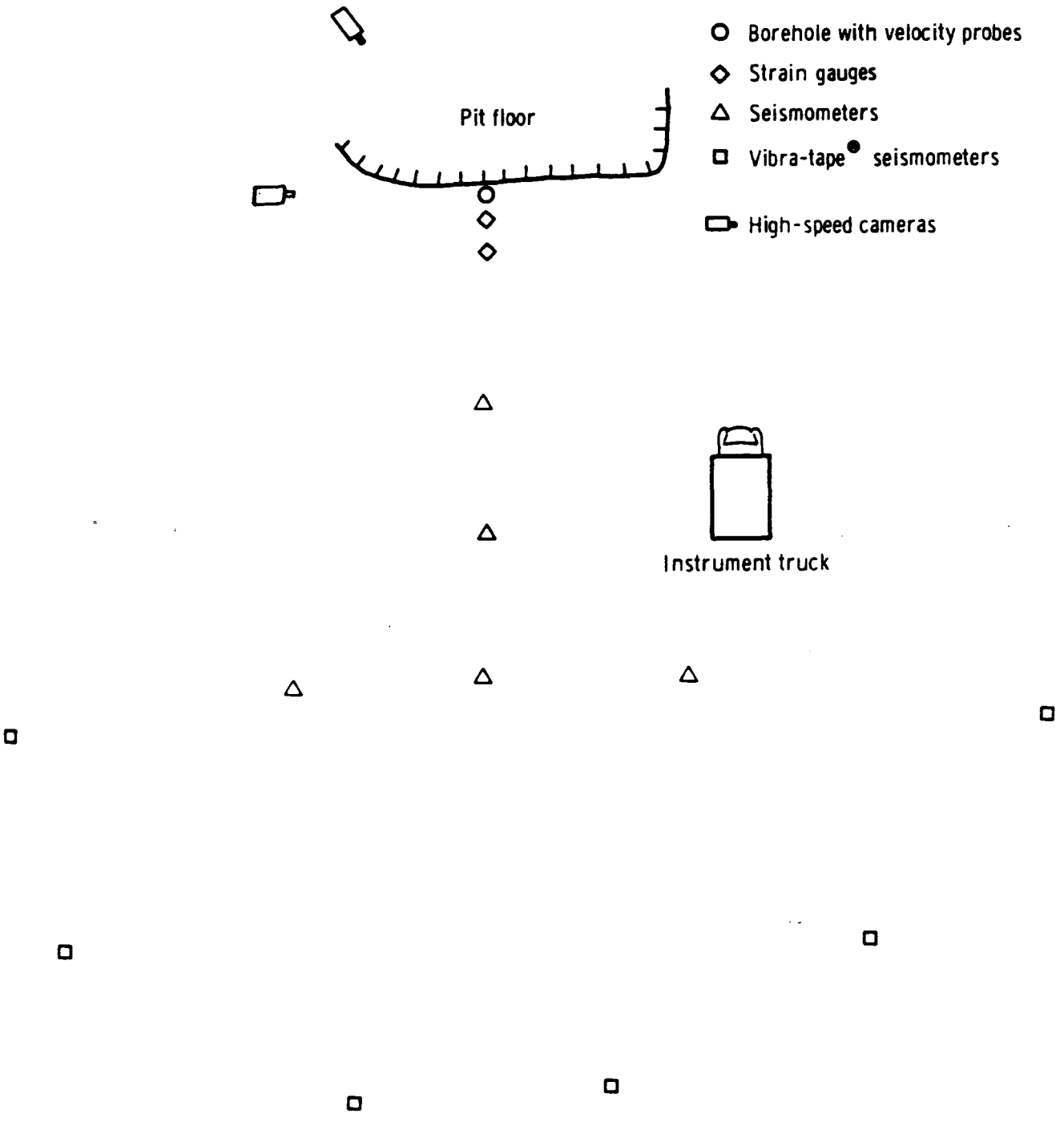

Figure 9. Schematic diagram of instrumentation layout for single-hole shot.

Blast pattern geometry was determined by current quarry practice. Standard dimensions at Marriottsville are: borehole diameter, 6 in.; burden and spacing, 15 ft x 17 ft; stemming, 13 ft; and hole depth, 50 ft. Standard dimensions at Downingtown are: borehole diameter, 8 in.; burden and spacing, 18 ft x 18 ft; stemming, 17 ft; and hole depth, 55 ft. The explosive was cut into 4- to 6-lb pieces to ensure positive coupling with the borehole sides and uniformity in loading density up the column length. The loading density for Tovex Extra is approximately 1.33 gm/cc; a 1-foot column therefore corresponded to either 16 lb (6-in. diameter) or 29 lb (8-in. diameter).

4.3.1.1 Single-Hole Shots

Two single-hole detonations were made at each site in the bench selected for the production shots. High-speed films, and strain gage and seismic measurements were taken for each of the single-hole shots, to establish reproducibility, and collect baseline data for comparison with the production shots. The time histories recorded on the seismographs outside of the quarry property were used as the basis for changes in delay sequences. The same seismograph locations were used for the duration of the test series at each quarry.

4.3.1.2. Production Shots

Shots were laid out in two rows, with four holes per row. The size of the shot was determined by the number of available circuits on the blasting machine. At Marriottsville the shots were located on the fourth level of the southwest face in what is known as the white stone; at Downingtown, the fourth level, northeast corner was used as the test site. The holes

for each blast were laid out with tape measure and drilled by the drilling crew of the host quarry. As mentioned, Tovex Extra was used throughout, in both dry and wet boreholes, whereas most of the quarry production holes at both sites are loaded with an ANFO-based dry explosive. Before loading each shot, individual hole depths were measured with a weighted tape. At Downingtown, if the hole was wet, is was pumped. Clean crushed stone (1/4-in.) was added to reach the correct depth. During loading, the explosive column was frequently measured to ensure correct placement of the primers and initiators. Stemming length was kept constant; however, some variation was necessary according to the measured burden and rock condition on the top third of the face along the first row of holes.

4.3.2 Shot Performance Assessment

4.3.2.1 Delay Timing

Identification of firing times of individual boreholes was made using a telltale consisting of Ensign-Bickford NONEL® cord. One end of a known length of the cord is placed in the top of the explosive column. The cord was brought up through the stemming and taped in a coil to a cardboard box which the explosives came in. When detonated by explosive, the cord emits a visible bright flash.

A rotating-prism high-speed camera, Redlake Fastax II, run at 2200 pictures/sec, was used to record the flashes of telltales in each hole of the test blasts. Except in early tests, this camera was placed directly behind and above the shots. Location of the camera is critical to getting all of the firing time data; it must not be placed where vertical venting of early firing holes would obscure the flashes from later holes.

Firing times are determined by counting the number of frames from a zero time flash up to, and including, the frame where the flash from the telltale is first seen. Because the high-speed camera varies by several percent from the selected framing rate while running at speed, these variations must be accounted for when doing the timing analyses. The changes in framing rate can be determined from timing marks placed on the edge of the film during the filming. A program that accounts for changes in the framing rate of the camera over the period of the event is used to calculate the elapsed time between the zero frame and the event.

Because the telltales are placed in the top of the explosive column, the firing times determined directly from the surface flashes are not the actual detonation time, since the column is bottom initiated. The time of the hole detonation is determined by subtracting the detonation time of the explosive column plus the detonation time of the telltale though the stemming from the surface firing time. Initiator locations within the column were logged for each hole, which, together with the stemming lengths, were used in correcting the surface firing times. Knowing the burning rate for the cord, its length, and the length and detonation velocity of the explosive, we can obtain the detonation time for the column with an accuracy of $\pm$0.3 ms.

The largest uncertainty in the firing times comes from the limits on time resolution in the high-speed films. At the framing rate used for these tests, there is an uncertainty of $\pm$0.45 ms in the timing of the surface flashes.

4.3.2.2 Detonation Velocity

Pin probes were used to determine the detonation velocity of the explosive columns. Two probes are required for the set-up, one each for a start and a stop signal, spaced a known distance apart. The probes are made by cutting off the end of a coaxial cable, verifying isolation of the center lead and the shield, and then insulating the end of the cable with a plastic-dip compound. The lengths of the cable were sufficient to permit connections to a lead line outside the backbreak zone of the blast with enough additional cable to place the probe at the desired borehole depth. In our tests, the start probe was placed 40 ft from the top of the hole and the stop probe 20 ft above it. When the explosive column was built up to the proper height, the insulated end of the coaxial cable was weighted with a small rock and lowered into the borehole. Fifty to 100 pounds of explosive were placed on top of the probe and the cable was anchored with a rock until the hole was loaded and stemmed. Safety procedures dictated that the probe cables would be connected to the lead line only during the final test preparations, i.e., usually when the caps were being wired together.

An electrical potential of ~ 15 V DC was placed across the center lead and shield of each probe before the blast was initiated. The circuits were current limited to less than 10 microamperes to minimize the possibility that a pin probe could set off any of the electric blasting caps. As the detonation front of the exploding borehole passes the insulated end of a pin probe, the surrounding ionized plasma is sufficiently conductive to short the center lead and the shield together, discharging a capacitor and allowing a voltage spike to be recorded at

the other end of the cable. To distinguish between the start and stop signals, which are recorded on the same channel, they have different polarity. The velocity probe data were recorded on magnetic tape and later analyzed using a digital oscilloscope.

4.3.3 Seismic Measurement

4.3.3.1 Far-Field

Three (3)-component FM recording seismographs (Vibra-Tape GMS-4 Series 2000 analog units, manufactured exclusively for Vibra-Tech Engineers, Inc.) were used for the far-field data acquisition. The Series 2000 records an analog waveform on magnetic tape with 30-minute recording capability. Each unit was turned on 10 to 15 minutes before each blast. A voice function button enabled the date, time, location, and calibration details to be directly recorded on tape for each site per detonation.

The manufacturer's specifications for the seismograph are as follows:

Sensitivity:

The two available range settings for ground motion are 0.02 to 1.0 in./s particle velocity and 0.10 to 4.0 in./s particle velocity.

Response:

Dynamic range of 24dB, with frequency response flat from 1 to 200 Hz.

Power:

Two self-contained, 6-volt dry lantern batteries, with up to 75 hours of operation. Battery level indicator ensures adequate voltage.

An internal calibration system was utilized each time the units were used. Analysis of each trace confirms the calibrated response of the unit. The instruments were calibrated both prior to the test series and after its conclusion using a shaker system traceable to the National Bureau of Standards.

4.3.3.2 Near-Field System

Martin Marietta Laboratories' researchers modified four Sprengnether S 6000 3-axis blast seismometers with 80 dB attenuators and PTS-9 micro-earthquake amplifiers, resulting in a full-scale dynamic range of -20 to +120 dB (4×10^{-7} to 4 in./s). The seismic data were recorded on a multi-channel magnetic tape recorder, Honeywell Model 101, at a tape speed of 120 ips, resulting in flat frequency response from 1 to 100 Hz.

The seismometers were placed at various distances behind the test blasts on the bench level of the quarry. The seismic and strain gage responses were recorded simultaneously. The seismic data were related to the film data by placing a zero-time pulse on each channel electronically at the instant the blast sequence was initiated.

4.3.4 Face Fragmentation Measurement

A pin-registered 16-mm high-speed camera, Redlake Locam, run at 500 frames/s, was used to film face fragmentation of all test blasts. The zero-time indicator was placed on the top of the bench so as to be visible in the films, and a scale was painted on the face to allow calibration during data analyses. A zoom lens was used to adjust the field of view to include all of the blast plus approximately one spacing distance on either side. When lighting conditions and face orientation were favorable,

tests were scheduled at a time of day when the face received the most sunlight to give the films maximum contrast. Unfortunately, changeable weather on some days resulted in fairly low contrast films for some tests, which tend to have less spatial resolution than high contrast ones.

Prints of the high-speed films were projected by a stop-frame analytical movie projector into a photo-optical digitizer. This equipment allows an image to be rear projected in an 11 x 14 inch format onto a ground glass screen or a piece of tracing paper. In our analyses, a tracing was made of each frame to be digitized, including the outline of every resolvable rock fragment. Figures 10 a and b show a print of one frame and its tracing, respectively, from the second production shot at the Marriottsville quarry. Typically, frames to be digitized were selected between 400 and 900 milliseconds after zero-time. The actual time at which each frame was selected was affected by the total amount of time needed for the front row of holes to detonate and for the rock to move off the face. After the front row of holes detonate, the rock mass must be allowed sufficient time to expand such that individual fragments can be well resolved, but not too much for the fragments to leave the field of view or be obscured by dust. Because the rock moves towards the camera, the different times selected for digitizing resulted in variations in the scale factor used to change the dimensions of the particles to their "real" size. We found that the corrections needed to adjust the scale factors did not significantly change the gross shape of the particle size distributions. Thus, no corrections to the scale factors were used when comparing the data.

(a)

(b)

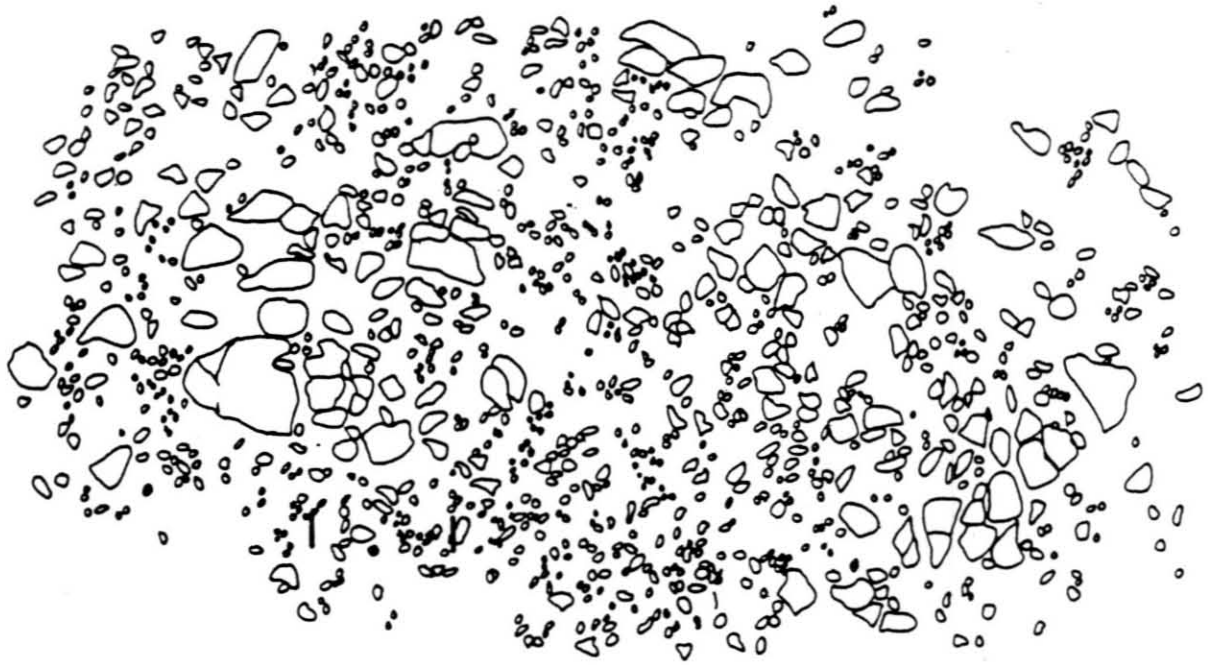

Figure 10. Face fragmentation determination: a) Typical frame from high-speed films, and b) corresponding trace of fragments.

According to the high-speed films, the smallest scaled dimension that could be restored was about 0.2 ft. After the tracings were generated, the individual fragments in each trace were numbered and their areas were determined using the digitizer calibrated to the actual scale of the bench. These tracings then formed the basis of the fragmentation data. The analytical procedures used to process the data will be discussed in Section 5.3.

4.3.5 Strain Wave Measurement

The fundamental design of the strain gages comes from R.P. Reed of Sandia Laboratories (Reed, 1979), but we have made minor modifications. The gage is made of six foil resistance strain gages embedded in a specific geometrical configuration in a cylindrical matrix, which is then grouted into a borehole.

The matrix material for the gage is an aluminum-filled thick-section epoxy (Ren Plastics 3269A) chosen because it is easy to work with and has low impedance mismatch with rock (Reed, 1979). A gage made of rock, such as that designed by the Bureau of Mines for static measurements, could not be used because the individual foil gages need to be as close to one another as possible, and recasting is necessary.

Six independent strain measurements are required to determine the complete strain tensor. Consequently, six foil resistance strain gages (MicroMeasurements CEA-13-125UT-120) were affixed with a standard epoxy to three surfaces of a 2.5-cm cube, with two gages per surface, as shown in Fig. 11. The arrangement of the gages is not trivial in that it is easy to have two gages on adjacent faces measuring the same strain, and

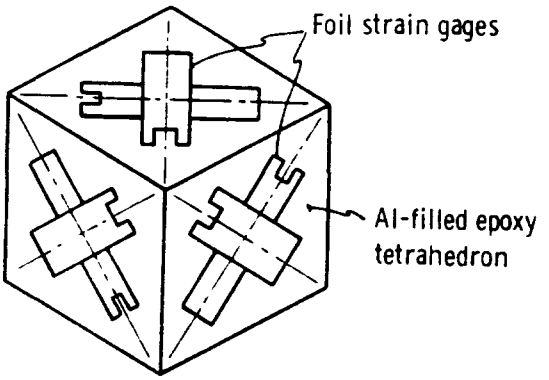

Figure 11. Strain-gage configuration on epoxy cube, viewed from top.

thus be redundant. Each gage is wired in true three-wire configuration, with an approximately 20-m cable consisting of nine, individually shielded, twisted pairs. The cable is strain relieved near the connections with room-temperature vulcanizing (RTV) rubber. The common three-fold axis of the cube is oriented vertically and recast into a 7.6-cm-diameter cylinder of the thick-section epoxy approximately 15-cm long. An array of light-emitting diodes is epoxied to the top of the cylinder and then oriented in a borehole, using a rifle-scope.

The strain-gage boreholes are approximately 7.5-m deep and of the diameter of the nearby explosively-loaded holes (for convenience). A modified garden sprayer wetted the inside of the borehole to reduce dust so that the LEDs could be seen, and to obtain good grout-rock contact along the walls. An expansive grout was used to put the gage under slight pre-compression. However, the amount of pre-compression was not measured. A 60-m extension cable was coupled to the gage after installation to carry the amplifier connections away from the blast. Each gage was independent, in quarter-bridge configuration. Strain gage amplifiers (Honeywell Model A218) were used to complete the bridge for each of the gages, and are rated to have flat frequency response from DC to 50 kHz. Gage excitation was 6 V DC, and gain was approximately 140:1. The dynamic signals were recorded on the 28-track FM analog tape recorder (Honeywell Model 101), running at 120 ips, with rated flat frequency response from DC to 40 kHz, which also recorded the bench seismograph signals.

5 ANALYTICAL PROCEDURES

The data collected in the test series were processed for analysis. To avoid confusion in the discussion of the results, we will describe the procedures used in this section.

5.1 VIBRATION

Analog waveforms for all of the seismic records were plotted for visual comparison. Peak particle velocities were calculated for each of the waveforms, using the instantaneous vector sum for all three components, which is the square root of the sum of the squares of the three particle velocity components at each digitization point.

In addition, response spectra were calculated. As recommended by Medearis (1977), the response spectrum method can be used to estimate the probability of damage to low-rise structures from blasting vibrations. The method calculates the response of a single degree-of-freedom system to a vibration time-history. The greatest potential for structural damage occurs when the frequency of the ground vibration matches the natural frequency of the structure, causing amplification of the ground motion within the structure. Various values of natural frequency are assigned to the single degree-of-freedom system, and the maximum response of these systems to a vibration time-history is calculated. The response spectrum is a plot of the maximum response at various natural frequencies. High response values for systems having a natural frequency from 3 to 18 Hz could adversely affect low-rise residential structures.

Response spectra for 5% critical damping were calculated for all three components of ground motion. The horizontal components are the most

critical in evaluating structural response, because a structure has less damping and more freely responds in a horizontal plane. In this analysis, the vertical components of the response spectra were also compared statistically because of difficulty maintaining the same alignment of the geophone's horizontal axis for all the testing as the blast locations moved along the quarry bench.

To complement the analysis of the vibration records, firing time frequency spectra were calculated for each blast by taking the Fourier transform of the time-series made from the blast delay times. The firing time function has a value of 1 at the time a hole is fired and a value of 0 at all other times. For example, a 3-hole blast with a 5-ms delay between holes could be represented by the firing time function as:

time	0	1	2	3	4	5	6	7	8	9	10	ms
amplitude	1	0	0	0	0	1	0	0	0	0	1	

f(t) = (1, 0, 0, 0, 0, 1, 0, 0, 0, 0, 1)

The Fourier amplitude at any particular frequency (n) for this firing time function can be calculated using the Fourier integral:

$$F(n) = \int_0^\infty f(t)\cos(2\Pi nt)dt + i \int_0^\infty f(t)\sin(2\Pi nt)dt$$

in this particular case dt = 1 ms.

The integral containing the cosine term is designated as real, while that containing the sin term is designated as imaginary, hence the use of the coefficient i. This is done as a mathematical convenience as the two terms cannot be added directly, but must be added vectorially.

Therefore,

$$F(n) = C(n) + i\ S(n)$$

where

$$C(n) = \int_0^\infty f(t)\cos(2\pi nt)dt$$

$$S(n) = \int_0^\infty f(t)\sin(2\pi nt)dt$$

Then for this particular 3-hole blast, the value of f(t) at all times other than 0, 5, and 10 ms would be zero. The Fourier amplitude would be equal to:

$$A(n) = [C(n)^2 + S(n)^2]^{1/2}$$

The Fourier amplitude for 10 Hz could easily be calculated as follows:

$$C(10) = 1 \times \cos(2\pi \times 10 \times 0) + 1 \times \cos(2\pi \times 10 \times 0.005) + 1 \times \cos(2\pi \times 10 \times 0.010)$$

$$= 1.0 + 0.952 + 0.81 \text{ (note: trig. function in radians)}$$

$$= 2.762$$

$$S(10) = 1 \times \sin(2\pi \times 10 \times 0) + 1 \times \sin(2\pi \times 10 \times 0.005) + 1 \times \sin(2\pi \times 10 \times 0.010)$$

$$= 0 + 0.307 + 0.586$$

$$= 0.893$$

$$A(10) = [(2.762)^2 + (0.893)^2]^{1/2}$$

$$A(10) = 2.90$$

5.2 STRAIN WAVES

The strain gage data collected from the test blasts were processed to determine the principal strains and the invariants of the strain tensor. Prior to analyzing the records, we did not know what to expect, since previous strain gage studies used either one component (e.g., Duvall and Atchison, 1957; Atchison and Tournay, 1959), or were from one- or two-hole shots (e.g., Reed, 1979; Anderson et al., 1984). Our philosophy was to manipulate the data in as many different ways as we could once we had the principal strains. We will discuss the results of the manipulations later and only describe the mathematics in this section.

Digitized data were first processed to determine the principal strain magnitudes from the six-component records. The six gage measurements must be transformed to give the six components of a symmetric strain tensor:

$$e_{ij} = \begin{vmatrix} e_{11} & e_{12} & e_{13} \\ e_{21} & e_{22} & e_{23} \\ e_{31} & e_{32} & e_{33} \end{vmatrix}$$

where $e_{21} = e_{12}$, $e_{31} = e_{13}$, and $e_{32} = e_{23}$. The strain gage components are numbered according to Fig. 10. The appropriate equations relating the strain components (E_k) to the tensor components (e_{ij}) are:

$$e_{11} = 1/2\ (E_1 + E_2 + E_3 + E_4 - E_5 - E_6)$$

$$e_{22} = 1/2\ (-E_1 - E_2 + E_3 + E_4 + E_5 + E_6)$$

$$e_{33} = 1/2\ (E_1 + E_2 - E_3 - E_4 + E_5 + E_6)$$

and for the shear components

$$e_{12} = E_3 - 1/2\ (e_{11} + e_{22})$$

$$e_{13} = E_2 - 1/2\ (e_{11} + e_{33})$$

$$e_{23} = E_5 - 1/2\ (e_{22} + e_{33}).$$

The principal strains, denoted e_1, e_2, and e_3, are determined by diagonalizing the strain tensor matrix. This diagonalization is accomplished by solving for the roots of the cubic equation:

$$-e + I_1 e^2 + I_2 e^3 + I_3 = 0.$$

The roots are the eigenvalues of the equation, and the equation may be solved using standard eigenvalue subroutines. The coefficients in the

cubic equation are called the strain invariants because they are invariant with respect to coordinate transformation. A full discussion of coordinate transformations is given in such standard texts as Nye (1963) and Fung (1965). The first strain invariant is the dilitation.

In addition to strain invariants, the strain deviation invariants may be calculated from the principal strains. The first strain deviation invariant is identically equal to zero, but the second and third strain deviation invariants are used in yield criteria. We will concentrate on the octahedral shear strain, which is proportional to the second strain deviation invariants:

$$9\tau_0^2 = 2\ I_1^2 - 6\ I_2 = 6\ J_2$$

where τ_0 is the octahedral shear strain, I_1 is the first strain invariant, I_2 is the second strain invariant, and J_2 is the second strain deviation invariant. The octahedral shear strain is the resultant shearing strain on a plane that makes the same angle with the three principal strain directions. This plane is called an octahedral plane since eight such planes form an octahedron. The shearing strain on each of these planes is of the same magnitude but varies in direction. Failure criteria (normally expressed as a function of stress rather than strain) often assume that yielding occurs at some constant value of the octahedral shearing strain. Some recent work on fracture has indicated that it may be viewed as a modified form of plastic yielding. This field is still under development, but the implications are that a yielding criterion based upon octahedral shearing strain or octahedral shearing stress may be appropriate.

5.3 FRAGMENTATION

Quanitative assessment of fragmentation at production scale is the most difficult task facing the investigator. The only fully quantitative method of assessing fragmentation is to screen the entire mass of fragment material; however, this is impractical at production scale. Other methods are statistical and rely on selective or random sampling of the muckpile, either photographically or through surface or trench sampling. Relying on quarry productivity figures is risky, because of the many variables affecting production parameters, such as loading rates and crusher throughput.

We have developed a somewhat different technique, which makes use of high-speed films to assess fragment size distribution. This technique is similar to that used by Winzer and Ritter (1979) to quantitatively assess the change in size distribution with time as rock fragments leave the face. The scaling factor for the photo-optical digitizer was determined from the scale markers on the face, and the amount of forward motion which had taken place at the stopped time. The were determined using the photo-optical digitizer. The areas and fragment number were stored in a computer file for use in a program which was written to calculate areas and mathematically screen the fragments to determine a size distribution. A separate program calculates the weight of each fragment, based upon the assumption that the maximum thickness of the fragment is calculated and multiplied by the density of the rock to find the weight. Weight or area passing a given size is then calculated. If the area of a fragment is smaller than the area of a square "screen" of a given dimension, then that particle passes that screen size. The program

accumulated both the number of particles and their total area that are retained on the selected screens. As with standard sieve analyses, screen sizes are related by a factor of two for consecutive fractions. Previous studies (Winzer, et al., 1983) comparing fragmentation obtained by this method with the results of screening have determined the validity of the method.

5.4 DELAY DESIGN TECHNIQUES

At this point we will discuss the techniques which we have used to determine the blast delays for the test series. We will be presenting some of the results of single-hole tests in the process; this presentation is somewhat out of order, but is being done to avoid a lengthy discussion of techniques in the results section.

We have chosen to vary between-hole relief to study the effect of delay on fragmentation, consistent with our discussion earlier, and previous work. Following Winzer et al. (1983), we have chosen delay times between holes in a row corresponding to relief of 1, 2, 3, and 4 ms/ft, based upon the appropriate spacings used at the quarry. We initially assumed that there would be no effect of the between-row relief on the face fragmentation, though we did not test this assumption. However, the between-row relief has been seen to affect displacement of the muck-pile, and this effect was observed, and utilized in the study.

The between-hole relief values were modified somewhat to mesh with the desired vibration control program, but to still study the effect of delay on fragmentation within this range of relief values. Once these values

were chosen, the vibration techniques could be used to modify the between-hole values as necessary, and the between-row times were chosen primarily to affect vibration.

We will now discuss in some detail the two techniques which were used to determine delay times for the vibration study.

5.4.1 Autocorrelation

Autocorrelation is a signal processing technique which determines the extent to which a time-lagged version of a signal matches the original signal. The procedure is a repeated convolution of the signal with its time-lagged version. The resultant of this calculation is a waveform, which assesses the degree of match. An example is shown in Fig. 12b for the single-hole waveform of Fig. 12a. The best match is at zero-delay, since each point perfectly matches the other in the two records. The autocorrelation function is then a measure of how well the two signals are in phase. High positive values of the function are found at times at which the signals are in phase, and negative values are found where they are out of phase.

Delayed blasting may take advantage of this situation; delay times may be chosen for the signals to be the most out of phase consistent with production practice. In this study, though, we have taken delay times corresponding to both negative and positive autocorrelation in order to determine how effective this method is in controlling vibration. Figures 12 c and d, respectively, show how constructive and destructive interference may be created by time-shifting the single-hole waveform according to the times determined by the autocorrelation.

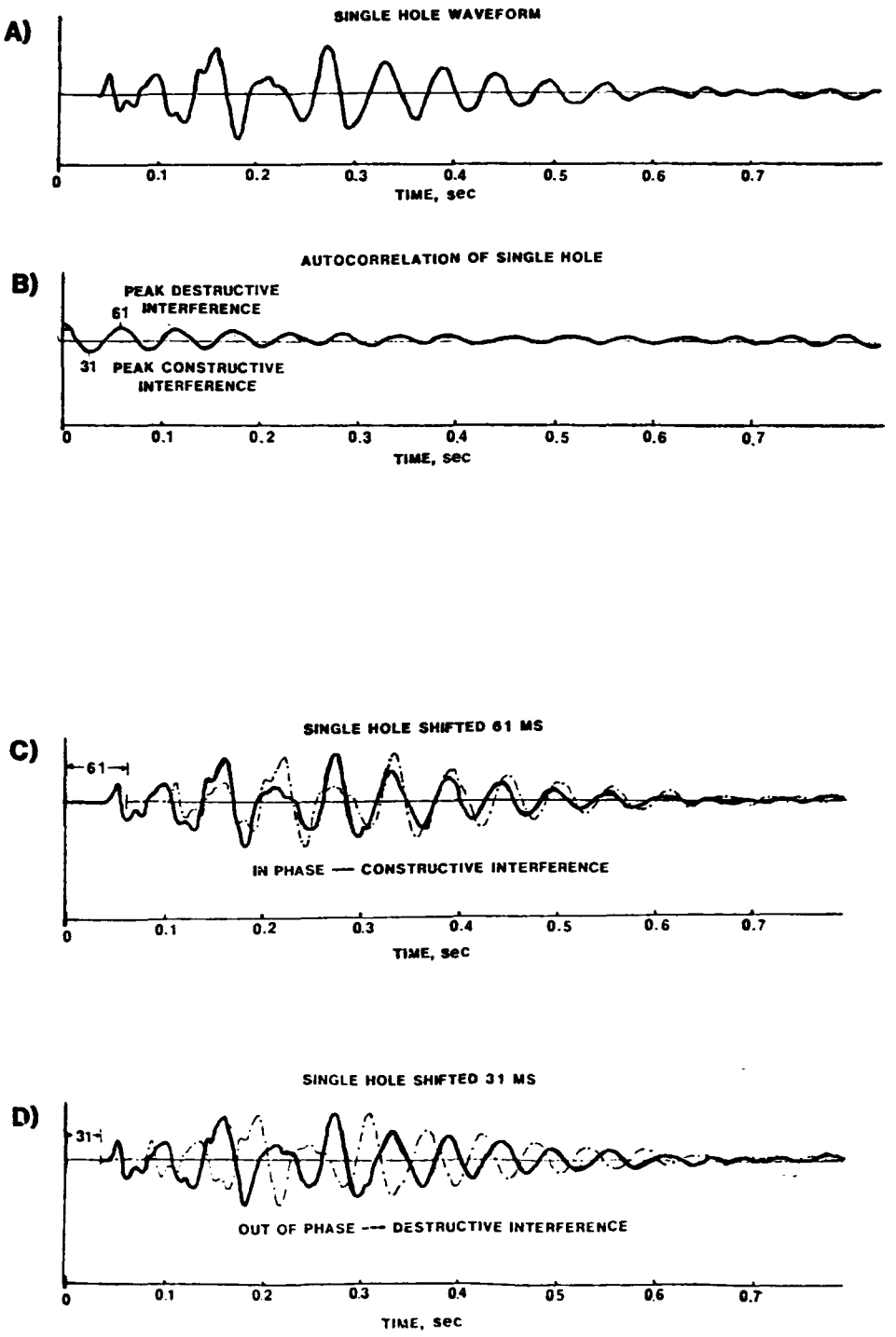

Figure 12. a) Time history and b) autocorrelation function for single-hole waveform. Constructive (c) and destructive (d) interference generated using autocorrelation times.

5.4.2 Fourmap

Fourmap is a site-specific method for choosing blast designs with predictable and controllable blast vibration. For the moment, we will assume that the first two hypotheses discussed in the methodology section have been verified, i.e., each hole in a multi-hole shot generates the same waveform, and single-hole waveforms may be linearly superposed to generate predicted production waveforms. In an optimum delay pattern, the waveforms generated by each of the holes in a shot, when summed, will destructively interfere. Later we will discuss deviations from this assumption, other assumptions, and details of the actual test series validating the method. At this point we will present one of the single-hole waveforms and its associated Fourmap plots as an illustrative example, and to indicate how blast designs were chosen for the test.

The seismic waveform generated by a single-hole shot will be dependent on shot parameters (e.g., explosive type, charge weight, hole size, burden, etc.), the wave path between the shot and the measuring transducer or seismometer and the characteristics of the seismometer. If all the blast parameters and the seismograph characteristics are kept constant, the variation between records obtained for single-hole shots at various seismometer locations should only be due to the different wave paths. A vertical seismogram recorded about 1000 feet from a single-hole shot is shown as Fig. 13a. The total length of the record is 1 s, and the detonation time was about 2 milliseconds (ms). A Fourier amplitude spectrum of this seismogram is shown as Figure 13b. It should be noted that high amplitudes are present at 9 and 15 Hz. These frequencies

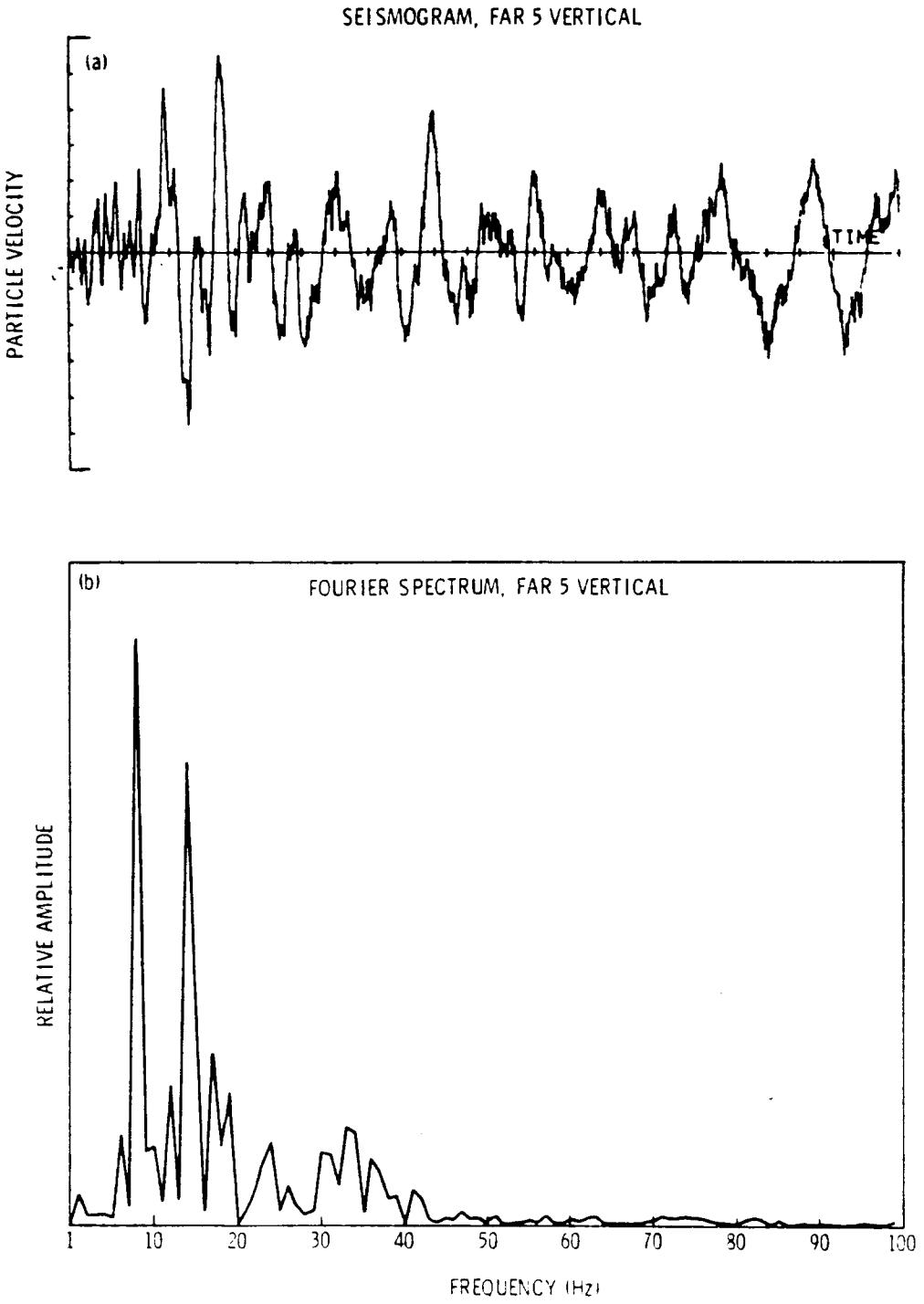

Figure 13. a) Single-hole waveform and b) its corresponding Fourier spectrum.

(Siskind, et al., 1980) are within the resonant range for residential structures. Enhancement of these frequencies by the blast design should be avoided.

We generate predictive synthetic seismograms for a production shot using time-lagged linear superposition of the single-hole waveform. This method involves repeated point-by-point addition of the single-hole waveform to a synthetic waveform starting at a point in the record determined by the desired time delay. The initial synthetic waveform is the single-hole record itself. A synthetic two-hole waveform is generated with the appropriate delay, and the single-hole waveform is then iteratively added to the resultant synthetic one until the number of holes desired is reached. Athough this procedure may be done with analog records, computer processing of digitized records is much more efficient and accurate. An example of how an eight-hole synthetic seismogram is created by time-lagging and linear superposition is shown as Fig. 14.

A Fourier spectrum of the synthetic seismogram will then determine whether the amplitude at the frequencies analyzed has been increased (constructive interference) or decreased (destructive interference).

The goal is to determine the appropriate delays to use for destructive interference of the total waveform, as much as possible, with particular emphasis on vibrations in the range 5 to 20 Hz. In order to do this, we need to vary the delays incrementally and determine the Fourier spectrum as a function of this incremental delay. In addition, we need to graphically display the spectra so that they may be compared. We will first

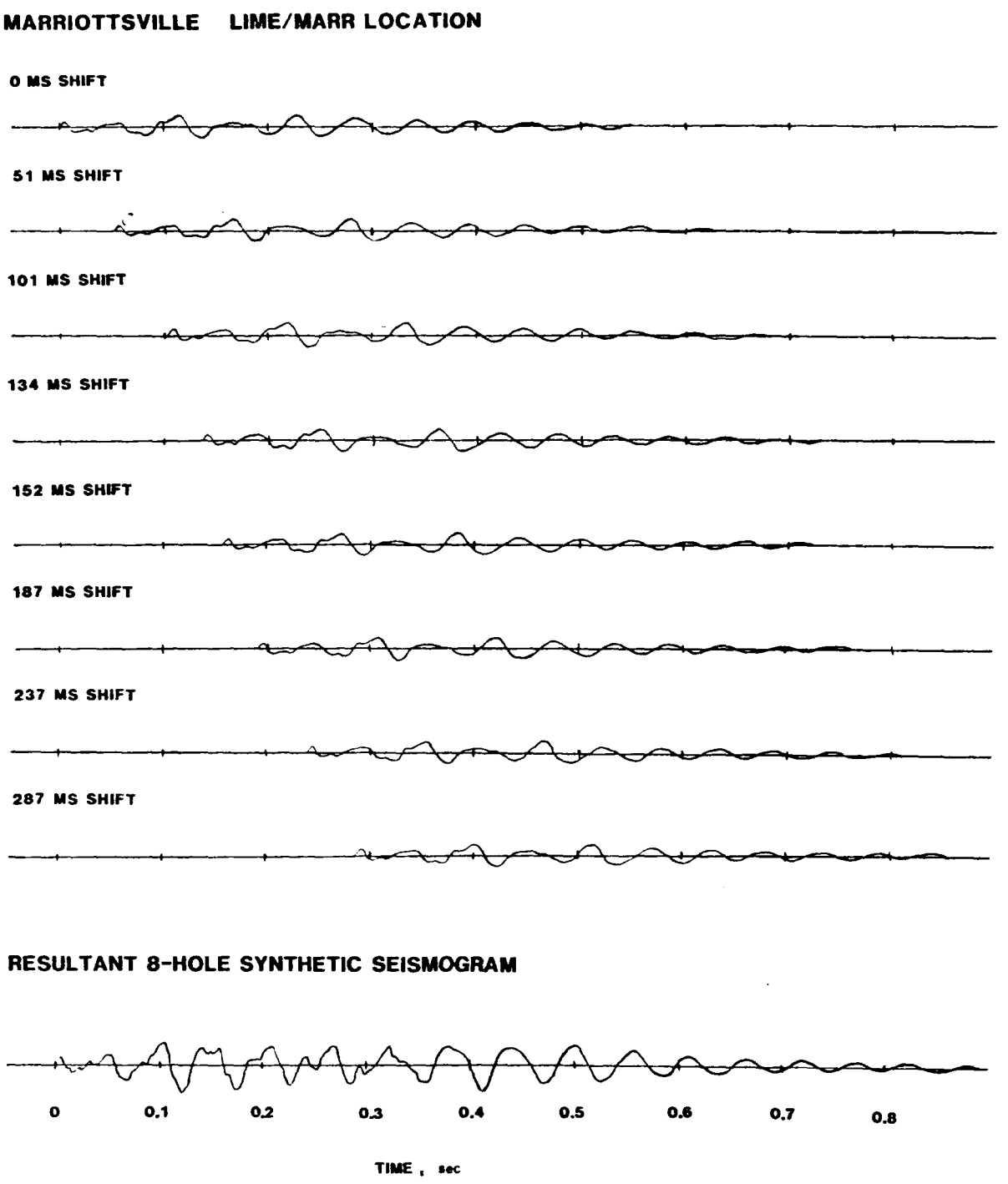

Figure 14. An eight-hole synthetic seismogram created by time-lagging and adding eight single-hole waveforms.

discuss systematic variations in delay between holes in a row, followed by systematic variations in delay between rows with constant delay between holes in a row.

The procedure is as follows: for a single row (single-circuit) shot, synthetic seismograms are systematically generated for 61 different delays between holes in a row and the Fourier spectra are calculated. The initial synthetic seismogram is for all holes detonating instantaneously, i.e., zero delay. The Fourier spectrum for this seismogram is computed and recorded for the range 5 to 50 Hz. The second synthetic seismogram is generated for 2-ms delay between successive holes in the circuit and the Fourier spectrum is computed and recorded. This procedure is repeated, with up to 120 ms between holes in a row for each of the 61 delays.

The results are then plotted using a printer graphics routine. Each spectrum is plotted on a separate line, with the amplitudes related to a seven-level gray scale: the highest amplitudes correspond to the darkest shading. The gray scale is calculated using the amplitudes for the entire data of 61 Fourier spectra. Each line then consists of characters corresponding to the amplitudes of the Fourier spectrum for a given delay, plotted vs logarithmic frequency on the horizontal axis. The vertical axis corresponds to delay in equal increments, increasing from 0 to 120 ms between holes in a row.

A sample Fourmap plot calculated for four holes in a row, using the seismogram shown in Fig. 13a, is shown in Fig. 15. The top line, with zero delay between holes, is the spectrum for four holes detonated simultaneously. The amplitude spectrum is proportional to that of the single-hole spectrum shown in Fig. 13b. Note the peaks at 9 and 15 Hz. The

Figure 15. Four-hole single-row Fourmap plot generated for single-hole waveform of Fig. 13a.

next line is the spectrum for 2-ms delay and so on. At short delays, the spectrum at low frequencies is essentially constant; however, interference, resulting in lower amplitude, may be seen at the higher frequencies.

On the remainder of the plot, two trends are apparent. The influence of the single-hole frequencies persist for all delays, as evidenced by vertical bands at 9 and 15 Hz. These bands are modulated by interference due to the delay. A curving domain of high amplitude is seen from about 24-ms delay at 40 Hz to 120-ms delay at 8 Hz. This domain corresponds to constructive interference for the frequency corresponding to the inverse of the given delay. Low-amplitude domains parallel to the constructive interference domain correspond to destructive interference for the corresponding frequency-delay pairs.

The frequency response for a particular delay between holes may be determined by looking at the line corresponding to that delay number or one close to that delay. The optimum delay is that for which there is destructive interference for those frequencies that are present in the single-hole spectrum. In this example, a delay of about 30 ms appears to be optimum. Conversely, a delay of about 68 ms will give high amplitudes at 15 Hz, one of the frequencies excited by the single-hole shot.

Calculation of the Fourmap plots for multiple-circuit shots uses a similar approach but with some minor modifications. A particular delay between holes in a given circuit must be selected, for optimum fragmentation and/or for the best vibration. This delay is then used to generate a synthetic seismogram from a single-hole waveform which then becomes the basis for creation of the synthetics for the multiple-circuit Fourmap plot. As with the single-row shots, synthetic seismograms are

generated by systematically delaying the initial waveform and adding delays incremented, in this case, by 3 ms. Similarly, the best delays are those having the minimum amplitude (the lightest gray-scale image) on the plot. An example for delays between holes in a circuit of 72 ms is shown as Fig. 16. Low amplitudes are indicated for delays of about 39 and 123 ms, respectively. Typically the delays between rows should be longer than delays between holes in a row, to allow sufficient relief, and the 123-ms delay is preferable.

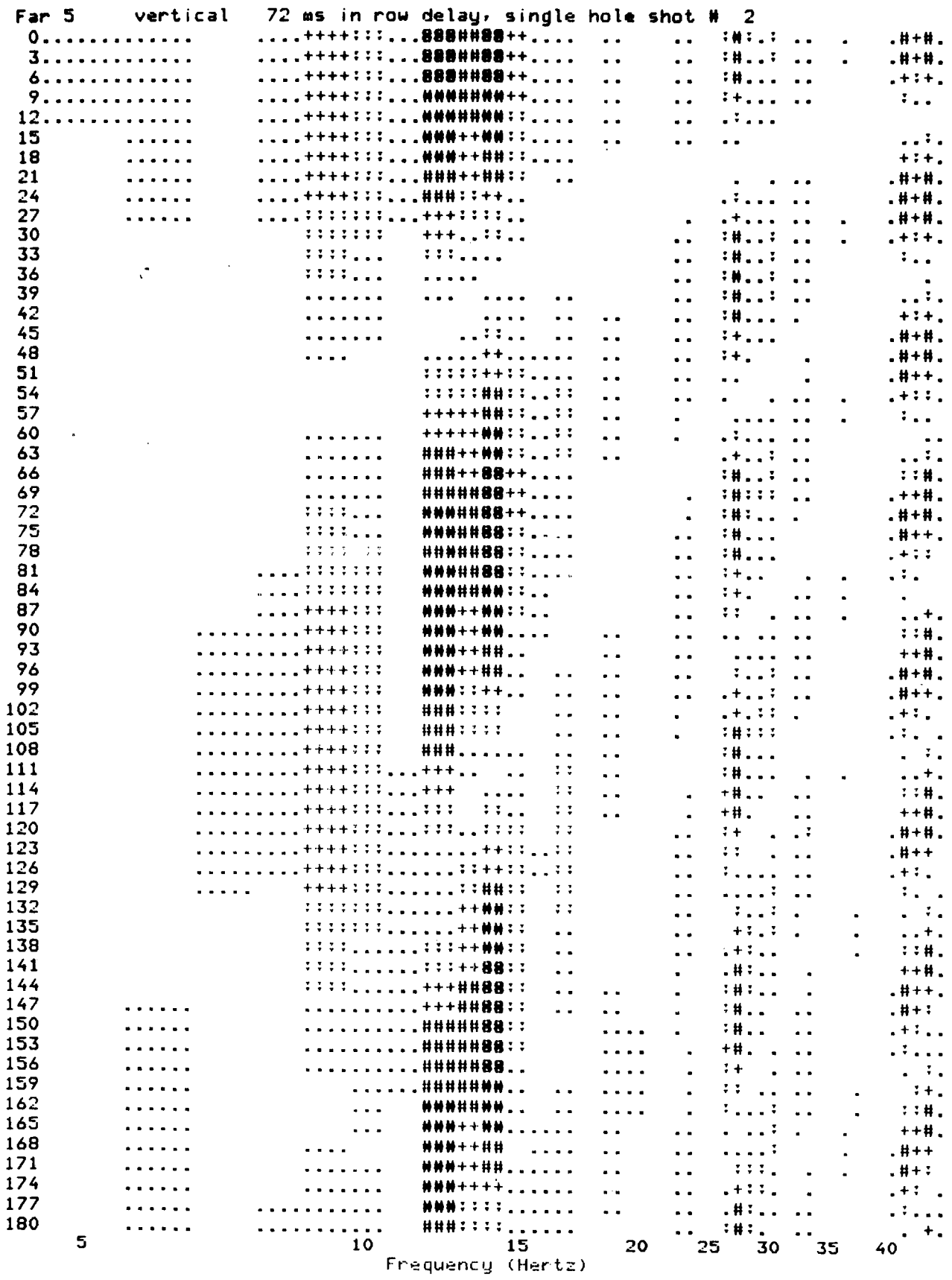

Figure 16. Two-row Fourmap plot generated using 72 ms delay in each four-hole row, from seismogram of Fig. 13a.

6 RESULTS AND DISCUSSION

In this section we will present the results and how they relate to the hypotheses of Section 3. We will first discuss the results of the site characterization and shot performance, as background to the rest of the results. The single-hole shot data will be discussed to show reproducibility. The use of the single-hole shots to design production shot delays will be discussed before the results of the production shots.

6.1 SITE CHARACTERIZATION

6.1.1 Marriottsville

As suspected from field observations, the Wissahickon Schist west of the Marriottsville Quarry is a deeply weathered, low velocity rock (3200-5000 ft/s). These velocities indicate a soft, decomposed and weathered rock. The average thickness of the soil overburden above the schist was approximately 30 ft along the fill road on the west side of the quarry. Along Marriottsville Road, southwest of the quarry, the overburden thickness was less (20 ft) and the velocities measured in the schist were higher (5500-7000 ft/s).

The Wissahickon-Cockeysville contact along the fill road on the west side of the quarry can be recognized as a lateral transition from low-velocity schist (3200-5000 ft/s) to high-velocity marble (9000-12,000 ft/s). A similar contact occurs southwest of the quarry along Marriottsville Road.

On the east side of the quarry, along Marriottsville Road, the near-surface rock velocities are high (13,000 ft/s), indicating the presence of the Hard Setters Formation. The refraction survey lines were run

along the west side of Marriottsville Road, close to the relocated channel of Falls Run. A 5000 ft/s velocity layer in this area may represent the ground water table. Figure 17 shows the thickness of the soil overburden, as well as the compressional wave velocities measured in the soil and upper rock horizons.

The results of the seismic refraction survey were used to predict the predominant frequencies that would be present at each of the recording locations, using the Gupta model discussed earlier. Table 1 lists the results and the frequencies predicted by the model.

No seismic refraction data were available for the seismograph at the wash house because of physical obstructions at that location.

Seismic velocity measurements were also taken on the quarry floor, immediately behind the test bench locations, and are summarized below:

	P-wave velocity (ft/s)	S-wave velocity (ft/s)
Parallel to strike	13,000	7,200
Perpendicular to strike	12,000	6,100

6.1.2 Downingtown

The seismic refraction survey at the Downingtown quarry indicates a 30- to 50-ft-thick overburden layer running east-west across the area where the seismographs were located (see Fig. 8). This is the area that has been mapped as being underlain by the Conestoga Formation. Figure 18 shows the thickness of the overburden.

Figure 17. Overburden thickness at Marriottsville.

TABLE 1

REFRACTION SURVEY RESULTS -- MARRIOTTSVILLE

Location	Soil Thickness (ft)	Soil Velocity (ft/s)	Rock Velocity (ft/s)	Frequency (Hz) Calculated
West Opposite	30	1800	4500	16.3
West Halfway	30	1600	3300	13.3
Lime/Fill	31	1700	5000	14.5
Lime/Marr	12	1700	13400	19.1
	12.5	3750		
Ward's Chapel	15.5	2300	17000	19.0
	35.5	5500		
East Halfway	13	2500	12000	28.3
	20	5500		
East Opposite	9	1100	12000	23.2
	13	5000		

Figure 18. Overburden thickness at Downingtown.

As indicated previously, the Conestoga formation in Chester Valley contains micaceous limestones and phyllites; this composition is reflected in the 4000 to 6000 ft/s rock velocities measured. Immediately adjacent to the quarry, the overburden is shallower (20 to 30 ft) and the rock velocities are higher (7000 to 9000 ft/s). As with the Marriottsville data, the refraction data at Downingtown were used with the Gupta model to predict the frequencies that would appear on the single-hole waveforms. Table 2 shows the results and predicted soil layer frequency.

Seismic measurements were also taken on the quarry bench used for the test blasting. The velocities measured were:

	P-wave velocity (ft/s)	S-wave velocity (ft/s)
North side, parallel to strike	5150	3700
South side, parallel to strike	8250	----
Perpendicular to strike	5900	3600

TABLE 2

REFRACTION SURVEY RESULTS — DOWNINGTOWN

Location	Soil Thickness (ft)	Soil Velocity (ft/s)	Rock Velocity (ft/s)	Frequency (Hz) Calculated
Close-1	37	1600	7500	11.0
Close-2	42	1200	4800	7.4
Close-3	30	1500	7000	12.7
Far-1	39	1800	6600	11.9
Far-2	41	1300	9300	8.0
Far-3	45	2000	4700	12.2
Far-4	51	1600	4300	8.5
Far-5	34	1500	8000	11.2

6.2 SHOT PERFORMANCE

We will now discuss the shot performance results to avoid confusing the discussion of the effects of delay changes. As will be seen, firing times were close to the nominal in all but two shots. The actually measured times were used for determining predictability. Detonation velocity was essentially constant at each location, except for one shot at Marriottsville.

6.2.1 Firing Times

As discussed earlier, a high-speed camera was used to obtain surface firing times by counting the number of frames from zero time up to and including the first frame where the flash of the tell tale is seen. The surface firing times of the Marriottsville and Downingtown multi-hole tests are given in Tables 3 and 4, respectively. The actual firing times were determined by subtracting the detonation times of the explosive column and the tell tale through the stemming from the surface firing time.

For example, hole #1 in the fifth production shot at Marriottsville quarry was programmed to fire at 25 ms after zero time. From the high-speed film, the surface flash of the tell tale in that hole was seen 29.2 ms after zero time. The 32-ft-long explosive column would detonate in 1.7 ms, using an average VOD of 19,2000 ft/s. The tell tale, with a VOD of 6,000 ft/s, would take 2.2 ms to shoot through the 13 ft of stemming in the hole before it could be seen by the high-speed camera. Therefore, to calculate an accurate detonation time for this borehole, we subtracted 3.9 ms from the surface firing time and got 25.3 ms. Corrected detonation times for all shots are also found in Tables 3 and 4.

TABLE 3

FIRING TIMES OF MARRIOTTSVILLE TEST BLASTS

Shot	Hole	Programmed Time (ms)	Surface Time (ms)	Firing Time (ms)
P1	1	25	28.8	25.1
P1	2	59	63.1	59.4
P1	3	93	97.1	93.4
P1	4	127	131.7	128.0
P1	5	110	114.2	110.5
P1	6	144	148.9	145.2
P1	7	178	182.9	179.2
P1	8	212	-- (a)	212 (b)
P2	1	25	29.6	25.9
P2	2	42	46.2	42.5
P2	3	59	-- (a)	59 (b)
P2	4	76	81.0	77.3
P2	5	90	95.4	91.7
P2	6	107	112.7	109.0
P2	7	124	130.0	126.3
P2	8	141	147.1	143.4
P3	1	25	29.3	25.4
P3	2	76	79.4	75.5
P3	3	127	129.8	125.9
P3	4	178	180.7	176.8
P3	5	137	140.0	136.1
P3	6	188	191.3	187.4
P3	7	239	241.0	237.1
P3	8	290	292.5	288.6
P4	1	25	30.0	25.2
P4	2	98	101.5	97.6
P4	3	171	174.7	170.7
P4	4	244	247.7	243.8
P4	5	160	163.3	159.4
P4	6	233	236.1	232.2
P4	7	306	309.0	305.1
P4	8	379	382.4	378.5
P5	1	25	29.2	25.3
P5	2	76	79.8	75.9
P5	3	127	129.9	125.8
P5	4	178	181.5	177.6
P5	5	160	163.1	159.2
P5	6	211	215.7	211.8
P5	7	262	265.8	261.9
P5	8	313	316.3	312.4

(a) No flashes were recorded
(b) The detonation time is assumed to equal the nominal

TABLE 4

FIRING TIMES OF DOWNINGTOWN TEST BLASTS

Shot	Hole	Programmed Time (ms)	Surface Time (ms)	Firing Time (ms)
P1	1	25	29.7	24.9
P1	2	61	64.6	59.8
P1	3	97	101.3	96.5
P1	4	133	138.1	133.3
P1	5	124	128.1	123.3
P1	6	160	165.2	160.4
P1	7	196	200.3	195.5
P1	8	232	236.3	231.5
P2	1	25	30.3	25.5
P2	2	97	100.6	95.8
P2	3	169	172.4	167.6
P2	4	241	-- (a)	241.0 (b)
P2	5	106	109.9	105.1
P2	6	178	181.6	176.8
P2	7	250	348.2	343.4 (c)
P2	8	322	419.9	415.1 (c)
P3	1	25	29.6	24.8
P3	2	97	99.6	94.8
P3	3	169	171.3	166.5
P3	4	241	243.4	238.6
P3	5	178	180.7	175.9
P3	6	250	252.4	247.6
P3	7	322	323.5	318.7
P3	8	394	394.3	389.5
P4	1	25	30.5	25.7
P4	2	61	65.9	61.1
P4	3	97	102.2	97.4
P4	4	133	137.9	133.1
P4	5	160	165.9	161.1
P4	6	196	201.3	196.5
P4	7	232	237.1	232.3
P4	8	268	273.5	268.7
P5	1	25	28.8	24.0
P5	2	47	47.0	42.2
P5	3	61	65.8	61.0
P5	4	79	-- (a)	79.0 (b)
P5	5	160	166.2	161.4
P5	6	178	184.1	179.3
P5	7	196	--	350.0 (c)
P5	8	214	410.2	405.4 (c)

(a) Indicates that no flashes were recorded
(b) Indicates that the detonation time is assumed to equal the nominal
(c) Indicates that the hole was fired by the back-up cap

For some holes, no surface flashes were seen in the high-speed films. If the first motion around the top of these boreholes was noted, and they appeared to fire in proper sequence with the rest of the shot, the nominal firing time of the hole was used for further work. However, in two cases, timing inaccuracies were documented.

In Downingtown production shots 2 and 5, the last two holes to fire did so at least 100 milliseconds later than designed. Firing times recorded for the last holes of these shots indicate that they were fired by the back-up delay caps which, for safety reasons, were initiated before the first explosive column detonated. The most plausible explanation for the failure of the seismic caps is that the cap wires to the seventh hole in each shot were broken, probably by settling of the explosive column as surrounding holes fired, causing the blasting machine to stop firing upon sensing an open circuit. In all cases, the measured firing times were used for subsequent data reduction rather than the programmed firing times, except when no surface flashes were recorded at a given hole.

6.2.2 Detonation Velocity

The explosive detonation velocities obtained in the tests are shown in Tables 5 and 6. In each test, only the first hole to fire was probed to get velocity data. The scatter seen in these data are attributed mostly to variations in the experimental techniques rather than to the performance of the bulk explosive that we used. The largest single source of error came from our method of locating the pin probes in the explosive column. Given the precision of the measuring tapes used in loading the blast holes in our tests and the plasticity of the bulk explosive, the locations of the pin probes in the explosive column were likely to vary

TABLE 5

DETONATION VELOCITIES — MARRIOTTSVILLE

Shot No.	Probe Spacing (ft)	Δ T (ms)	VOD (ft/s)
S1	20	1.05	19,050
S2	20	incomplete record	
P1	20	1.03	19,420
P2	19.5	1.10	17,730
P3	20	1.03	19,510
P4	19.5	0.99	19,750
P5	20	1.01	19,800

average detonation velocity: 19,200 $\pm$ 800 ft/s

TABLE 6

DETONATION VELOCITIES — DOWNINGTOWN

Shot No.	Probe Spacing (ft)	Δ T (ms)	VOD (ft/s)
S1	20	0.95	21,050
S2	20	0.98	20,510
P1	20	0.98	20,510
P2	20	1.00	20,000

average detonation velocity: 20,500 $\pm$ 500 ft/s

about 0.5 ft for each probe, giving a possible location error of ± 1 ft for the set of the probes. For the 20 ft pin-probe spacing we used, this error translates to a possible error of about 5%, corresponding to about 1000 ft/s variation in detonation velocity simply due to pin-probe location errors.

Given the scatter induced by measurement techniques, the detonation velocity of the explosive was constant for all tests except for the second production blast at Marriottsville quarry. As a result, the detonation velocities were averaged together for each site to give a representative velocity that was used in reducing the firing time data and correlated with the strain gage data. Note that the higher detonation velocities measured at Downingtown correspond to an increase in borehole size from 6 in at Marriottsville to 8 in at Downingtown. The detonation velocities measured in our tests agree with the product specifications for the Tovex Extra®. The lower velocity measured for the second Marriottsville production blast (P2) correlates with a lower explosive loading density noted for the test. Shot P2 had approximately 13% less explosive than the other shots at Marriottsville. This difference is believed to be due to excessive water in the boreholes which, despite our precautions, was not completely displaced during loading.

6.3 SINGLE-HOLE TESTS

6.3.1 Vibration

6.3.1.1 Reproducibility

The ground vibration data from the single-hole shots were compared to assess reproducibility. This was a test of the first hypothesis.

Waveforms from the first single-hole shot were plotted adjacent to the waveforms from the second single-hole shot to allow a visual judgment of the match. Figure 19 shows this type of comparison for several of the recordings.

As can be seen, the waveforms produced at each location from the first single-hole were nearly identical to the waveforms produced by the second single-hole. The instantaneous vector sum particle velocities for the single-hole test blasts at Marriottsville and Downingtown can be compared in Tables 7 and 8. The Marriottsville data indicate that the single-hole peak particle velocities are very reproducible at all locations. At Downingtown, the close locations show some substantial differences, while the far location values are quite comparable. Note that at Downingtown the single-hole shots were separated by about 100 ft, and the second shot was detonated partially in a mud seam.

Detailed comparisons of power spectra for the single-hole shots at one location at each quarry (Lime/Marr. at Marriottsville and Far 5 at Downingtown) are shown in Fig. 20. Note the striking similarity between the power spectra for the two single-hole shots at each location.

It can be seen that the comparisons between the two single-holes at Marriottsville are in closer agreement than those at Downingtown. Because of the quarry bench configuration, the single-hole blasts at Downingtown were separated by approximately 100 feet so that the first single-hole shot at Downingtown was in the "harder" rock to the south, while the second single-hole was in the "softer" rock to the north. A deeply weathered clay seam was also in the area of the second single-

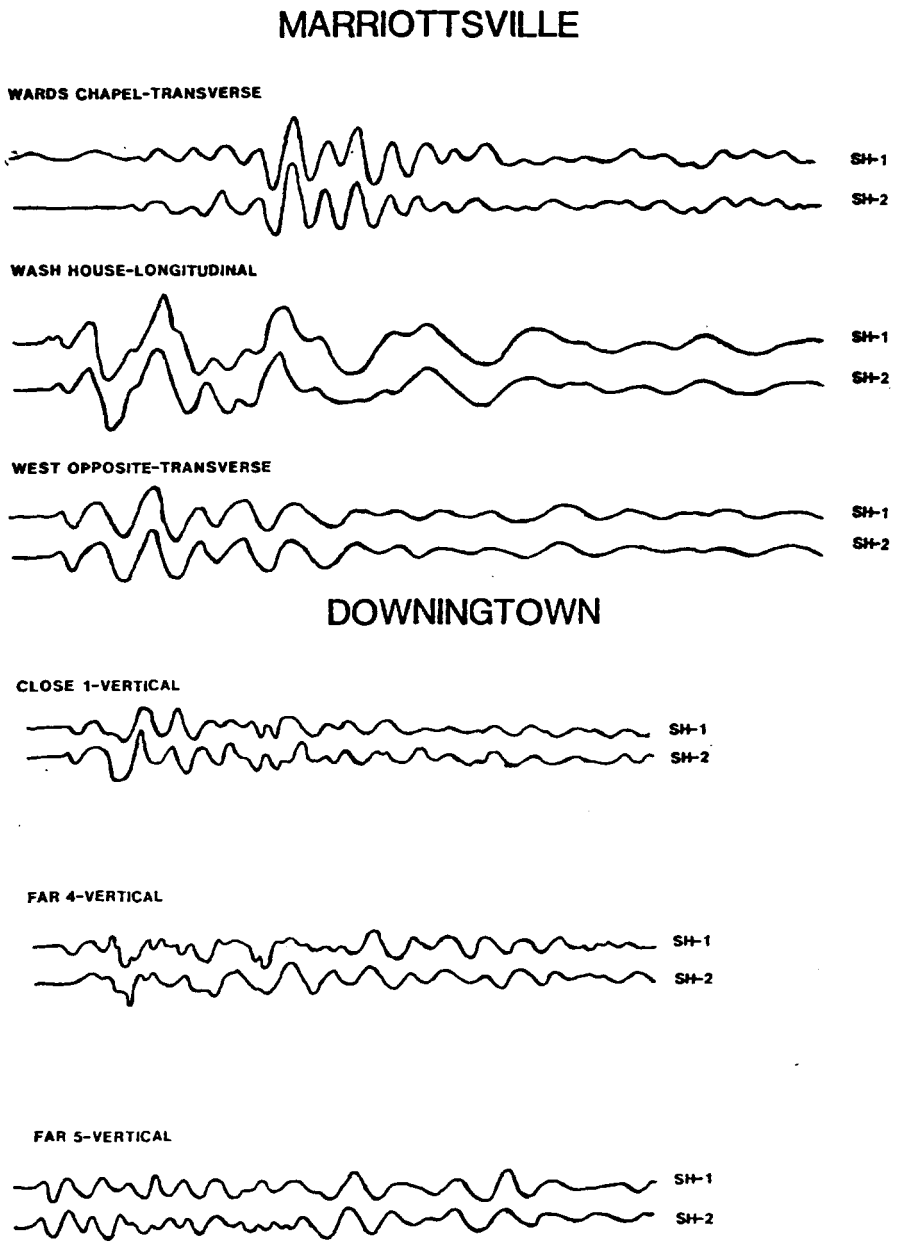

Figure 19. Two single-hole waveforms from three locations at each quarry. Note the reproducibility of the waveforms.

TABLE 7

PEAK PARTICLE VELOCITY (INSTANTANEOUS VECTOR SUM) - IN./S

MARRIOTTSVILLE QUARRY

Seismograph Location	SH1	SH2	(SH1/SH2)
West Opposite	0.36	0.31	1.16
West Halfway	0.26	0.23	1.13
Lime/Fill	0.40	0.49	0.82
Lime/Marr.	0.19	0.15	1.27
Ward's Chapel	0.09	0.11	0.82
Wash House	0.09	0.11	0.82
East Halfway	0.34	0.32	1.06
East Opposite	0.48	0.52	0.92
		Mean	1.00
		Standard Dev.	0.17

TABLE 8

PEAK PARTICLE VELOCITY (INSTANTANEOUS VECTOR SUM) - IN./S

DOWNINGTOWN QUARRY

Seismograph Location	SH1	SH2	(SH1/SH2)
Close 1	0.10	0.13	0.77
Close 2	0.15	0.27	0.56
Close 3	0.25	0.34	0.74
Far 2	0.11	0.11	1.00
Far 3	0.08	0.10	0.80
Far 4	0.12	0.13	0.92
Far 5	0.16	0.12	1.33
		Mean	0.87
		Standard Dev.	0.23

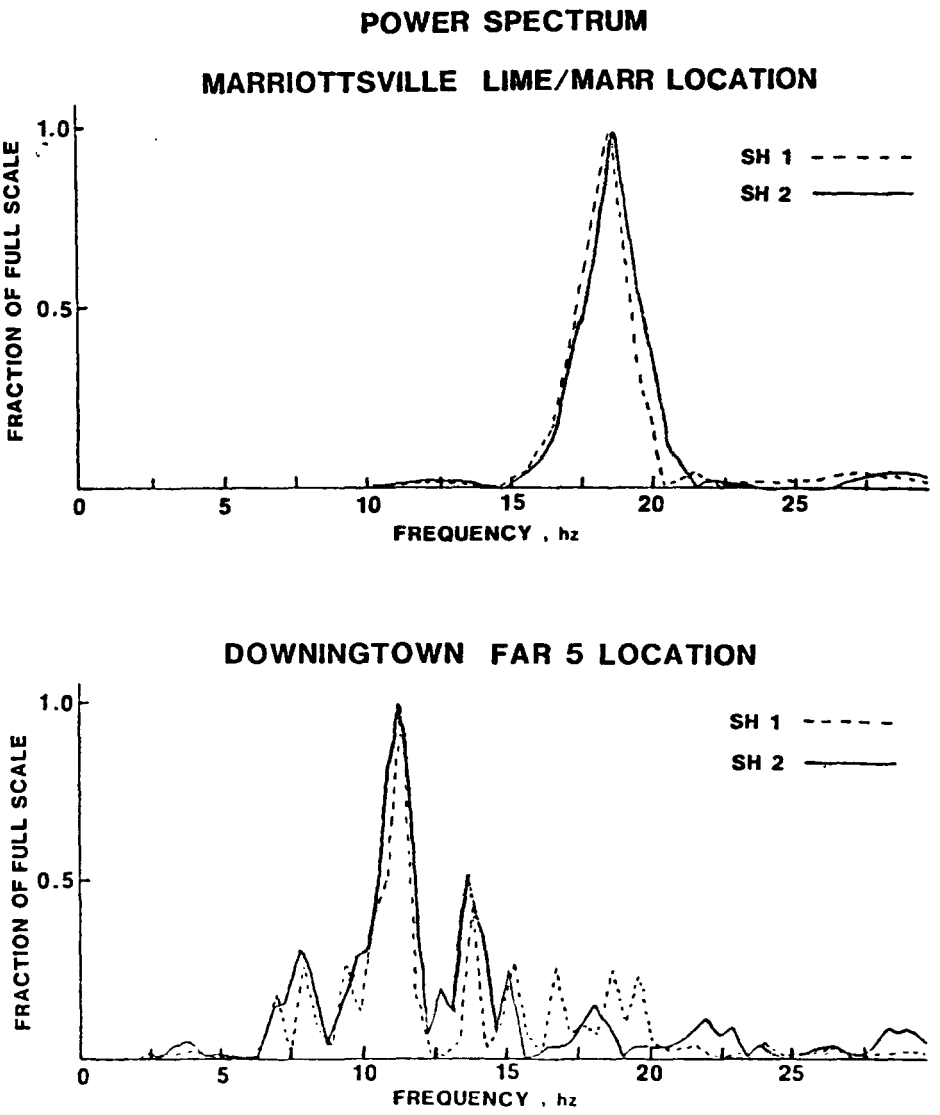

Figure 20. Power spectra from single-hole shots at both quarries. Note the similarity of spectra at each site.

hole. One of the objectives of the Downingtown testing was to determine what effect this variation in the test-bench geology would have on the resulting ground vibrations. The results showed that local geology had a greater effect on the vibration levels at the close seismograph locations than at the far locations.

Response spectra for the single-hole tests, calculated for single degree-of-freedom systems having 5% critical damping over a frequency range from 3 to 50 Hz, were compared. The response spectra plots for the two single-hole shots (Figs. 21 and 22) at each of the seismograph locations at the Marriottsville and Downingtown quarries show the reproducibility of the single-hole shots. The results clearly show that single-hole blasts with constant blast design parameters will generate reproducible waveforms at a given seismometer location. We will next discuss how these waveforms are related to the local geology.

6.3.1.2 Comparison with the Gupta Model

The observed resonant vibration frequencies, discussed in Section 6.1, were compared with those predicted by the Gupta model, using the geologic information gathered from the seismic refraction surveys. The results of these comparisons are shown in Tables 9 and 10 for Marriottsville and Downingtown, respectively. Figures 23 and 24 are plots of the single-hole power spectra at Marriottsville and Downingtown, respectively. Peaks at the resonant frequencies predicted by the Gupta model are highlighted on these plots. Resonant vibrations with high amplitudes were found at frequencies which correspond to the frequencies calculated from the model. Although vibration at other frequencies was observed, the

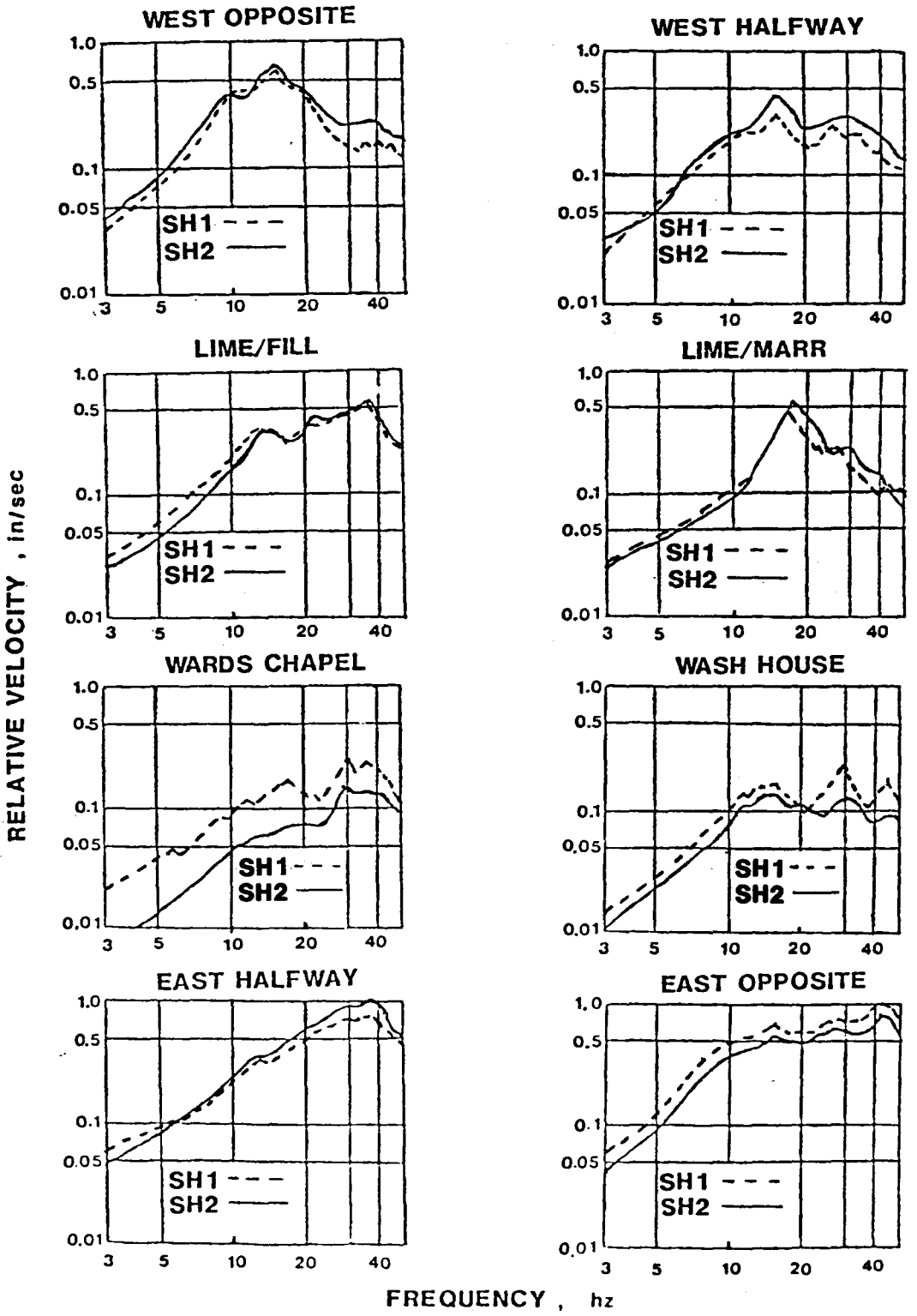

Figure 21. Response spectra from single-hole shots at Marriottsville.

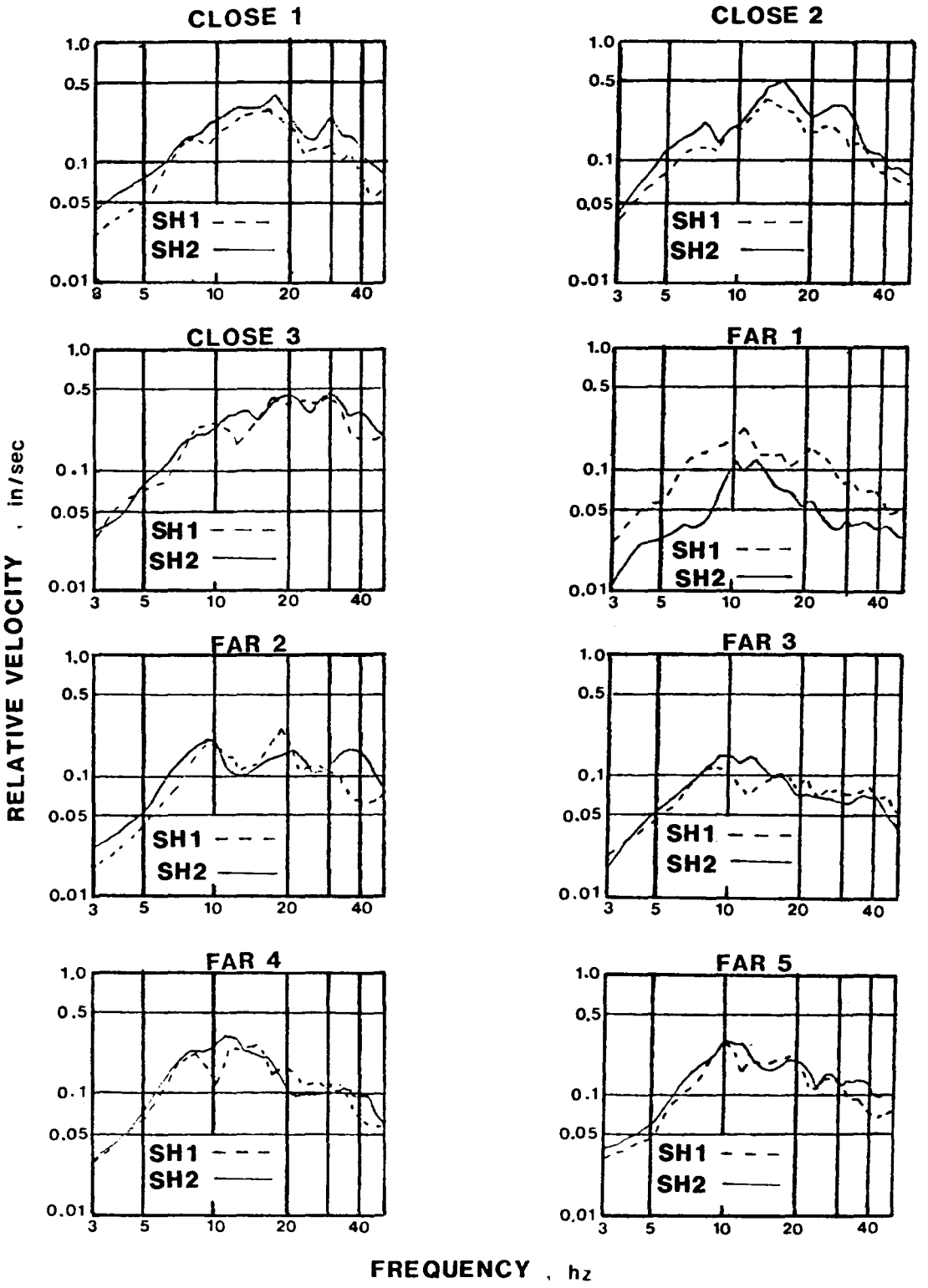

Figure 22. Response spectra from single-hole shots at Downingtown.

TABLE 9

COMPARISON OF PREDICTED AND OBSERVED RESONANT VIBRATION FREQUENCIES

MARRIOTTSVILLE

Location	Frequency (Hz) Calculated	Observed
West Opposite	16.3	16.5
West Halfway	13.3	12.8
Lime/Fill	14.5	14.0
Lime/Marr.	19.1	18.5
Ward's Chanel	19.0	18.0
East Halfway	28.3	29.0
East Opposite	23.2	23.5

TABLE 10

COMPARISON OF PREDICTED AND OBSERVED RESONANT VIBRATION FREQUENCIES

DOWNINGTOWN

Location	Frequency (Hz) Calculated	Observed
Close 1	11.0	10.0
Close 2	7.4	7.5
Close 3	12.7	12.0
Far 1	11.9	11.5
Far 2	8.0	8.75
Far 3	12.2	11.75
Far 4	8.5	8.5
Far 5	11.2	11.0

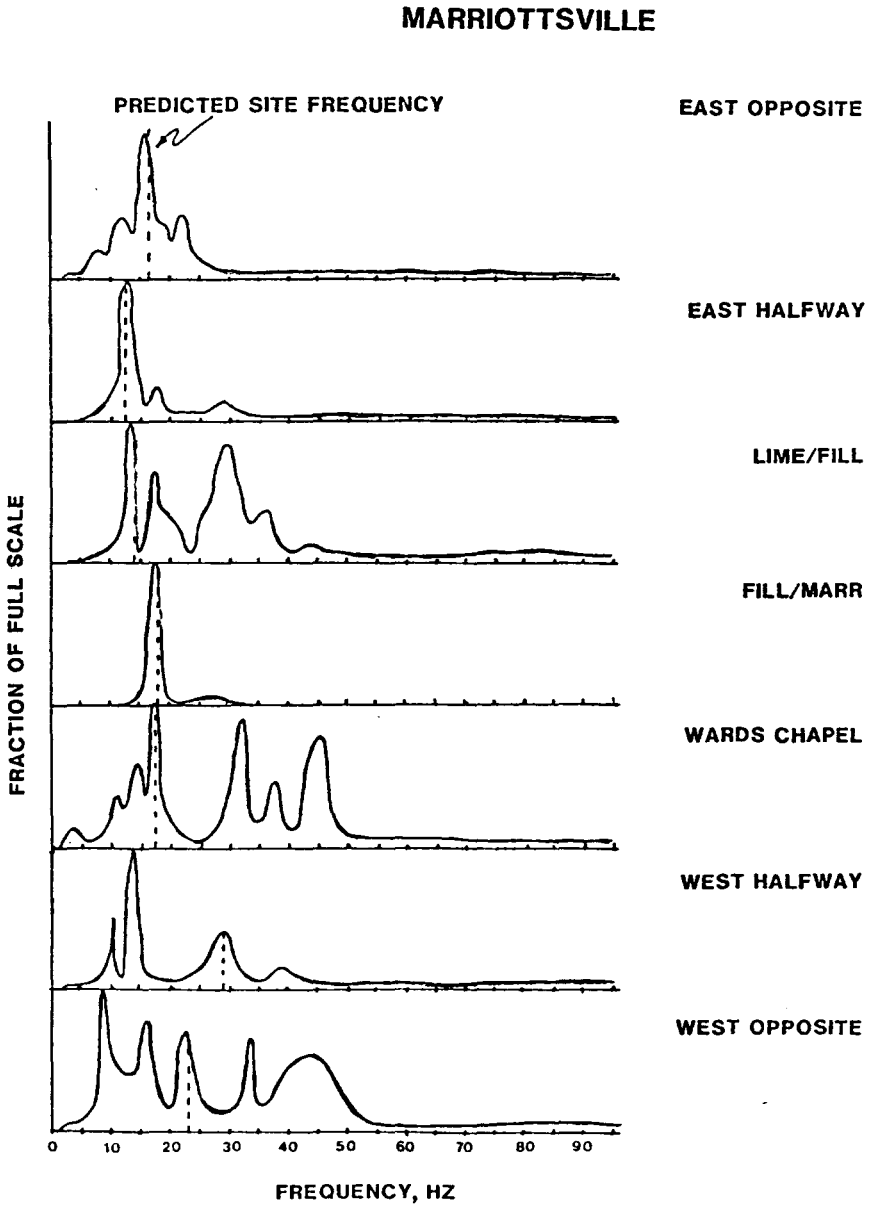

Figure 23. Single-hole power spectra, Marriottsville. Predicted resonant frequency highlighted.

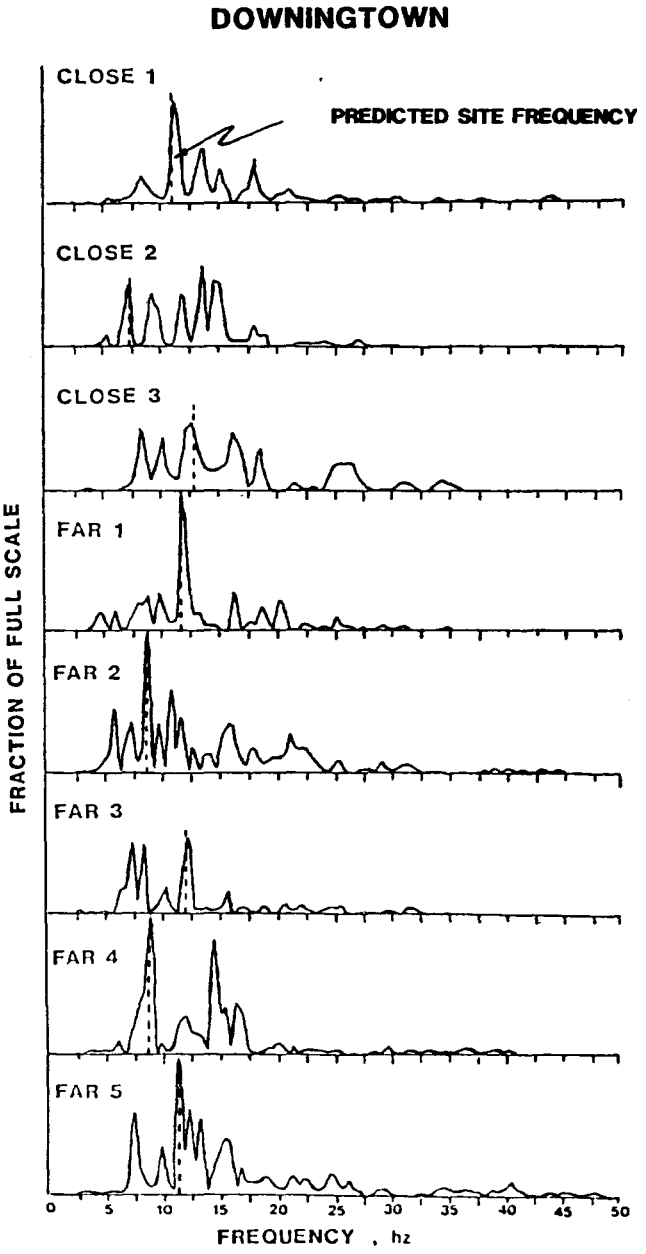

Figure 24. Single-hole power spectra, Downingtown. Predicted resonant frequency highlighted.

consistency of the observations indicate that the Gupta model has been reconfirmed at these two sites.

6.3.2 Strain Waves

Although we will emphasize the common features apparent from all of the strain-gage records, it must be emphasized that each record observed thus far is somewhat different from each of the others in detail. Two factors are likely to explain this difference. The bonding of the gage to the borehole may be variable from test to test. We try to ensure that all of the gages have the same surface characteristics and the grout has cured. A more likely cause for the variation is that the rock through which the strain waves pass from explosive hole to gage is not the same from test to test. We know from observation of the face that fracture densities vary from test to test, and this certainly is observed. At present we have not related these effects systematically.

In order to determine the principal-strain time-histories, all six strain components must be collected. Of the 14 strain gage records at Marriottsville, 8 had all six components active for significant portions of the shot: two of these are for the second single-hole shot, and two were for production shot 2 (17 ms between holes, 65 ms between rows). Of the 10 strain gage records obtained at Downingtown, only 3 had all six components active. We will focus on the Marriottsville records for the single-hole shot and production shot 2 because the most important conclusions can be drawn from those shots for which the most complete data are available.

The single-hole strain records obtained in this test series are similar to those observed in granite in the work discussed earlier (Anderson, et al., 1984). Figure 25 shows the principal-strain time-history from a gage located 5 ft from the explosive borehole and at the same distance from the free-face. It should be noted that the distances of the gage from both the borehole and the free-face are substantially shorter in this shot than in production shots.

Even with the variability from record to record, certain common features are apparent in all of the records. The three traces correspond to maximum compressive strain, which is downward pulse on the figure, and the minimum and intermediate principal strains. In strain time-histories the minimum strain is always very close to a mirror image of the maximum strain, with a lower amplitude. We interpret this to be the Poisson expansion of the gage due to the compression. The intermediate strain has a somewhat different character, which is apparently important in determining the shear strains, discussed later. Because the gage is located quite close to the hole, and the detonation of the column takes approximately 2 ms, the individual phases are not separated.

The features that we noted in the granite study are present in this record. First, there is an impulsive wave with a rise-time of the order of 100 microseconds (Note: absolute rise times are probably shorter than those observed in the records due to data smoothing routines). A secondary pulse, best observed on the intermediate principal strain record, is probably associated with the arrival of the shear wave. A broad pulse which begins about 6 ms after the first arrival, and which has a pulse-width of about 14 ms, may be related to the reflections from

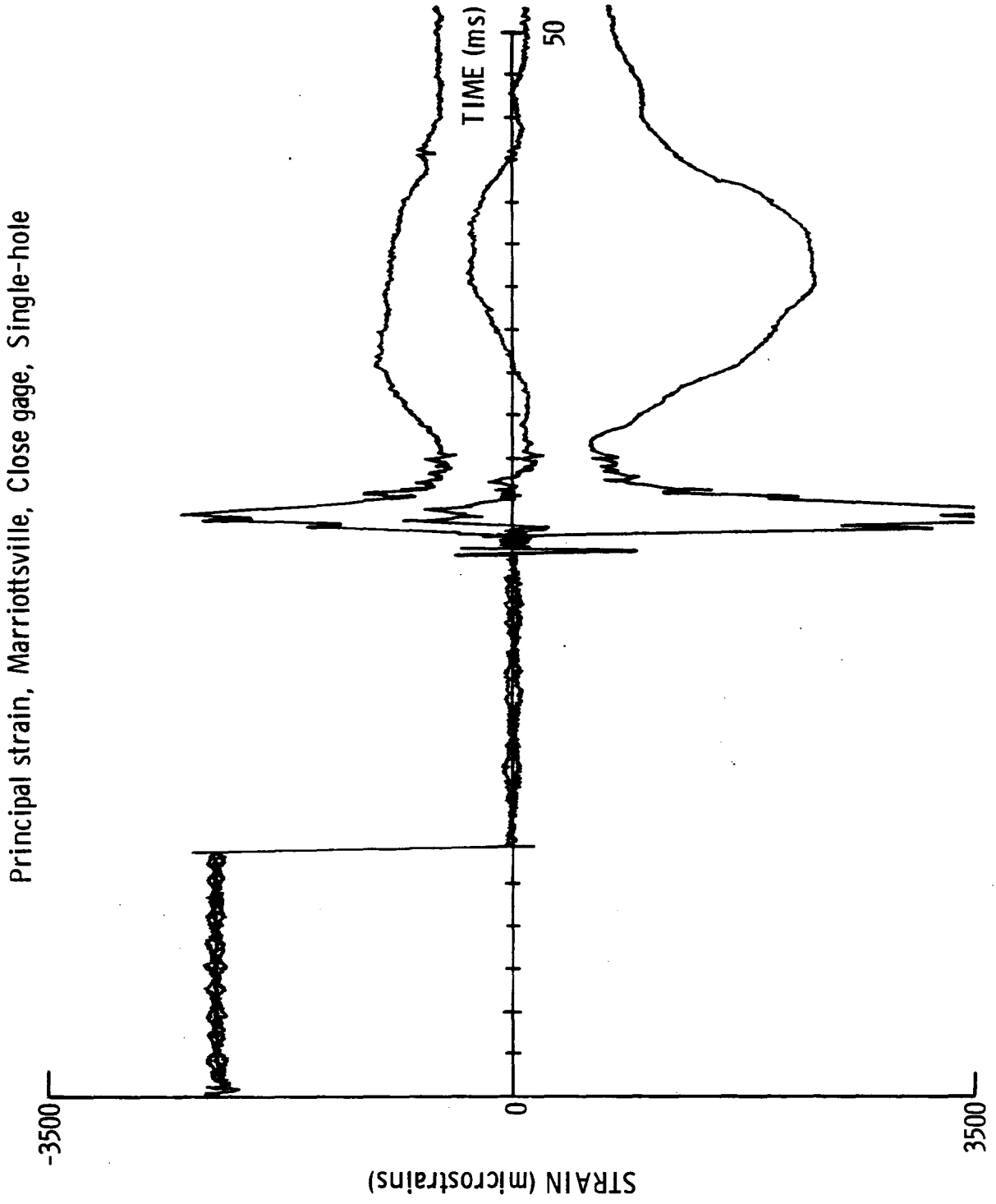

Figure 25. Principal-strain time-history for single-hole shots at Marriottsville. Compressive strain is downwards. "Boxcar" at left is zero-time pulse. Note sharp pulse of short duration, followed by broader pulse. See text for discussion.

the free-face and the bench top, as discussed in detail in Anderson, et al. (1984); however, the width and late arrival of the pulse are consistent with the strain being caused by gas pressurization of new or existing cracks near the gage. This point will be discussed in more detail later, in Section 6.5.2.

The octahedral-shear-strain time-history for this record is shown in Fig. 26. The shape of this plot is quite similar to that of the principal-strain time-history. This would indicate that the predominant shear strains acting upon the gage are simply the distortional part of a compressional pulse. In the work in granite (Anderson, et al., 1984), some shear strain not associated with the compressional pulse was observed. The reasons for this difference are not known; however, the most likely explanation is that some differences in rock type or structure were responsible.

6.3.3 Fragmentation -- Reproducibility

Figure 27 shows the size distributions determined for the two single-hole blasts at Marriottsville quarry. The two distributions are similar except in the coarsest fractions. This difference is due to the presence of one piece of oversize that falls in the 4-foot screen fraction in shot S2. S1 had no fragments of rock in that fraction. If the one piece of oversize is removed from the fragment file of shot S2 and the size distributions are recalculated and plotted (Fig. 28) the closeness of fit between the two distribution curves is quite good. This suggests two things -- our measurement techniques are valid and the blasting tests are reproducible. This comparison also shows that

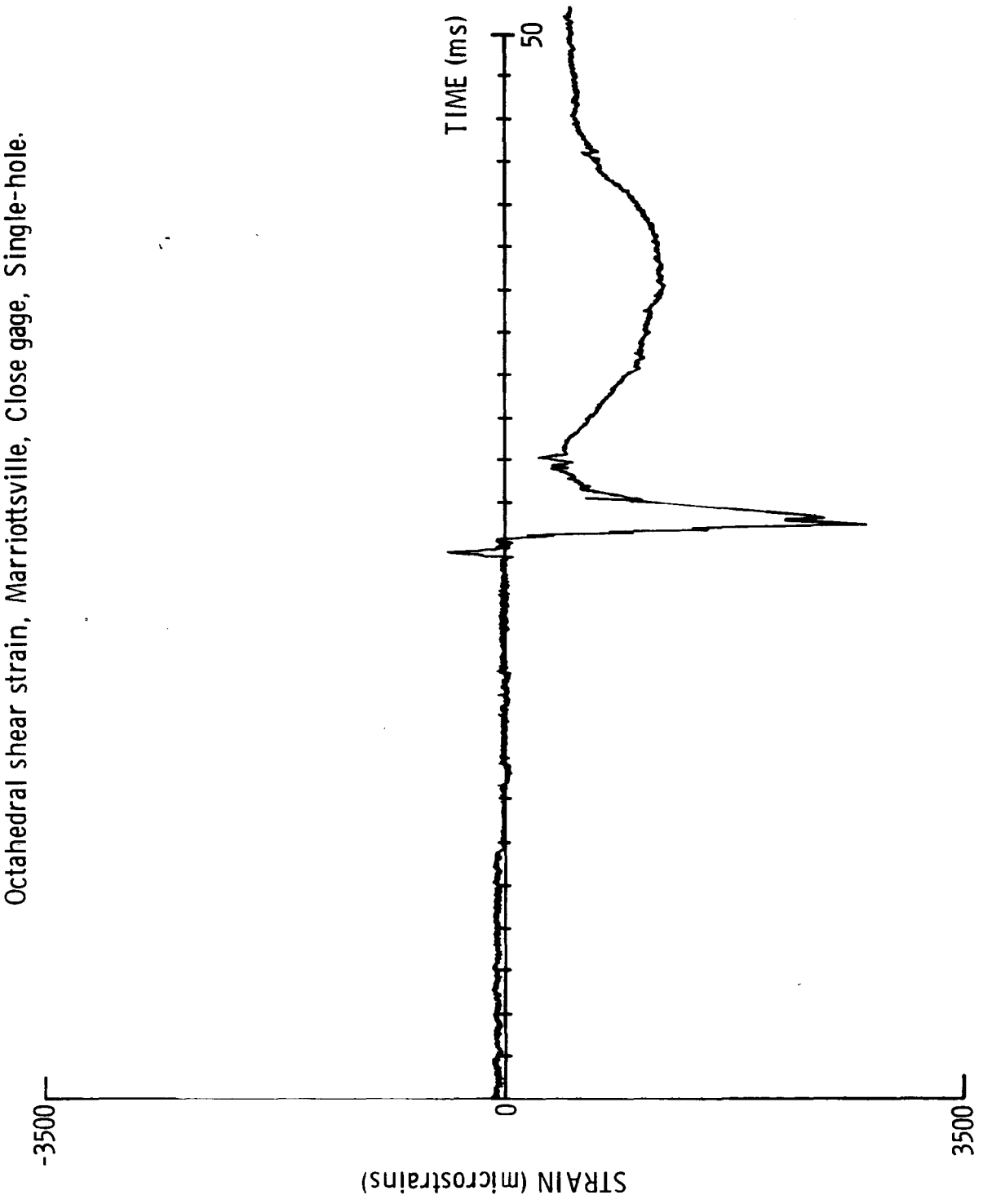

Figure 26. Octahedral-shear-strain time-history calculated from principal strains in Fig. 25.

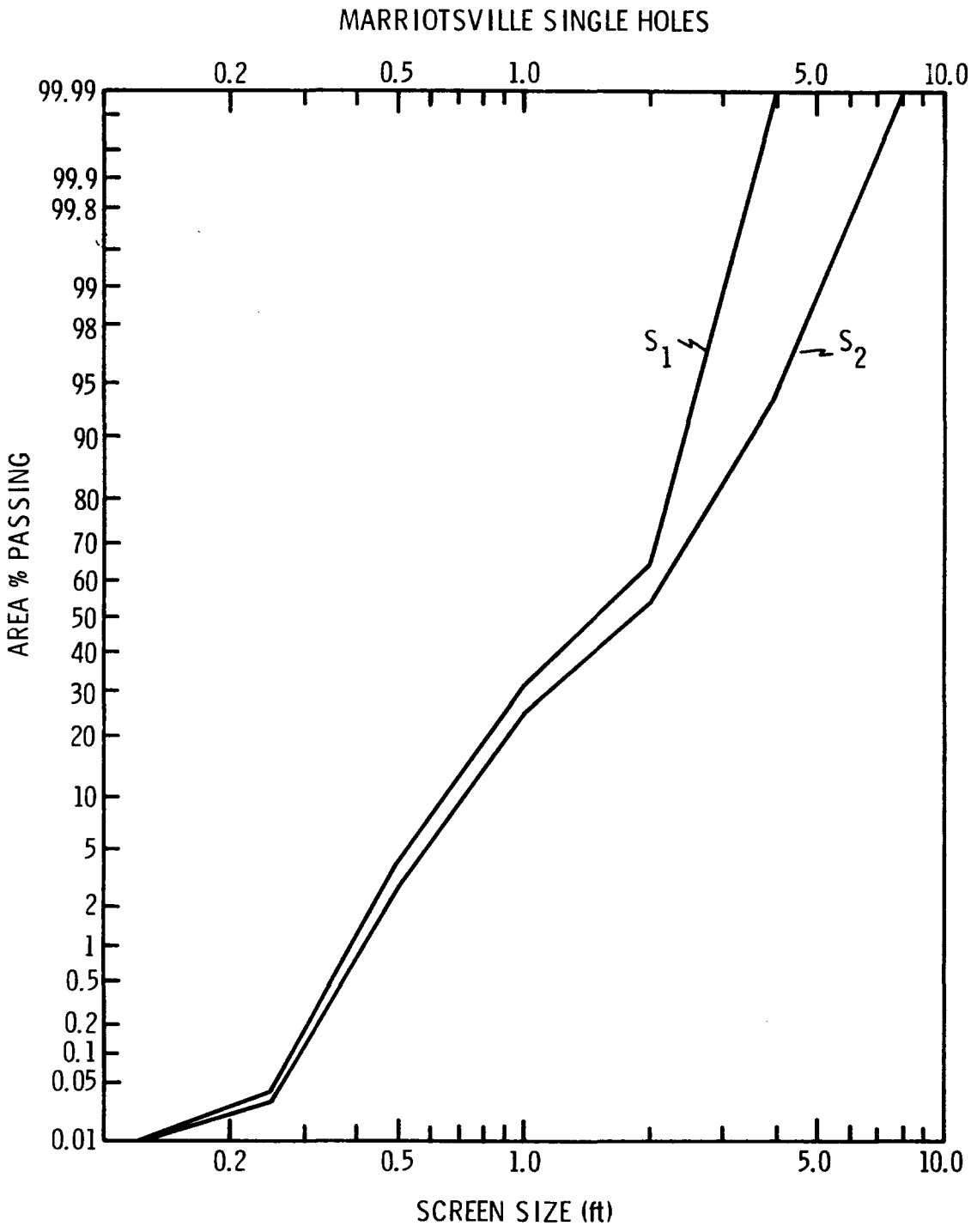

Figure 27. Size distribution calculated from high-speed films for single-hole shots at Marriottsville.

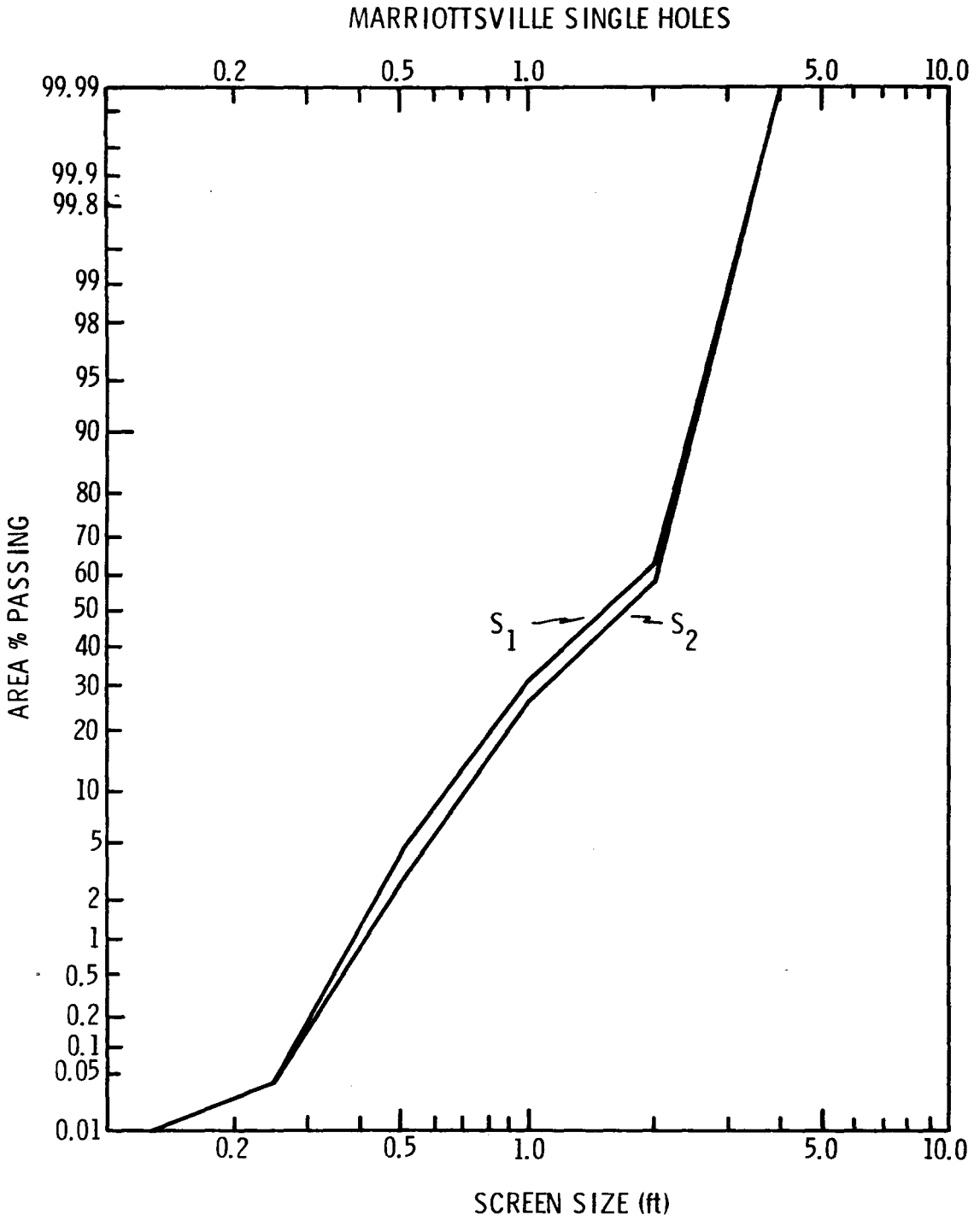

Figure 28. Size distribution as in Fig. 27 with one piece of oversize removed from fragment file of shot S2.

the presence of even small numbers of oversize fragments can greatly skew the fragment size distributions.

As stated previously, the shots at Downingtown were of two types: those in competent rock and those in more weathered rock. Shots in the weathered portions produced a lot of dust, obscuring the face and compromising the high-speed camera recording of face fragmentation. Subsequent data analyses of those films proved virtually impossible. We decided not to digitize the first single-hole test nor production shots P-1 and P-3 at Downingtown (raw data for the shots is on file at the Twin Cities Research Center of the U.S. Bureau of Mines). Therefore, comparisons of the two single-hole shots are not presented here.

6.4 DELAY DESIGN GENERATION

The results of the single-hole shots were generally reproducible. Therefore, they were used to select the firing times for the five production test blasts to be detonated at each of the quarries. Precise timing was to be obtained using a ten-circuit programmable sequential blasting machine with seismic blasting caps. Since one circuit was needed to fire the zero time signal and one was needed to fire the backup standard electric delay caps, test blasts of eight holes each were planned. Each production test blast was to consist of 2 rows of 4 holes. It was planned to use the delay interval between holes in a row primarily to study fragmentation effects, and the delay interval between rows to study vibration effects.

6.4.1 Fragmentation

Delays to be chosen on the basis of fragmentation were to correspond as closely as possible to relief of 1, 2, 3, and 4 ms/ft, as per the studies

of Winzer, et al. (1983). At Marriottsville, with spacing of 17 ft, the nominal delays would then be 17, 34, 51, and 68 ms between holes in a row. At Downingtown, with spacing of 18 ft, the nominal delays would be 18, 36, 54, and 72 ms between holes in a row. Deviations from this basic scheme will be discussed in the next section.

6.4.2 Vibration

The study was also designed to determine if delay patterns could be used to modify vibration based on constructive or destructive interference of summed single-hole waveforms. Since the single-hole waveforms were shown to be reproducible, dependent upon the site geology, we then chose delay intervals to test the hypothesis regarding predictability by linear superposition.

As discussed earlier, the two methods chosen to select delay times to enhance or minimize the low-frequency motion were the autocorrelation function and the Fourmap routine.

The autocorrelation function was used to determine time shifting of single-hole waveforms where constructive or destructive interference would occur. Constructive interference will take place at time shifts with the largest positive correlation values, and destructive interference at time shifts with the largest negative correlation.

The Fourmap method was also used to determine delay times and to determine which frequencies would be selected for either constructive or destructive interference. Although Fourmap plots for all three components at each seismograph location were generated for each single-hole shot, we will only present vertical-component composite Fourmap plots

for each delay sequence, since a total of 432 plots were generated. The composite plots average the response for all of the seismograph locations. Those which had the strongest low-frequency vibration dominated the composite plots.

Autocorrelation and Fourmap calculations were first performed for the single-row shots, to determine appropriate between-hole delay times for constructive and destructive interference, consistent with the delay times chosen for fragmentation. Delay between rows was then generally chosen to augment the desired interference caused by the between-hole delay. Delay sequences for each quarry will be discussed separately.

6.4.2.1 Marriottsville

Autocorrelation and Fourmap calculations were first performed to determine the appropriate four-hole single-row delay times. The results of the autocorrelation calculations are shown in Table 11. On this and the following tables, the delays corresponding to maximum and minimum autocorrelation values are shown for both single-hole shots. Generally the delays are quite similar. Constructive interference, resulting in maximum vibration, is obtained for delays with the maximum autocorrelation values. Conversely, destructive interference, resulting in minimum vibration, is obtained for delays with the minimum autocorrelation values.

A single-row Fourmap plot for the vertical component is shown as Fig. 29. In some cases, different patterns were observed for the different components; however, at Marriottsville all three components have similar Fourmap plots. Resonance is observed most strongly at 8-10 Hz and 15-17 Hz. The range of delays for constructive interference in the

TABLE 11

MARRIOTTSVILLE QUARRY — TIME SHIFTS FOR MAXIMUM AND MINIMUM

SINGLE-HOLE AUTOCORRELATION VALUES

	Maximum		Minimum	
Location	S.H. 1 (ms)	S.H. 2 (ms)	S.H. 1 (ms)	S.H. 2 (ms)
West Opposite	55	55	27	28
	133	130	98	99
West Halfway	73	75	34	37
	161	166	118	120
Lime-Fill	30	33	17	18
	58	66	41	46
	--	--	73	81
Lime-Marr.	61	66	31	31
	120	126	93	94
Ward's Chapel	131	136	18	17
	--	--	45	--
Wash House	120	121	38	39
	--	--	171	171
East Halfway	29	29	17	16
	47	47	35	34
	89	92	58	56

Figure 29. Single-row composite Fourmap plot, vertical component, Marriottsville.

15-17 Hz range is from about 50 to 80 ms between holes. These values are consistent with the autocorrelation results at most locations.

Two times were then selected for constructive interference, corresponding to the two long-relief times for fragmentation of 51 and 73 ms. This second time is a bit longer than the time of 68 ms indicated for 4 ms/ft relief, but we decided to use the vertical component as the primary criterion for choosing delays, and 73 was thus chosen. The other two delay times used, 17 and 34 ms, were consistent with destructive interference for most of the shots, particularly in the 15-17 Hz range. The 17-ms delay does show some possible constructive interference at about 8 Hz. We decided to stick with this time as a destructive interference time, and use the between-row delays to further decrease the possible vibration.

Tables 12 and 13 show the between time shifts for destructive interference for four holes at 17 and 34 ms between holes, respectively. Figure 30 is the corresponding Fourmap plot for 17 ms, and Fig. 31 is the Fourmap plot for 34 ms.

The Fourmap plot for the 17-ms between hole delay shows a minimum at a delay of about 65 ms between rows, with some constructive interference at 18 Hz. However, from the single-row plot, constructive interference at 8 not 18 Hz was a possible problem, so this time appears appropriate. The time of 65 ms is consistent with the results of the autocorrelation.

The Fourmap plot for 34 ms shows a minimum at about 85 ms. The only substantial constructive interference on this plot is at 25 to 35 Hz, and the 85-ms delay was chosen to minimize this interference. This time is also consistent with the autocorrelation. We chose not to use the

TABLE 12

MARRIOTTSVILLE QUARRY - TIME SHIFTS FOR DESTRUCTIVE INTERFERENCE

FOR 4 HOLES @ 17 MS SYNTHETIC SEISMOGRAM

Location	Time Shifts (ms)			
West Opposite	28	68	150	
West Halfway	44	133		
Lime/Fill	27	44	68	125
Lime/Marriottsville	29	77	135	
Ward's Chapel	64	203		
Wash House	63	188		
East Halfway	43	67	150	
East Opposite	66	161		

TABLE 13

MARRIOTTSVILLE QUARRY -- TIME SHIFTS FOR DESTRUCTIVE INTERFERENCE

FOR 4 HOLES @ 34 MS SYNTHETIC SEISMOGRAM

Location	Time Shifts (ms)			
West Opposite	21	57	94	138
West Halfway	18	58	87	122
Lime/Fill	17	50	85	118
Lime/Marriottsville	20	47	85	142
Ward's Chapel	16	49	82	148
Wash House	19	53	89	128
East Halfway	17	51	85	118
East Opposite	17	53	90	132

Figure 30. Two-row Fourmap plot, 17 ms between rows, vertical component, Marriottsville.

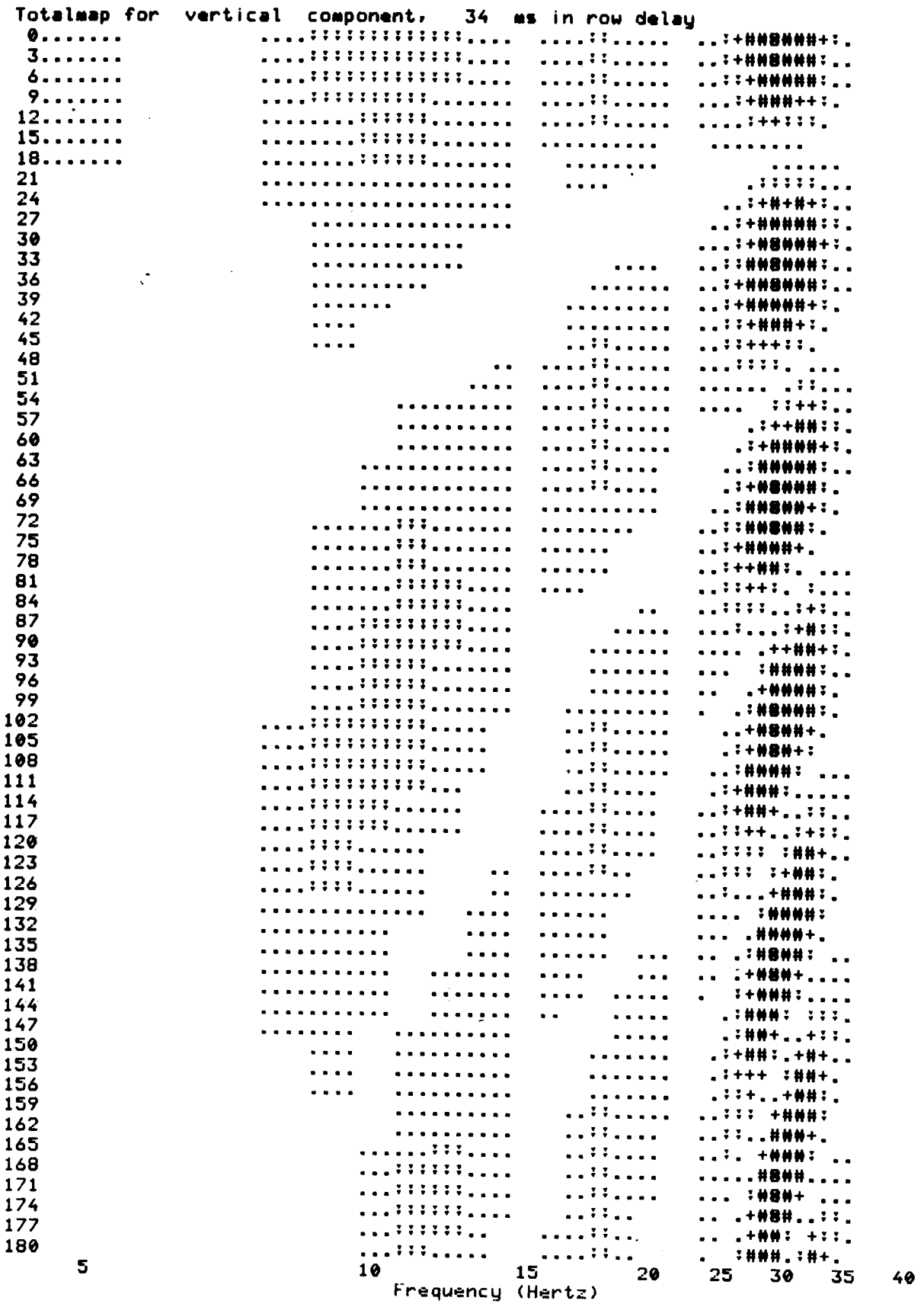

Figure 31. Two-row Fourmap plot, 34 ms between rows, vertical component, Marriottsville.

delays of 50 or 120 because we wanted to keep the ratio of between-hole and between-row relief fairly constant. As we discussed earlier, such effects are not yet understood.

Tables 14 and 15 show the time shifts for constructive interference for four holes at 51 and 73 ms between holes, respectively. Figure 32 is the corresponding Fourmap plot for 51 ms, and Fig. 33 is the Fourmap plot for 73 ms.

The Fourmap plots for 51 ms show a maximum at about 102 ms, consistent with the results of the autocorrelation. A between-row delay time of 110 ms was selected instead of 102 ms in order to maintain a minimum of 9 ms between delay intervals on the eight-hole blast, thus keeping the "pounds per delay" constant for the test series. The "eight-millisecond criterion" is widely used as a means for reducing vibration. We did not want to confuse the hypotheses we were testing with the verification of this criterion. It may be noted on the Fourmap plots that the predicted amplitudes for 102 and 110 ms differ only slightly. Again, we did not choose the other possible ranges of delay times around 51 or 170 ms to keep the relief ratio fairly constant.

The Fourmap plots for 73 ms show a maximum at about 146 ms, consistent with the autocorrelation plots. We chose a time of 135 ms, again to keep the pounds per delay constant.

The last production blast at Marriottsville used a 51 ms between-hole delay time; the blast with this delay appeared to have the best fragmen tation and diggability, according to the quarry operating personnel. A between-row delay interval of 135 ms was selected from the Fourmap plot to minimize adverse vibrations, and to improve move-out from the face.

TABLE 14

MARRIOTTSVILLE QUARRY — TIME SHIFTS FOR CONSTRUCTIVE INTERFERENCE

FOR 4 HOLES @ 51 MS SYNTHETIC SEISMOGRAM

Location	Time Shifts (ms)	
West Opposite	102	204
West Halfway	102	204
Lime/Fill	102	204
Lime/Marriottsville	102	204
Ward's Chapel	102	204
Wash House	102	204
East Halfway	102	204
East Opposite	102	204

TABLE 15

MARRIOTTSVILLE QUARRY - TIME SHIFTS FOR CONSTRUCTIVE INTERFERENCE

FOR 4 HOLES @ 73 MS SYNTHETIC SEISMOGRAM

Location	Time Shifts (ms)	
West Opposite	146	293
West Halfway	146	293
Lime/Fill	146	293
Lime/Marriottsville	146	293
Ward's Chapel	146	293
Wash House	146	293
East Halfway	146	293
East Opposite	146	293

Figure 32. Two-row Fourmap plot, 51 ms between rows, vertical component, Marriottsville.

Figure 33. Two-row Fourmap plot, 73 ms between rows, vertical component, Marriottsville.

The delay patterns used for the Marriottsville test blasting are summarized in Table 16 and in Fig. 34.

6.4.2.2 Downingtown

At Downingtown it was decided to test the effects of local quarry-bench geology on the ground vibration produced from blasting. As described earlier in this report, the north half of the test bench was more deeply weathered and had lower seismic wave velocities than the southern half. The test plan was to detonate two identical blasts — one located on the north side of the test bench and the other on the south side — each having destructive interference delay times. The same procedure would be followed for two identical blasts with constructive delay times.

As with Marriottsville, autocorrelation and Fourmap calculations were first performed to determine the appropriate four-hole single-row delay times. The results of the autocorrelation calculations are shown in Table 17. The single-row Fourmap plot for the vertical component is shown as Fig. 35. Somewhat different patterns were observed for the three components; however, the same general trend was observed, i.e., destructive interference at short delays and constructive interference at longer delays. Resonance is observed most strongly in the range from 8-20 Hz. The range of delays for constructive interference is then above about 50 ms between holes. These values are consistent with the autocorrelation results at most locations.

Only one between-hole delay time was then selected for constructive interference, corresponding to the long-relief time for fragmentation of

TABLE 16

DELAY INTERVALS FOR MARRIOTTSVILLE

MULTI-HOLE TEST BLASTS

Shot No.	Between-Hole Delay (ms)	Between-Hole Relief (ms/ft)	Between-Row Delay (ms)	Between-Row Relief (ms/ft)	Remarks
1	34	2.0	85	5.7	Destructive
2	17	1.0	65	4.3	Destructive
3	51	3.0	112	7.5	Constructive
4	73	4.3	135	9.0	Constructive
5	51	3.0	135	9.0	Best fragmentation with destructive

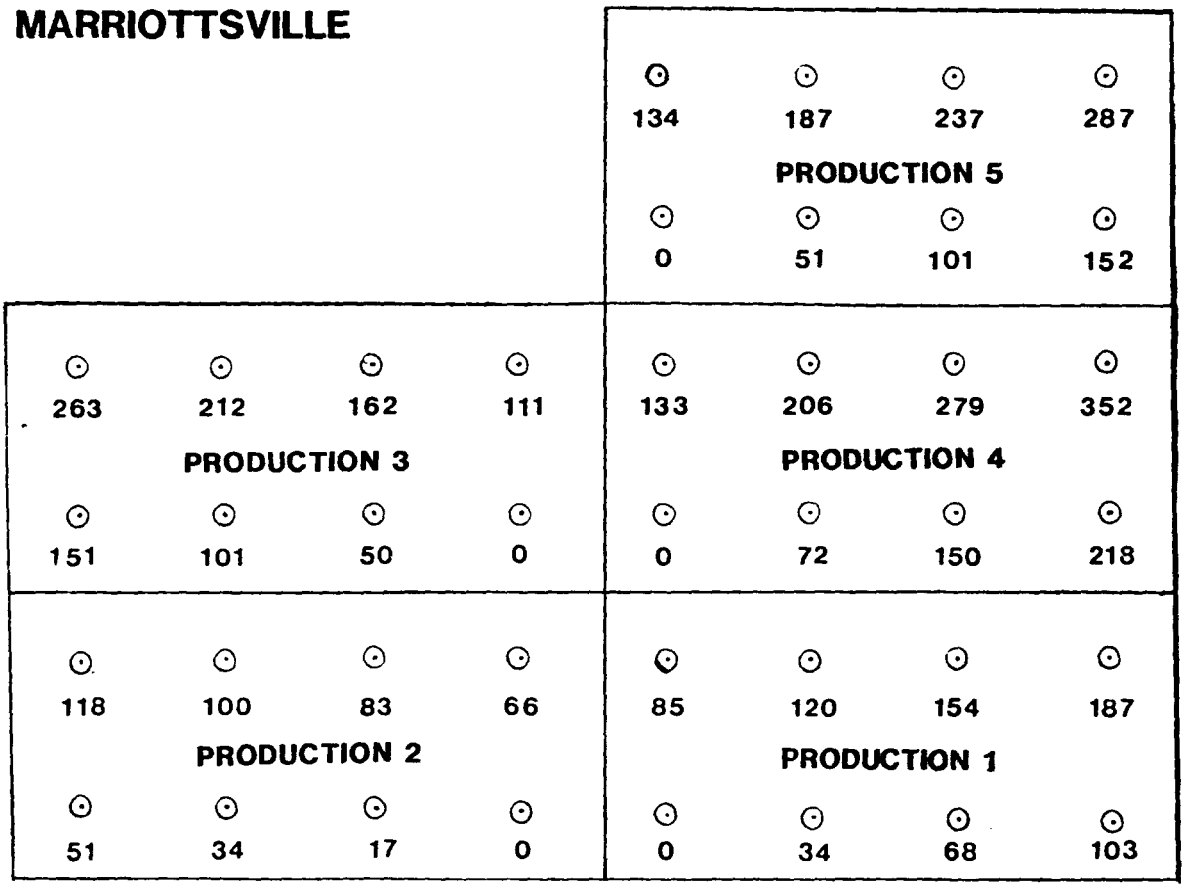

Figure 34. Delay patterns used at Marriottsville.

TABLE 17

DOWNINGTOWN QUARRY — TIME SHIFTS FOR MAXIMUM AND MINIMUM

SINGLE-HOLE AUTOCORRELATION VALUES

Location	Maximum		Minimum	
Time shifts	S.H. 1 (ms)	S.H. 2 (ms)	S.H. 1 (ms)	S.H. 2 (ms)
Close 1	102	116	38	40
	174	206	142	156
Close 2	76	78	36	38
	144	144	108	112
Close 3	120	34	38	40
	238	70	142	156
Far 1	96	—	44	—
	200	—	140	—
Far 2	110	124	38	68
	188	240	168	178
Far 3	108	108	48	48
	182	186	146	152
Far 4	78	82	40	40
	142	146	104	110
Far 5	90	100	40	44
	202	174	142	144

Figure 35. Single-row Fourmap plot, vertical component, Downingtown.

72 ms. A short delay time, 36 ms, was consistent with destructive interference for most of the shots. These times then correspond to relief of 4 and 2 ms/ft, respectively.

Tables 18 and 19 show the between-row time shifts for constructive interference at 72 ms and destructive interference at 36 ms, respectively. Figure 36 is the corresponding Fourmap plot for 72 ms and Fig. 37. is the Fourmap plot for 36 ms.

The Fourmap plot for 72 ms shows a maximum at about 144 ms, consistent with the autocorrelation plots. We chose a time of 153 ms, again to keep the pounds per delay constant.

The autocorrelation for 36 ms show a minimum at about 144 ms. A time of 135 ms was chosen from the Fourmap plots to keep the pounds per delay constant. As with the destructive interference shots at Marriottsville, the only substantial constructive interference on the Fourmap plots is at 25 to 35 Hz, and the between-row delay provides destructive interference.

For the fifth production blast at Downingtown, it was decided to attempt to generate a low-frequency signal by firing a short time between holes (18 ms) and a relatively long time between rows (136 ms). Eighteen milliseconds would be short enough to minimize destructive interference for low frequencies generated by adjacent holes, while the 136-ms time was intended to cause constructive low-frequency interference between rows. The Downingtown delay times are in Table 20 and Fig. 38.

TABLE 18

DOWNINGTOWN QUARRY - TIME SHIFTS FOR CONSTRUCTIVE INTERFERENCE

FOR 4 HOLES @ 72 MS SYNTHETIC SEISMOGRAM

Location	Time Shifts (ms)		
Close 1	72	143	215
Close 2	72	144	216
Close 3	72	144	217
Far 1	74	145	214
Far 2	72	144	218
Far 3	72	144	216
Far 4	72	144	216
Far 5	72	144	216

TABLE 19

DOWNINGTOWN QUARRY -- TIME SHIFTS FOR DESTRUCTIVE INTERFERENCE

FOR 4 HOLES @ 36 MS SYNTHETIC SEISMOGRAM

Location	Time Shifts (ms)			
Close 1	20	54	88	152
Close 2	22	54	92	134
Close 3	20	54	94	140
Far 1	20	56	94	142
Far 2	18	54	90	122
Far 3	20	56	92	144
Far 4	20	54	86	128
Far 5	22	52	86	144

Figure 36. Two-row Fourmap plot, 72 ms between rows, vertical component, Downingtown.

Figure 37. Two-row Fourmap plot, 36 ms between rows, vertical component, Downingtown.

TABLE 20

DELAY INTERVALS FOR DOWNINGTOWN

MULTI-HOLE TEST BLASTS

Shot No.	Between-Hole Delay (ms)	Between-Hole Relief (ms/ft)	Between-Row Delay (ms)	Between-Row Relief (ms/ft)	Remarks
1	36	2.0	135	7.5	Destructive - North
2	72	4.0	153	8.5	Constructive - South
3	72	4.0	153	8.5	Constructive - North
4	36	4.0	135	7.5	Destructive - South
5	18	1.0	136	7.5	Low Frequency - South

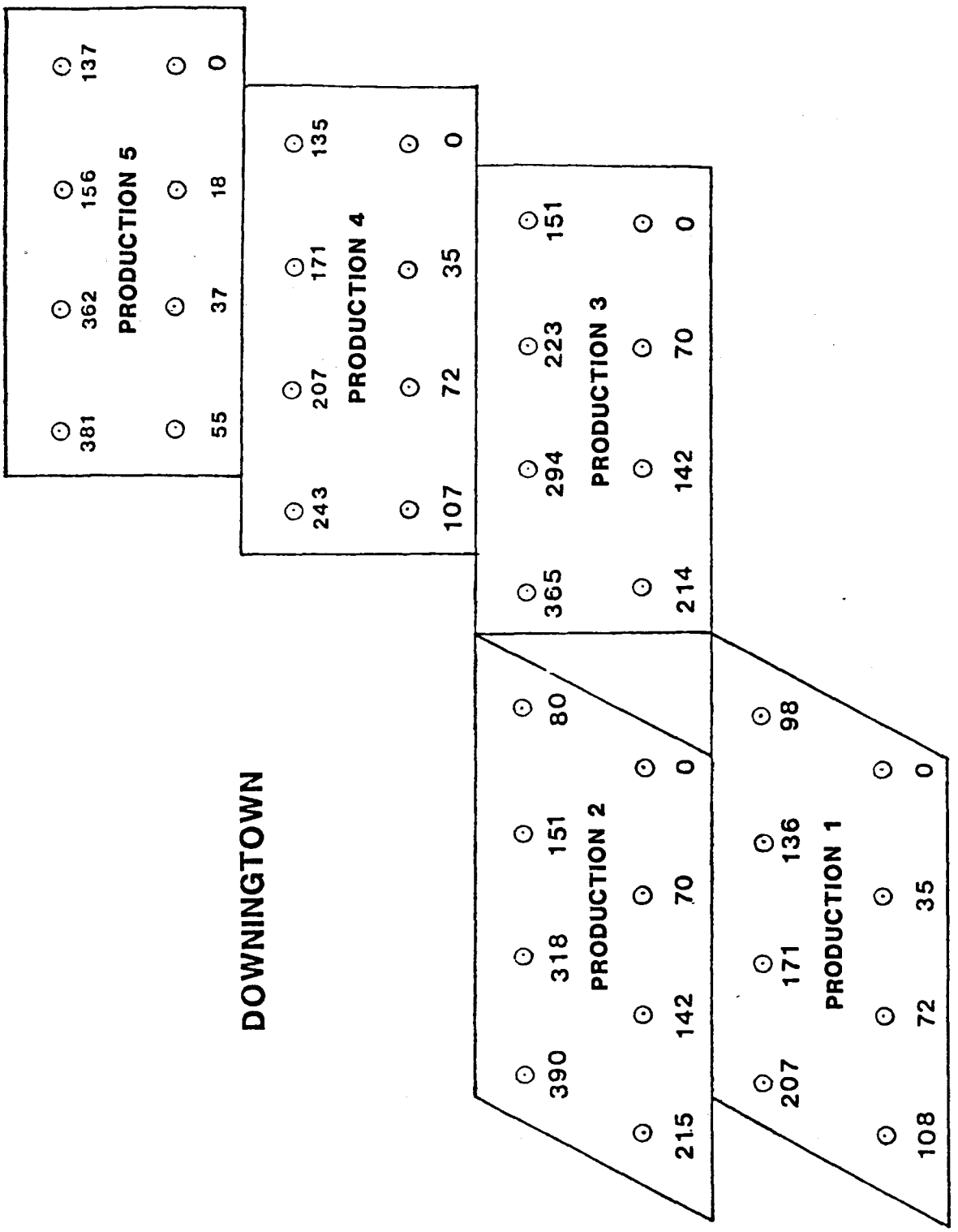

Figure 38. Delay pattern used at Downingtown.

6.5 PRODUCTION TESTS

6.5.1 Vibration

6.5.1.1 Predictability

Although we discuss the effect of delay design on vibration in more detail in the next section, Figs. 39 and 40, for Marriottsville and Downingtown, respectively, show comparisons of the measured and predicted response spectra. The predicted response spectra are calculated using time-lagged linear superposition of the single-hole waveforms, with the times used for the calculations being those actually observed. As noted earlier, there were two deviations from the nominal times at Downingtown.

As can be seen, the measured and predicted compare quite well at both locations. This effect is apparent at all locations. The hypothesis regarding the predictability of the vibration is therefore confirmed. There are some slight deviations of the observed from the predicted. The implications of these deviations will be discussed with respect to fragmentation efficiency in a later section.

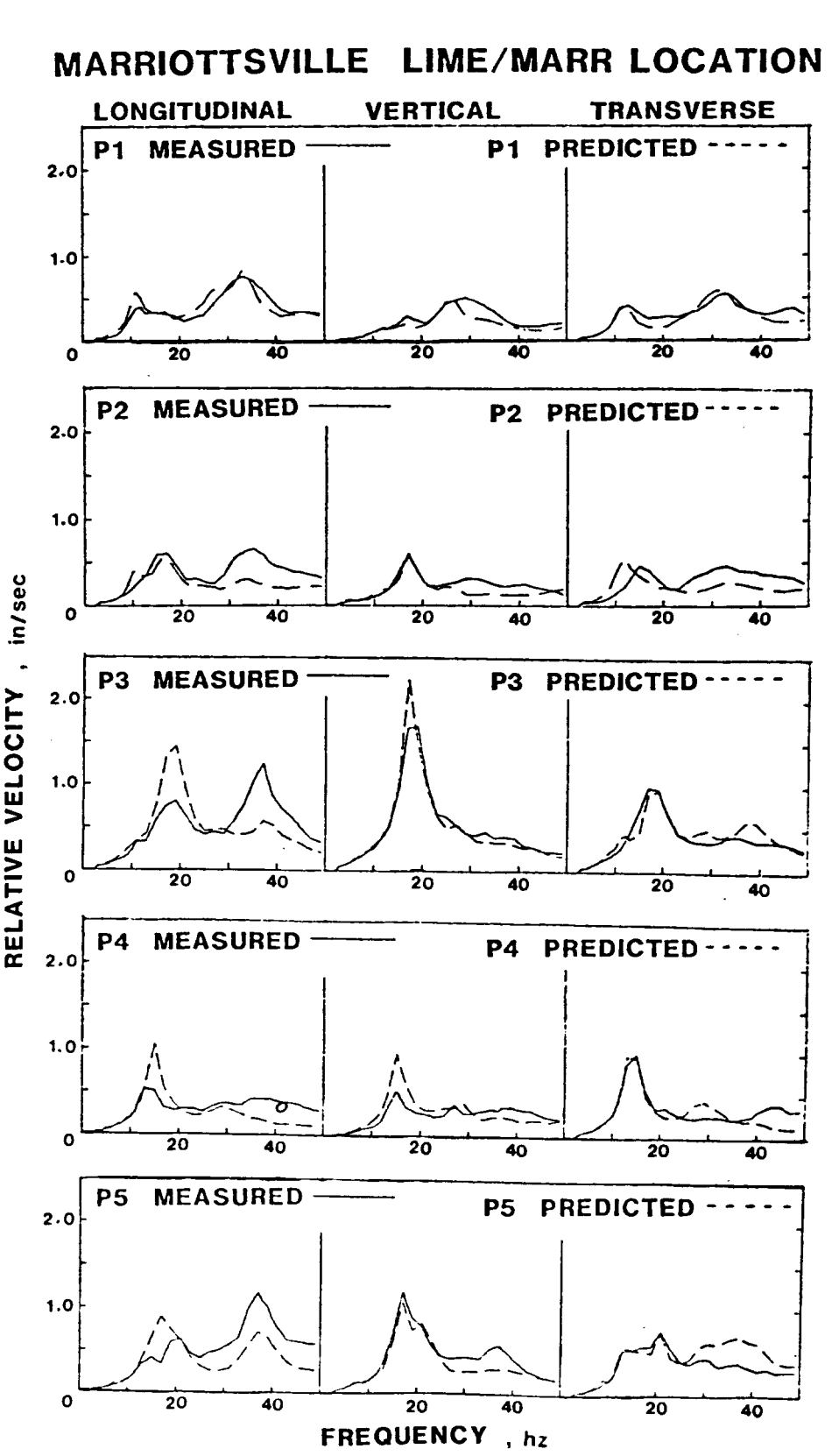

Figure 39. Predicted and measured response spectra, Marriottsville.

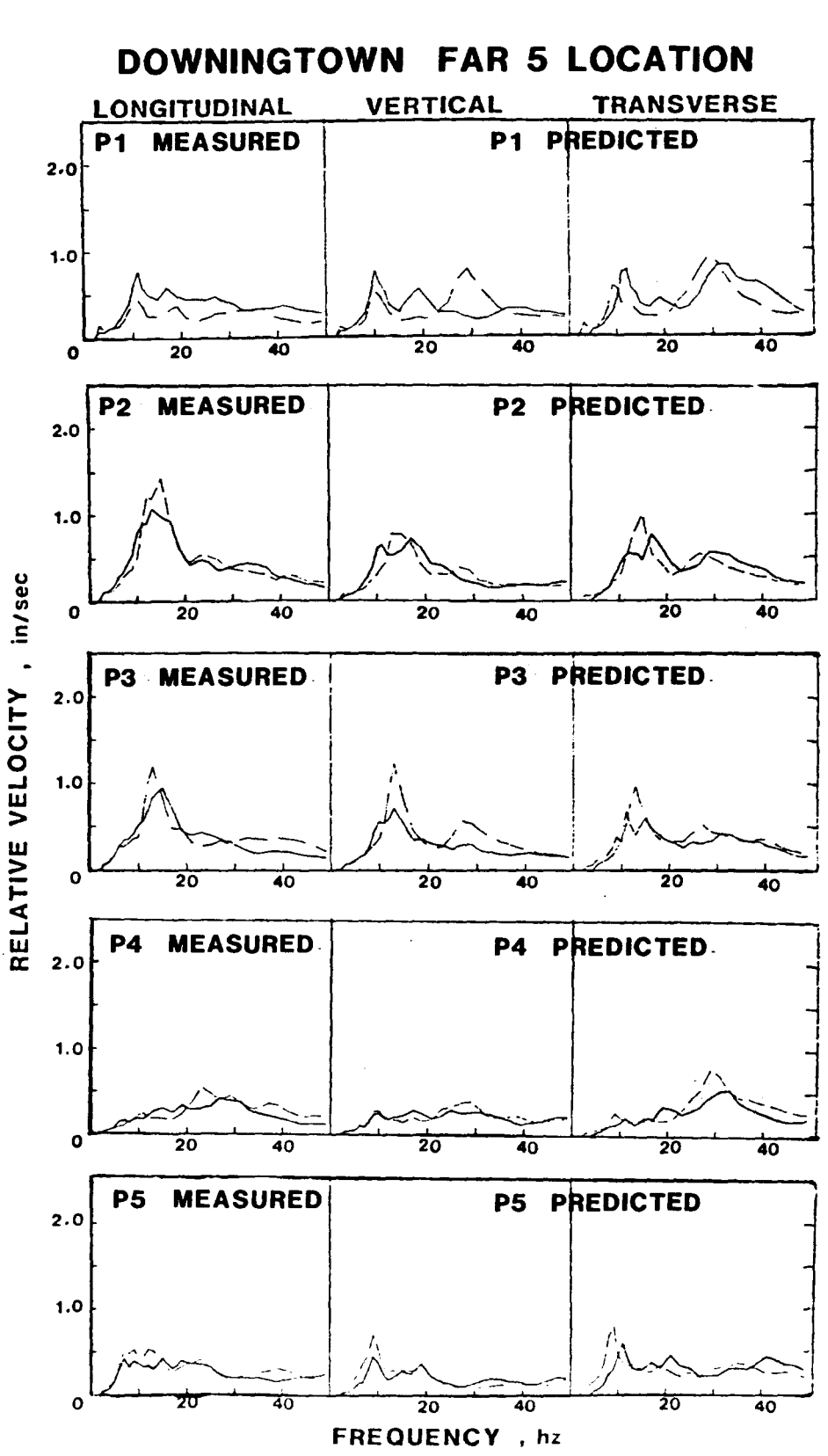

Figure 40. Predicted and measured response spectra, Downingtown.

6.5.1.2. Control Effectiveness

The data on the use of changes in delay to control vibration are shown in the next several tables and figures. The techniques used for analysis have been discussed earlier, and their use has been discussed with respect to the single-hole tests. At this point we will simply present the tabulated data, and the design criteria for the shots (i.e., constructive or destructive interference) for each quarry. A summary is given following the plots to indicate the relative success in controlling vibration.

6.5.1.2.1 Marriottsville

Production shots 3 and 4 were designed to produce constructive interference (marked "C" on tables) and shots 1 and 2 were designed to produce destructive interference (marked "D" on tables). Shot 5 had a constructive between-hole delay time, the same as shot 3; the between-row time for this shot was chosen to prevent further constructive interference. Note in particular the results for shots 2 and 3, which were predicted to have the extremum values.

Maximum peak particle velocities for the production shots at Marriottsville are shown in Table 21. Means for all shots at a given location are shown; for each shot the values at all locations are summed and the increase over the single-hole values are indicated. Shot 2 increased only 0.04 over the single-hole value, while shot 3 increased 0.33.

The ratios of production shot peak particle velocity versus that for the single-hole shot are shown in Table 22. Note that for the same set of locations, the average peak particle velocity for shot 2 was slightly less than that for the single-hole, while that for shot 3 was about 1.4 times that for the single-hole shot.

TABLE 21

MARRIOTTSVILLE

MAXIMUM INSTANTANEOUS PEAK PARTICLE VELOCITY (IN./S)

Location	Average Single Hole	Blast No. 1D	2D	3C	4C	5	Mean	Standard Deviation
West Opposite	0.34	0.48	0.28	0.50	0.39	0.58	0.43	0.11
West Halfway	0.25	0.39	0.25	0.37	0.45	0.46	0.36	0.09
Lime/Fill*	0.40	0.36	0.40	0.47	0.37	0.43	0.41	0.04
Lime/Marr.*	0.17	0.23	0.23	0.36	0.22	0.28	0.25	0.06
Ward's Chapel*	0.10	0.11	0.07	0.10	0.12	0.12	0.10	0.02
Wash House*	0.10	0.14	0.11	0.17	0.15	0.15	0.14	0.03
East Halfway	0.33	0.32	0.27	0.32	0.24	0.29	0.30	0.04
East Opposite	0.50	0.52	0.32	0.52	0.37	0.55	0.46	0.09
Sum	2.19	2.55	1.93	2.81	2.31	2.85	2.45	

*Using only locations behind to eliminate shield effects

Sum	0.77	0.84	0.81	1.10	0.86	0.98	0.90
Increase over single hole		0.07	0.04	0.33	0.09	0.21	0.13

TABLE 22

MARRIOTTSVILLE

INSTANTANEOUS PEAK PARTICLE VELOCITY

RATIOS: PRODUCTION/SINGLE-HOLE

Location	Blast No.				
	1D	2D	3C	4C	5*
West Opposite	1.41	0.82	1.47	1.15	1.71
West Halfway	1.56	1.00	1.48	1.80	1.84
Lime/Fill*	0.9	1.00	1.18	0.93	1.08
Lime/Marr.*	1.35	1.35	2.12	1.29	1.65
Ward's Chapel*	1.10	0.70	1.00	1.20	1.20
Wash House*	1.40	1.10	1.70	1.50	1.50
East Halfway	0.97	0.82	0.97	0.73	0.88
East Opposite	1.04	0.64	1.04	0.74	1.10

*Using only locations behind to eliminate shield effects

Mean	1.22	0.93	1.37	1.17	1.37
Standard Deviation	0.23	0.22	0.38	0.35	0.33

Finally, maximum response spectrum values and their associated frequencies are shown in Table 23. For shot 2 the sum is 1.1, while for shot 3 the sum is 2.9. An illustration of the strong effect on response spectra is seen in Fig. 41, the response spectra for vertical component for all shots recorded at the Lime/Marr. location. Noting again shots 2 and 3, the potential response in residential structure may be altered significantly by blast design.

Summarizing, all of the comparative analyses indicate that the delay times intended to create constructive interference produced a higher vibration level than those intended to create destructive interference. Because of the geometry of the test bench with respect to the seismograph locations, some shielding occurred because of an open face between the blast and the seismograph. The locations would be the West Opposite, West Halfway, East Halfway, and East Opposite. If we eliminate these locations from consideration, the following summary can be made, ranking the blasts in terms of decreasing vibration intensity.

	Peak Particle Velocity	Response Spectra
High Vibration	3C	3C
	5*	5*
	4C	4C
Low Vibration	1D	2D
	2D	1D

C = Constructive
D = Destructive

*Blast no. 5 has a constructive between-hole delay time, the same time that blast no. 3 had. The between-row delay time was chosen in an attempt to pick the best time to prevent further constructive interference.

TABLE 23

RESPONSE SPECTRA - MAXIMUM RELATIVE VELOCITY (m/s) 3-18 Hz 5% DAMPING

	Blast No.				
Location	1	2	3	4	5
West Opposite	0.43-18 hz	0.68-15 hz	0.99-18 hz	1.36-15 hz	0.80-18 hz
West Halfway	0.34-15 hz	0.40-15 hz	1.05-17 hz	1.31-15 hz	0.96-18 hz
Lime/Fill*	0.35-12 hz	0.34-15 hz	1.00-17 hz	0.97-15 hz	0.85-17 hz
Lime/Marr.*	0.30-17 hz	0.60-17 hz	1.68-18 hz	0.53-15 hz	1.20-17 hz
Ward's Chapel*	0.09-13 hz	0.07-18 hz	0.13-18 hz	0.12-15 hz	0.12-17 hz
Wash House**	0.17-11 hz	0.09-15 hz	0.09-18 hz	0.21-15 hz	0.19-15 hz
East Halfway	0.40-12 hz	0.31-18 hz	0.49-18 hz	0.36-14 hz	0.37-13 hz
East Opposite	0.47-11 hz	0.50-17 hz	0.79-18 hz	0.37-13 hz	0.45-18 hz
Sum	2.55	2.99	6.22	5.23	4.94

*Using only locations behind blasting to eliminate shield effects.

Sum	0.91	1.10	2.90	1.83	2.36

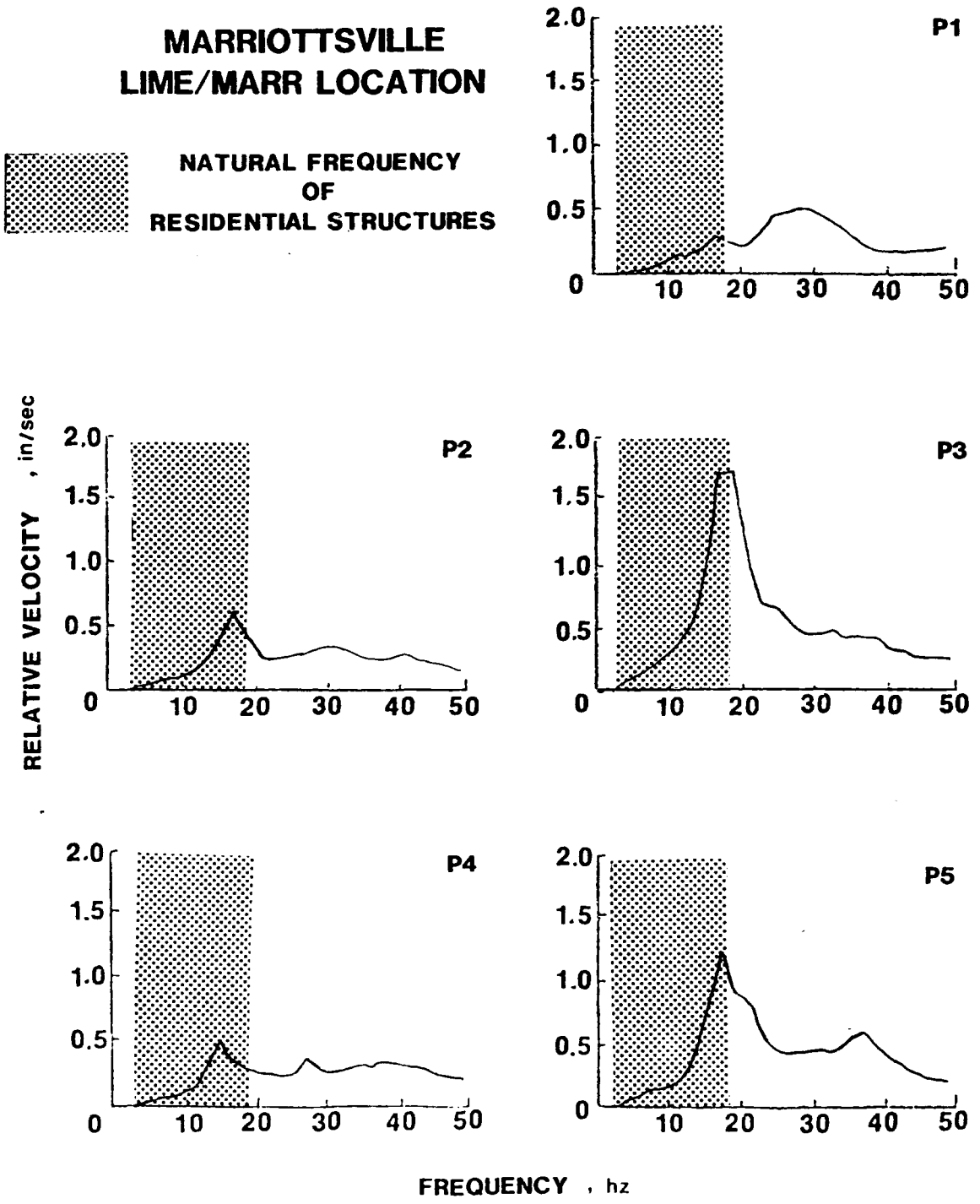

Figure 41. Response spectra, vertical component, for all shots at Lime/Marr. location, Marriottsville.

Even if all of the locations are included, the same trend is seen. The preceding analysis has indicated that at Marriottsville, vibration effects from blasting can be reduced if knowledge of the geology and precise delay times are available.

6.5.1.2.2 Downingtown

Production shots 2 and 3 were designed to produce constructive interference (marked "C" on tables) and shots 1 and 4 were designed to produce destructive interference (marked "D" on tables). Shot 5 was a composite shot designed to increase lowfrequency vibration. Note in particular the results for shots 3 and 4, which were predicted to have the extremum values. The anomalous values for shot 1 will be discussed at the end of this section.

Maximum peak particle velocities for the production shots at Downingtown are shown in Table 24. Again, means for all shots at a given location are shown; for each shot the values at all locations are summed and the increase over the single-hole values are indicated. Shot 4 increased only 0.54 over the single-hole value, while shot 3 increased 1.46. The ratio of production shot peak particle velocity versus that for the single-hole shots are shown in Table 25. Note that for the same set of locations, the average peak particle velocity for shot 4 was 1-1/2 times that for the single-hole shot, while that for shot 3 was 2-1/3 times that for the single-hole shot. Finally, maximum response spectrum values and their associated frequencies are shown in Table 26. For shot 4 the sum is 2.9, while for shot 3 the sum is 8.4. Again, an illustration of the effect on response spectra is seen in

TABLE 24

MAXIMUM INSTANTANEOUS PEAK PARTICLE VELOCITY (in./s)

DOWNINGTOWN

Location	Average Single Hole	Blast No. 1	2	3	4	5	Mean	Standard Deviation
Close 1	0.12	0.25	0.27	0.26	0.14	--	0.23	0.06
Close 2	0.21	0.56	0.46	0.54	0.29	0.29	0.43	0.13
Close 3	0.30	0.83	0.53	0.70	0.34	0.61	0.60	0.18
Far 1	0.09	0.30	0.35	0.24	0.13	0.21	0.25	0.08
Far 2	0.11	0.27	0.24	0.33	0.26	0.18	0.26	0.05
Far 3	0.09	0.24	0.17	0.16	0.18	0.19	0.19	0.03
Far 4	0.13	0.24	0.24	0.27	0.21	0.21	0.23	0.03
Far 5	0.14	0.31	0.33	0.29	0.20	0.24	0.27	0.05
Sum (excluding location C-1)	1.07	2.75	2.32	2.53	1.61	1.93	2.23	
Increase over single hole		1.68	1.25	1.46	0.54	0.86	1.16	

TABLE 25

DOWNINGTOWN

INSTANTANEOUS PEAK PARTICLE VELOCITY

RATIOS: PRODUCTION/SINGLE-HOLE

	Blast No.				
Location	1D	2C	3C	4D	5L
Close 1	2.08	2.25	2.17	1.17	--
Close 2	2.67	2.19	2.57	1.38	1.38
Close 3	2.77	1.77	2.33	1.13	2.03
Far 1	3.33	3.89	2.67	1.44	2.33
Far 2	2.45	2.18	3.00	2.36	1.64
Far 3	2.67	1.89	1.78	2.00	2.11
Far 4	1.85	1.85	2.08	1.62	1.62
Far 5	2.21	2.36	2.07	1.71	1.71
Mean	2.50	2.30	2.33	1.57	1.83
Standard Dev.	0.43	0.63	0.37	0.39	0.31

TABLE 26

RESPONSE SPECTRA - MAXIMUM RELATIVE VELOCITY (m/s) 3-18 Hz 5% DAMPING

Location	Blast No. 1	2	3	4	5
Close 1	0.54-17 hz	0.95-13 hz	0.79-13 hz	0.20-18 hz	----
Close 2	0.78-17 hz	1.49-13 hz	2.29-13 hz	0.55-17 hz	0.65-09 hz
Close 3	1.19-18 hz	1.63-15 hz	1.56-13 hz	0.56-15 hz	0.64-09 hz
Close 4	0.90-19 hz	1.19-15 hz	1.02-15 hz	0.59-18 hz	0.51-18 hz
Far 1	0.62-10 hz	0.65-15 hz	0.64-15 hz	0.27-15 hz	0.48-08 hz
Far 2	0.49-09 hz	0.59-10 hz	0.51-09 hz	0.22-09 hz	0.57-09 hz
Far 3	0.43-09 hz	0.50-13 hz	0.72-12 hz	0.15-09 hz	0.36-08 hz
Far 4	0.85-11 hz	0.84-11 hz	0.94-13 hz	0.29-13 hz	0.69-08 hz
Far 5	0.75-10 hz	0.72-17 hz	0.71-13 hz	0.28-17 hz	0.46-08 hz
Sum (excluding location C-1)	6.01	7.61	8.39	2.91	4.36

Fig. 42, the response spectra for the vertical component for all shots recorded at the Far 5 location. Noting shots 4 and 3, it may again be seen that the potential response in residential structure may be altered significantly by blast design.

Using all of the various measures of vibration intensity shown, we made the following ranking in terms of increasing vibration levels for the Downingtown test blasts.

	Peak Particle Velocity	Response Spectra
High Vibration	1D	3C
	3C	2C
	2C	1D
Low Vibration	5	5
	4D	4D

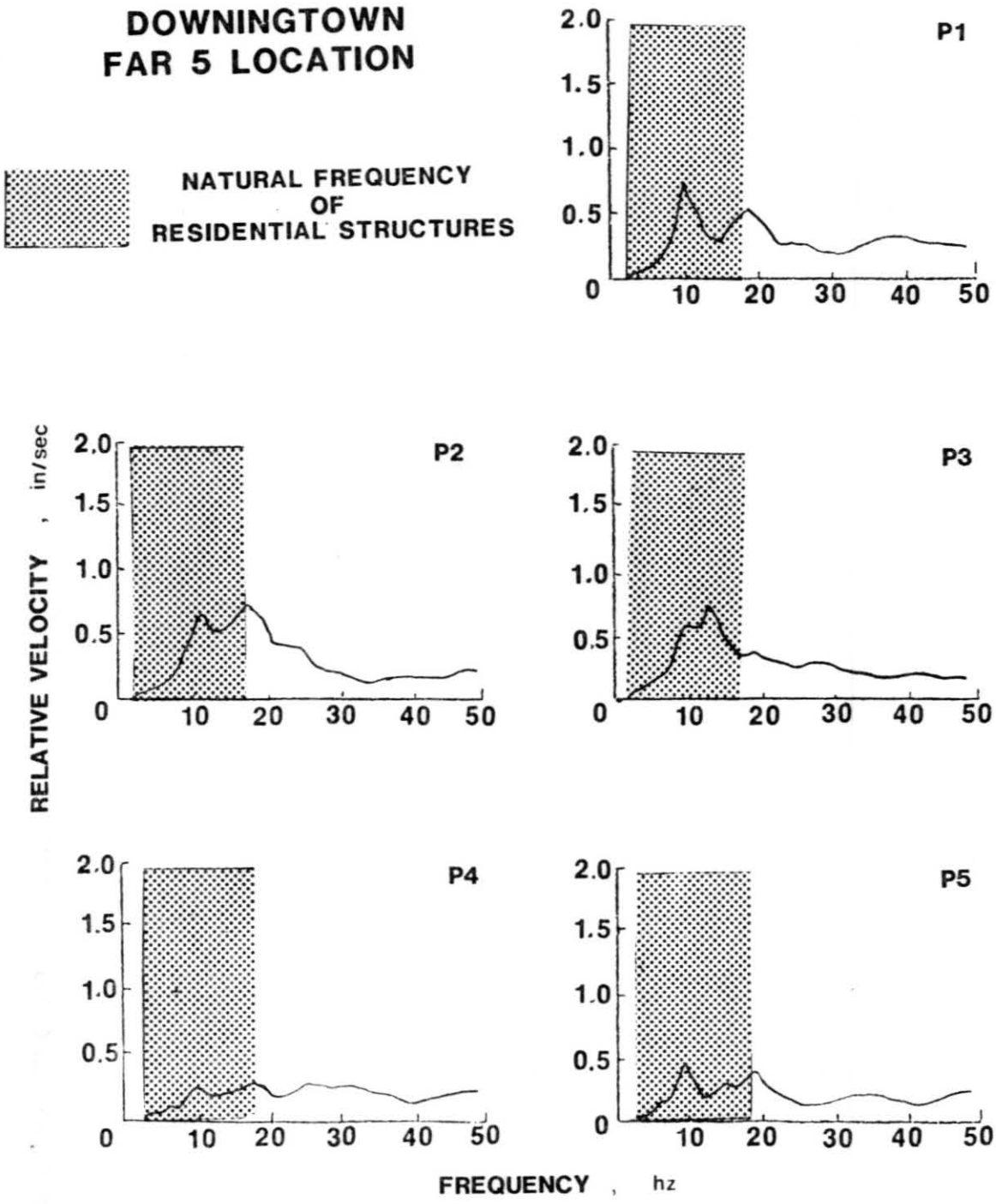

Figure 42. Response spectra, vertical component, for all shots at Far 5 location, Downingtown.

The analysis indicates that the vibration levels at Downingtown can be reduced if the quarry is consistent, the geology at the recording site is known, and precise timing is used. The deeply weathered clay seam on the north side of the quarry bench appears to have caused an increase in the vibration levels for blast no. 1. The vibration control method loses some of its effectiveness when the single-hole blast is not in material that is representative of the rock in a production shot, or if part of the production shot is in rock and part in a clay seam.

The various intensity level comparisons have been normalized by calculating a ratio of the maximum intensity to the intensity measured. These comparisons are shown below.

Marriottsville

Blast No.	PPV	Response Spectra	Total	
P1 D	0.76	0.31	1.07	"best"
P2 D	0.74	0.38	1.12	
P3 C	1.00	1.00	2.00	"worst"
P4 C	0.78	0.63	1.41	
P5	0.89	0.81	1.70	

Downingtown

Blast No.	PPV	Response Spectra	Total	
P1 D	1.00	0.72	1.72	
P2 C	0.74	0.91	1.65	
P3 C	0.87	1.00	1.87	"worst"
P4 D	0.32	0.35	0.67	"best"
P5	0.52	0.52	1.04	

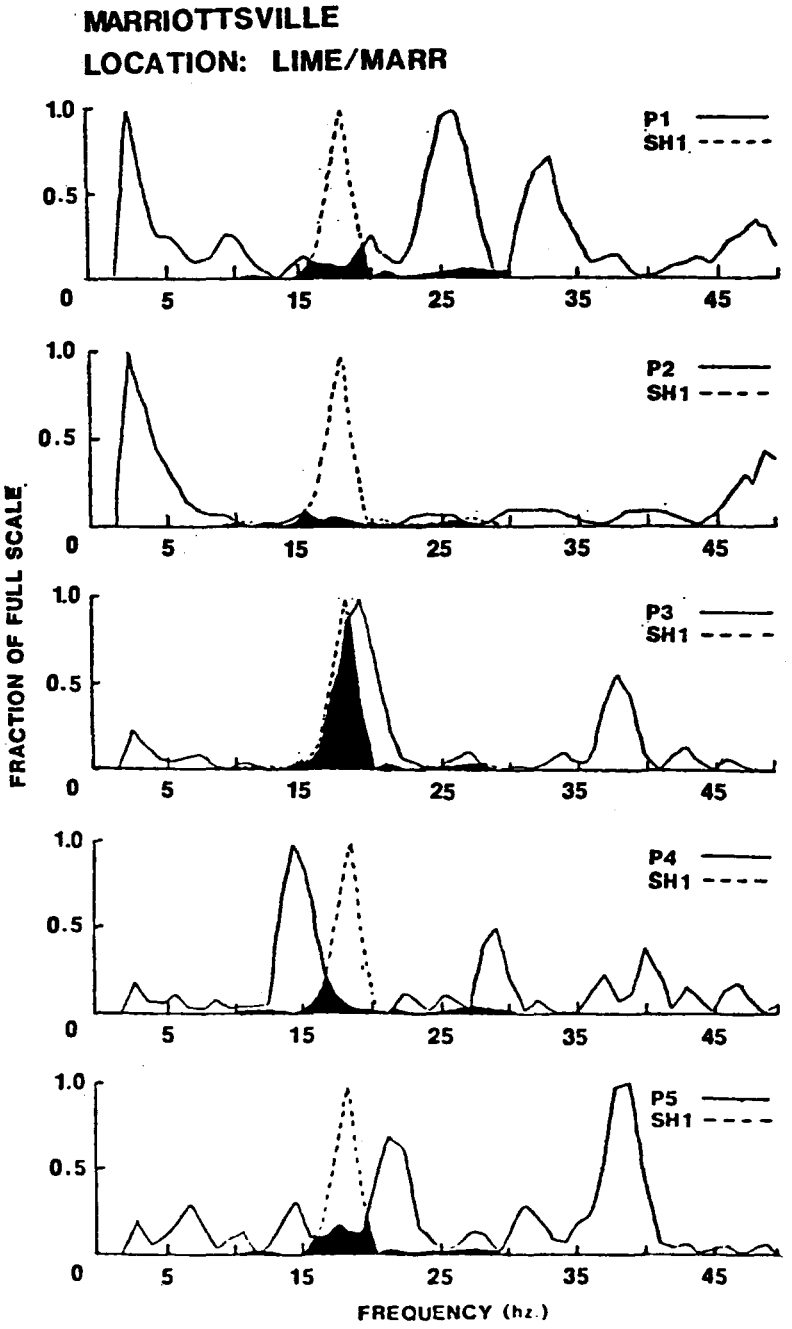

Figure 43. Power spectral density, plotted with firing-time spectra, Lime/Marr. location, Marriottsville.

at the Lime/Marr. seismograph location. At this location, the highest peak particle velocity and response spectrum values were recorded on blast no. 3. It produced the "worst" vibration of any of the blasts at this location, consistent with the firing-time spectrum.

Figure 44 is a similar comparison between the PSD for the Downingtown blasts and the single hole. Again, the areas in common under both curves are shaded black. The total shaded areas for blasts 2, 3, and 5 appear to be approximately equal. These areas represent common frequencies found on the single hole plots and the firing-time plots. There is a very significant difference and that is the area of the firing-time spectra for shots 2 and 3 at these common frequencies, and the area under the firing time spectra for shot 5 at these common frequencies. There is much more area on shots 2 and 3 than on shot 5. Shot 2 has more area than shot 3. In terms of the recorded vibration intensities shot 2 was "slightly worse" than shot 3 and "much worse" than shot 5 at the far 5 location.

Shots 2 and 3 were planned to test the effects of quarry-bench geology on delay times designed to produce constructive interference at 13-15 Hz. The vibration results were very similar, both shots producing high vibrations. Shots 1 and 4 were planned to test the effects of quarry-bench geology on delay times designed to produce destructive interference. Shot 1, located in the soft rock and clay seam on the north side of the bench, produced high vibrations, while shot 4, located on the harder rock on the south side of the bench, produced the lowest vibrations of all the shots at Downingtown.

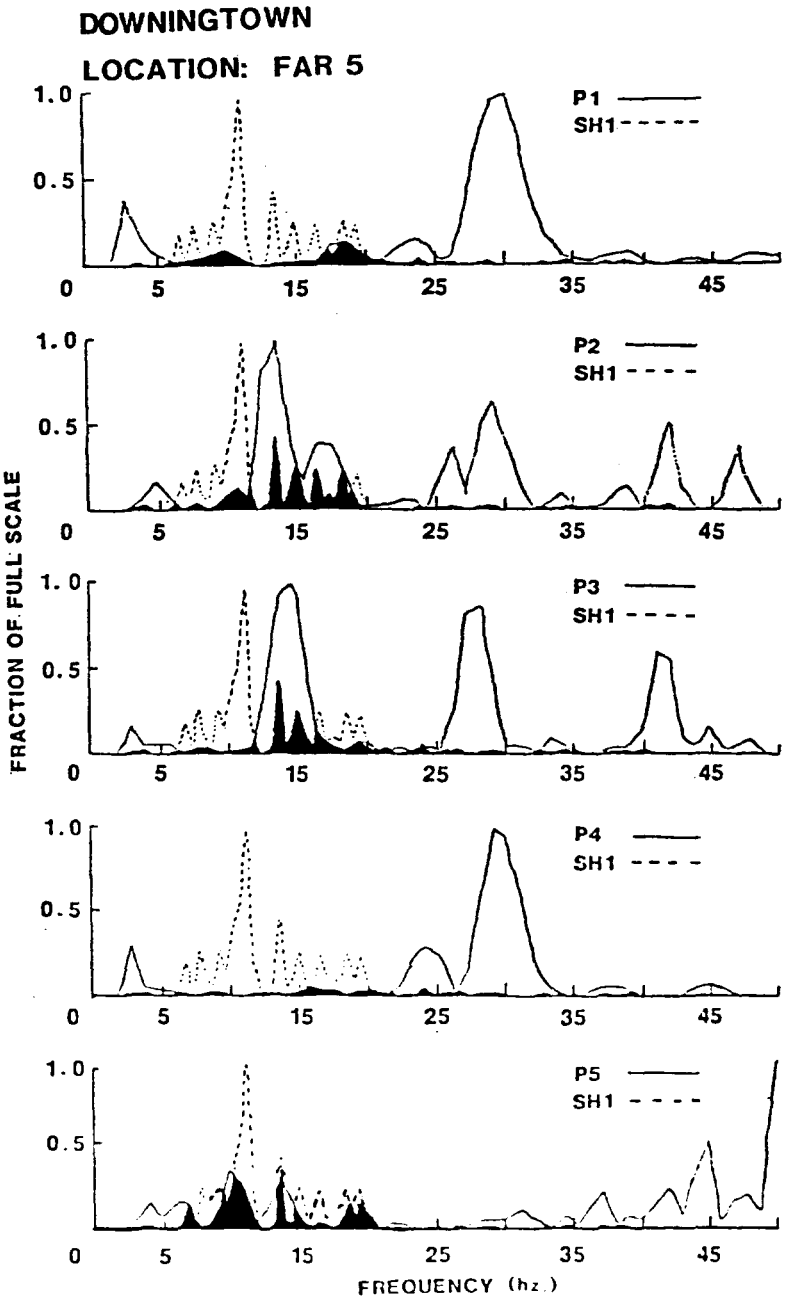

Figure 44. Power spectral density, plotted with firing-time spectra, Far 5 location, Downingtown.

6.5.2 Strain Waves

The original rationale for studying the strain waves was two-fold: first, the source characteristics of the explosive were to be determined and second, attenuation in the rock as a function of distance from the explosive column was to be assessed. We also hoped that the characteristics of the strain waves in larger shots than had been studied before with strain gages would offer insight into the mechanisms of fragmentation. In particular, we were interested in why delay affects fragmentation.

The study of strain waves was complicated by several factors. First, in most of the long-delay shots at Marriottsville, and almost all of the shots at Downingtown, the gage failed after only a few of the strain pulses had been recorded. Examination of the individual records showed that failure occurred on all components of the gage almost simultaneously. This failure was reflected in the records by a step-function offset to full-scale output. This type of signal is indicative of an open circuit and leads us to conclude that the cable to the gage was cut. This was probably due to some shifting of the rock around the cable. For future studies of this sort, we have concluded that a braided-wire sheath around the cable might lengthen the life of the gage sufficiently to allow a more complete record to be obtained. We do not know how this might affect the pick-up of noise.

For those records we were able to obtain, the signal levels were not sufficiently regular in their distribution that attenuation characteristics could be determined. In contrast with the vibration records, which indicated that the vibration signature was generally the same for

each location, we found that strain-wave behavior was very inhomogeneous. However, we believe that some of this inhomogeneity contains information about the fragmentation mechanisms.

We will discuss the records for Marriottsville only, because they form the more complete set. Several of the records will be shown which illustrate some of the problems encountered. We will conclude with discussions of the implications for fragmentation.

Figures 45 and 46 show the front-gage principal-strain records for two shots at Marriottsville. Note that the time and strain scales for all of these records are different than those for the single-hole shot records. A shot diagram, indicating the firing times and gage location with respect to the boreholes, is shown on the figures. The stars on the figures show the hole firing times with respect to the record.

The first thing to note is the impulsive nature of the strain pulse, comparable in width with that for the single-hole record (Fig. 25). The broad pulse seen in the single-hole records is sometimes seen and will be discussed in some detail later. Each of these records show failure of the gage at about 200 ms after shot initiation.

Of particular interest in these two figures is the relative amplitude of the strain pulses from the second and third holes in the front row. Each of these holes was the same distance from the gage; however, in Fig. 45 the pulse from the second hole was substantially greater than that from the third, and in Fig. 46 the converse was true. In Fig. 45 the broader pulses following the firing of the fourth hole are due to the failure of one component of the gage; such failures of only one component are rare. In Fig. 46, the broad pulse following the detonation

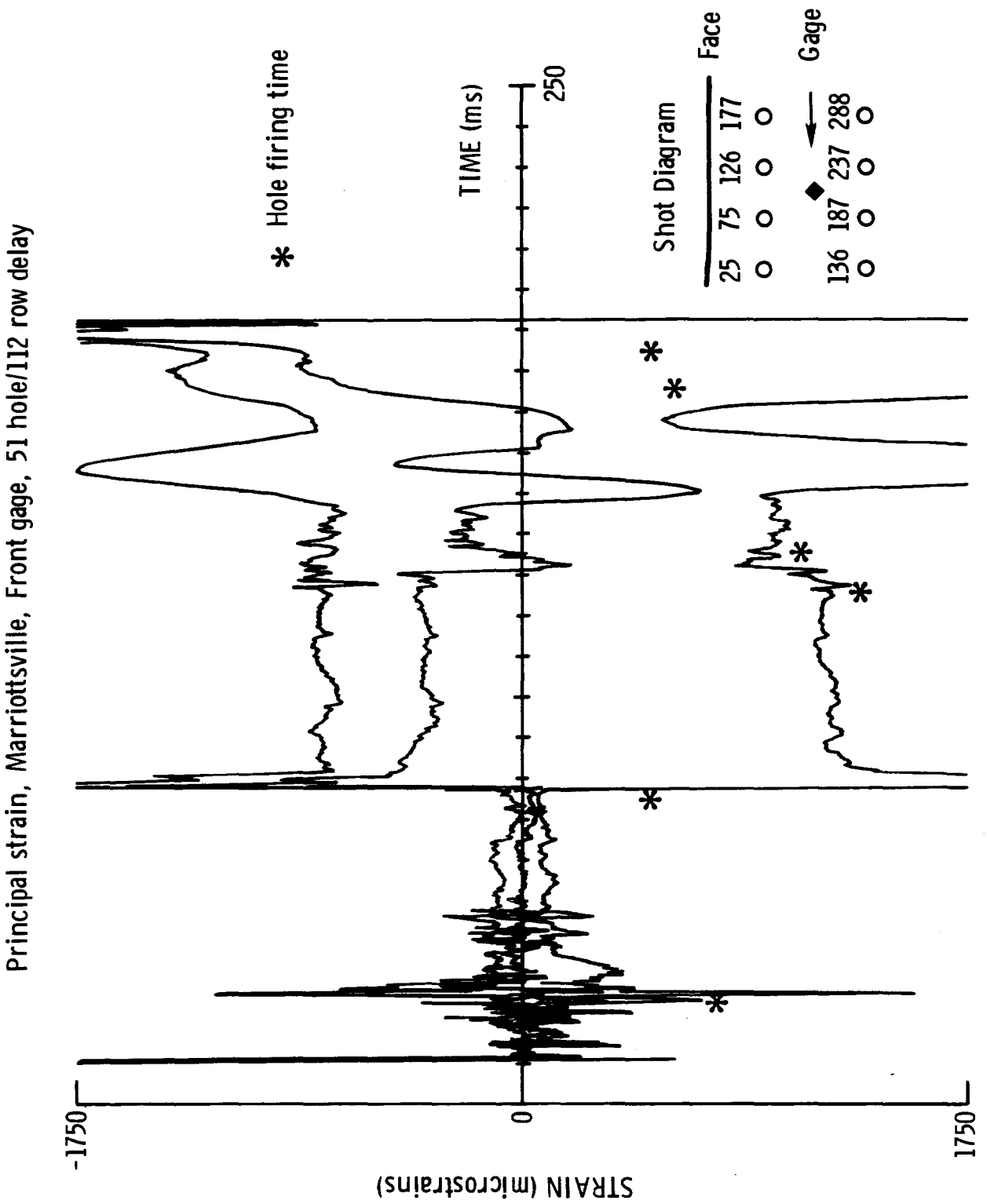

Figure 45. Front-gage principal-strain record for shot P3 at Marriottsville.

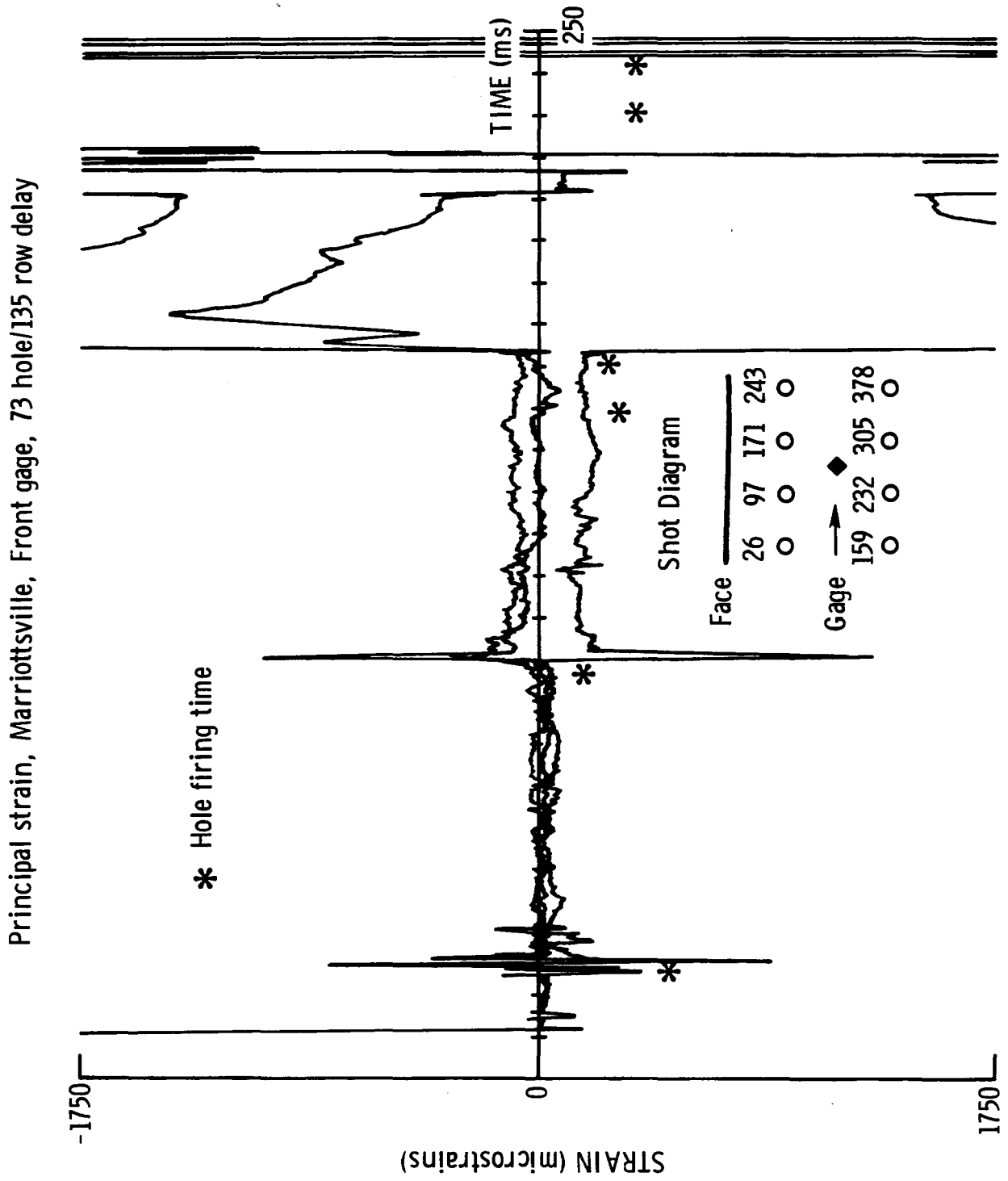

Figure 46. Front-gage principal-strain record for shot P4 at Marriottsville.

of the third hole in the front row is comparable to the pulses found in the single-hole shots. It may also be noted that pulses from the back row of holes are very small.

This variability in the records from gages at comparable distance is probably due to differences in the local transmission characteristics of the rock, such as may be due to jointing or cracks in the rock. The difference is not due to orientation because the principal strains are orientation independent. We were not able to confirm these possible differences in transmission characteristics because we could not map cracks in the face back through the bulk of the rock mass, and cracks on the bench surface were hidden by fines. At this point we can only infer that such differences are due to inhomogeneities in the rock.

Figure 47 shows the strain record from the rear gage on one of the shots with somewhat shorter delay than the previous figures. In this case, the gage fails late in the event even though it is behind the bulk of the shot; this indicates that some rock movement was present behind the bulk of the rock actually displaced by the shot (i.e., back-break).

Note the waves generated by the sixth and seventh holes to fire, which are the central two holes in the back row. Each of these has a broad pulse somewhat similar to that shown for the single-hole records. The broad pulse differs from that shown in the single-hole shots in that it is tensile rather than compressive. This tensile pulse was only observed for rear gages. It is not likely that tensile waves reflected from the free-face would generate such a strong pulse for these holes since there is no evidence of this pulse for any of the other holes. Therefore it appears that these pulses are direct. The tensile nature is also unusual. We would infer that this indicates either the pulling of the rock away

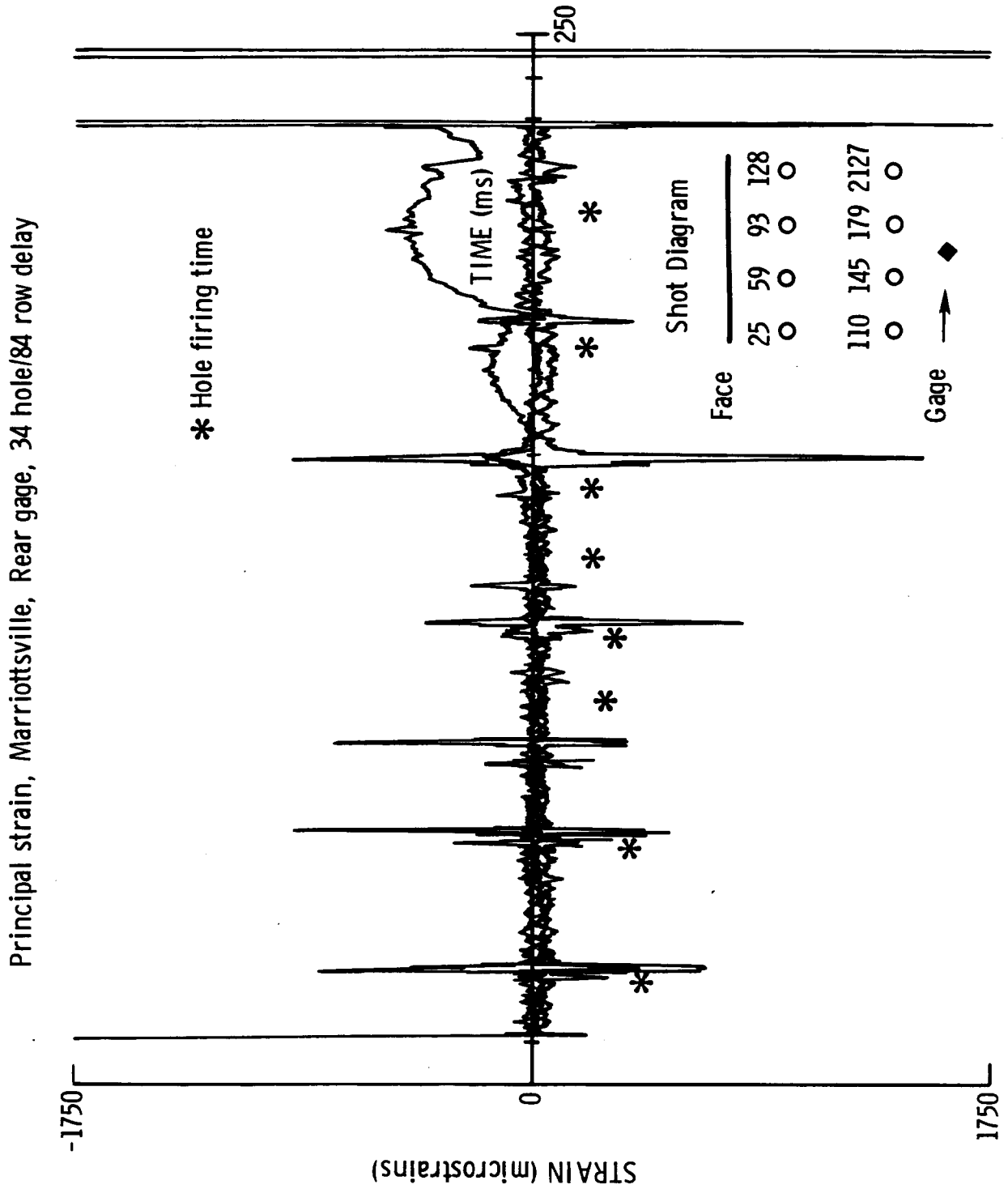

Figure 47. Rear-gage principal-strain record for shot P1 at Marriottsville.

from the gage, perhaps due to back-break or due to late gas-pressurization. We will refer to this more, but it is important to note that the pulse at the gage is declining in amplitude, almost to the baseline, by the time the next hole fires. It is also important to note that this is the shot with the optimum fragmentation. Unfortunately, we did not obtain a front gage record for this test.

Figure 48 shows the rear gage record for the shortest delay shot in the test series. Two things are notable: first, the primary pulses are generally broader than those of the previous figure and second, a tensile pulse is observed, but very late in the event. The broadness of the pulses is probably due to differences either in the transmission through the rock mass or the coupling of the gage. Because all of the primary pulses are broader, we would infer that this is due to gage coupling, although this could not be tested. The tensile pulse may be related to back-break, in this case because it follows late in the event, and is not associated with any particular hole firing. The tensile pulses associated with specific holes, as seen in the previous figure, are not noted here.

The octahedral shear strain for this record is shown in Fig. 49. As noted in the single-hole record, the octahedral shear strain tracks fairly well with the principal compressive strain, although the sense of shear for the tensile pulse is also of the same sign. The significance of the sign changes in the octahedral shear strain are not currently understood.

Figure 50 shows the principal strain record for the front gage from the shot recorded in the previous two figures. Several interesting points may be observed here. Note that the amplitude and broadness of the pulses, in general, are smaller than for the rear gage. This is not consistent with the fact that the waves should attenuate more with

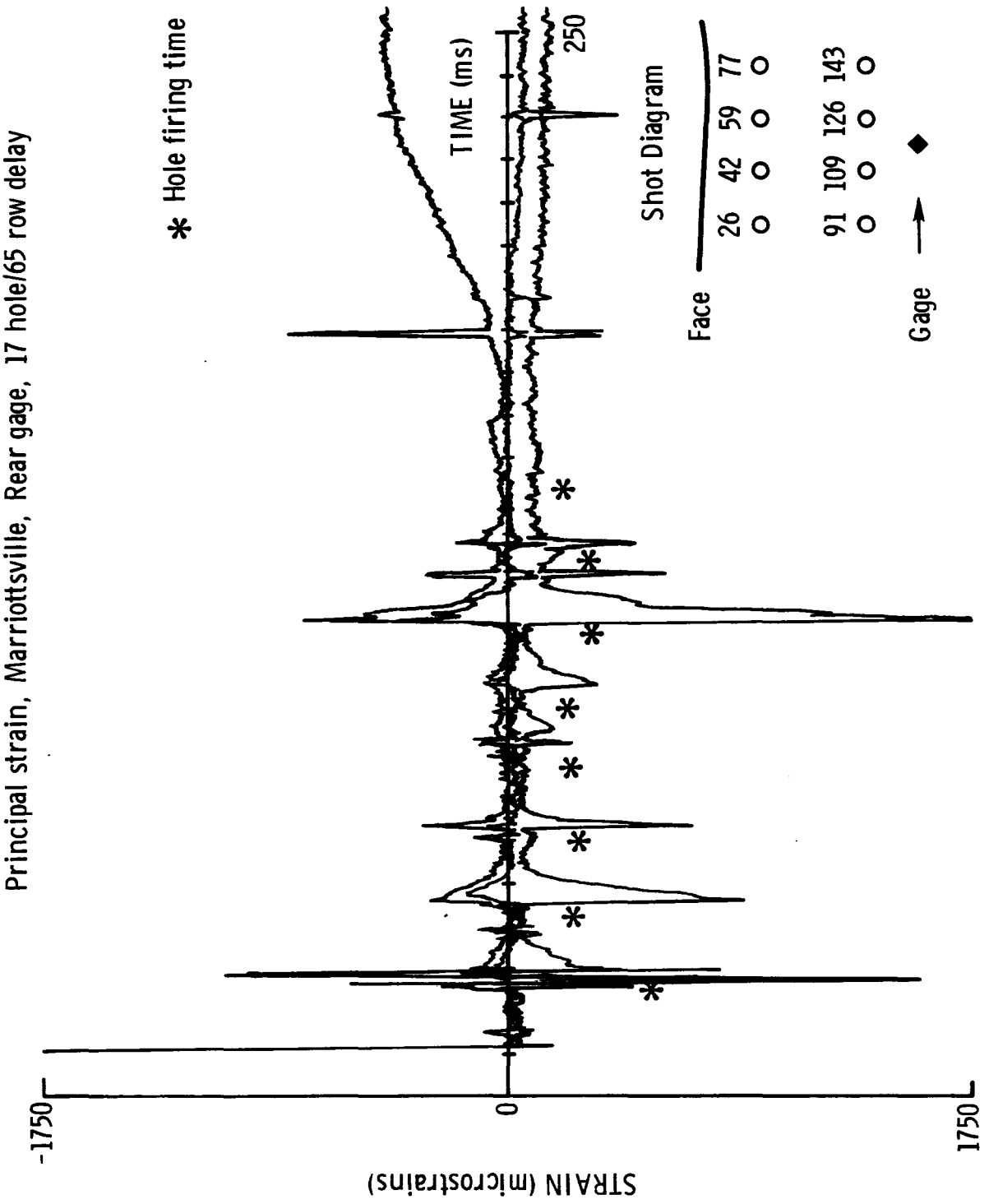

Figure 48. Rear-gage principal-strain record for shot P2 at Marriottsville.

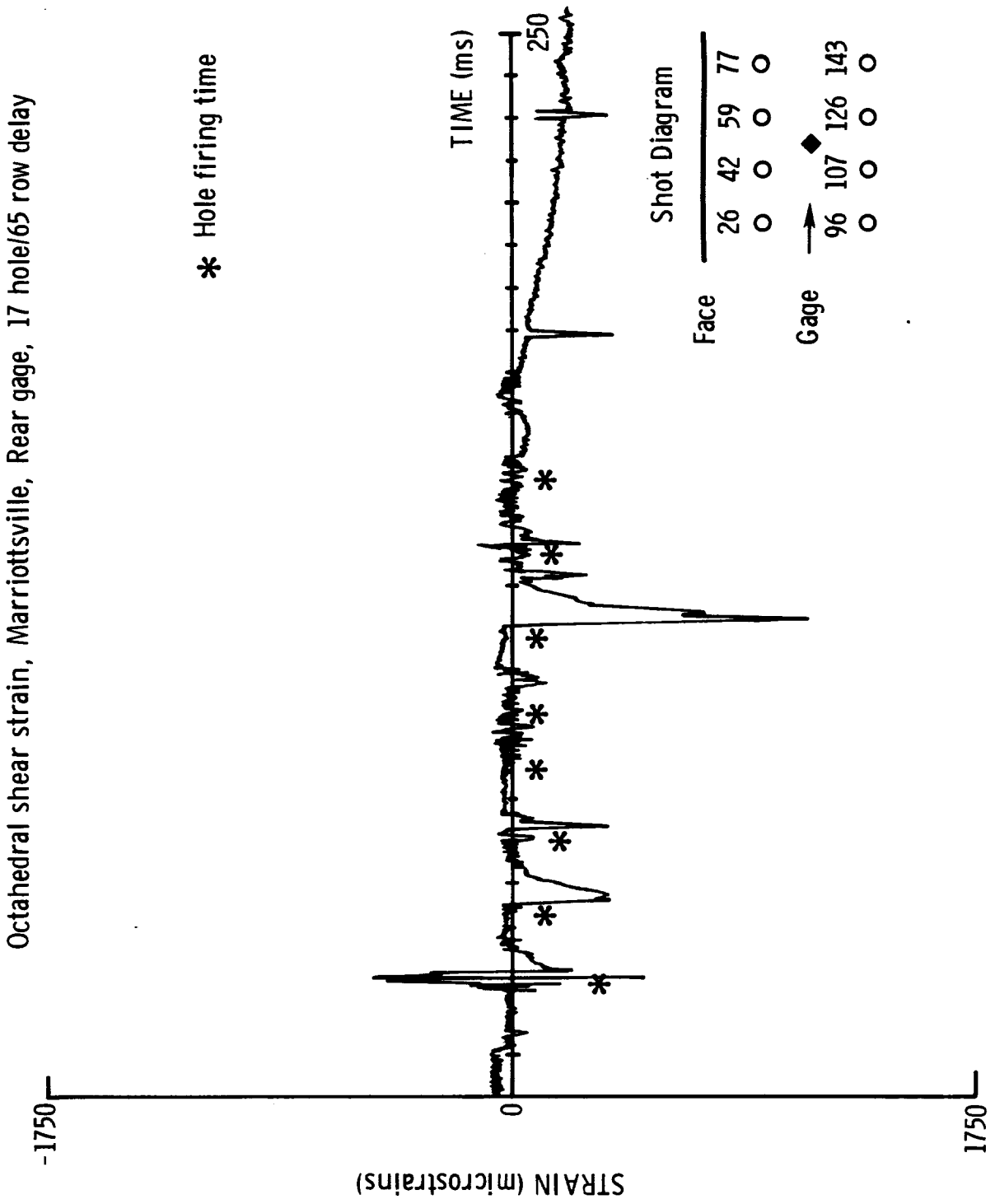

Figure 49. Octahedral-shear-strain record calculated from principal strains on Fig. 48.

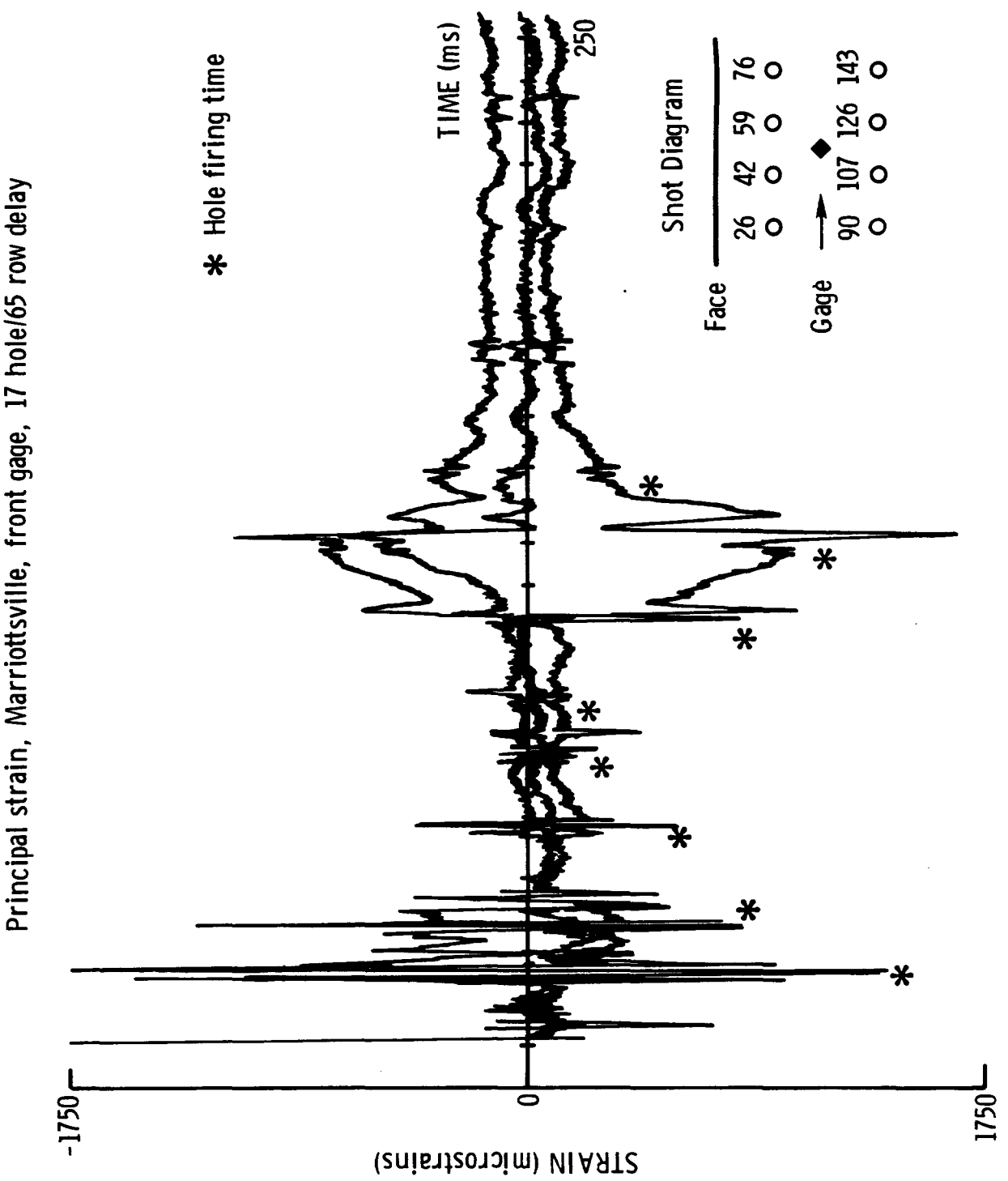

Figure 50. Front-gage principal-strain record for shot P2 at Marriottsville.

greater distance; however, it is consistent with the interpretation that the rear gage on this shot had very good coupling, relative to this gage record and the rear gage record of Fig. 47.

The broad pulse following the sixth hole firing is similar to that seen earlier. Figure 51 shows the octahedral shear strain for this record. The octahedral shear strain is again consistent with previous results. Notable in both of these records is the fact that no broad pulse is found for the holes in the front row, rather it is found for the holes in the rear row. If reflected waves from the free-face account for the broad pulses, then the holes in the front row should generate such pulses. This suggests that the broad pulses are due to one of two causes. Local discontinuities which are formed during the shot may reflect stress waves, or, more probably, these pulses are due to gas pressurization of new or existing cracks. The broad pulse reaches a maximum about 12 ms after the initiation of the hole that causes the pulse. It is unlikely that reflected strain waves would be remaining in the region of the gage for such a long period of time, even if the waves were multiply reflected. If the gas pressure travels at the velocity of sound in air (~ 1.1 ft/ms), then the pulse should arrive at the gage about 10 ms after the detonation of the hole, since the gage is about 11 ft from the hole. These calculations are rough, but indicate that the times are of the right order.

These broad pulses are not always found. This is consistent with the gas pressurization hypothesis, since such strain on the gage is likely to be significant only if a pressurized crack is near the gage. Cracks at a

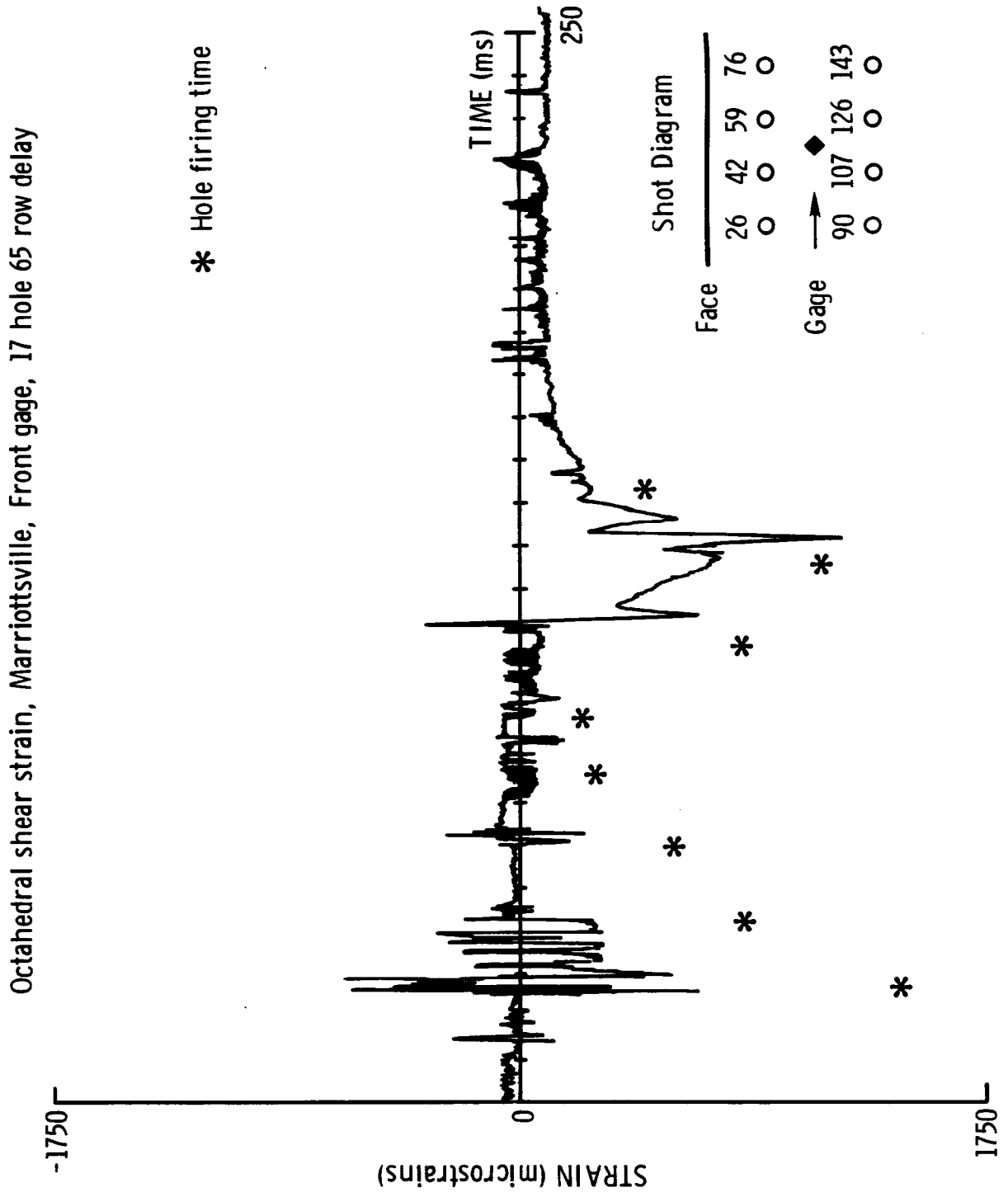

Figure 51. Octahedral-shear-strain record calculated from principal strains of Fig. 50.

distance from the gage will not exert significant strain in the rock mass, but will only locally extend new or previously-existing cracks.

We also note that in this case the strain wave from the next hole to fire interacts with the strain on the gage for the firing time of 17 ms between holes, corresponding to relief of 1 ms/ft. As indicated in previous work, and as we shall show in the next section, fragmentation is poor at such short relief.

We therefore hypothesize that the strain records, as sparse as they are, may suggest a reason for the effect of delay on fragmentation. At short delays, the cracks near a borehole may still be pressurized with gas, impeding the propagation of strain waves generated by the next hole to fire. At delay corresponding to relief of 2 ms/ft, the gas pressures have died down to the extent that strain waves may be propagated across fractures which were extended by the gas-pressure pulse. At longer delays, the rock will be in motion due to the gas pressurization and the strain waves then may be impeded from propagation due to the progressive separation of the rock pieces from the rock mass.

An optimum time for firing the next hole would be just after the gas pressure pulse dies down. Different explosives may generate gases at different rates and different rocks may fracture at different rates; however, the general concept appears consistent with the results observed. Further research, perhaps on scale models, may indicate whether this hypothesis conforms to the actual behavior of strain generated by explosives.

6.5.3 Face Fragmentation

The calculated screen sizes are plotted on log/probability axes for comparison. The size distributions from the tests at Marriottsville and those from Downingtown are seen in Figs. 52 and 53, respectively.

From the particle size distributions, we can determine the sizes of the mathematical screens at the 80-, 50-, and 20-percent passing points, corresponding to the coarse, median, and fine fractions, respectively, of the distributions. In the discussions that follow, we will emphasize the 50% passing size as the more representative of the three comparisons. As noted previously in the comparisons of the single-hole shots at Marriottsville (see the Fragmentation - Reproducibility section), small numbers of oversize rock, which may account for less than 5% of the total area analyzed, can greatly skew the particle size distributions. Thus, comparisons of the screen sizes at the 80% passing points are included here for completeness, but they will not be discussed further. The comparisons of the 20% passing screen sizes are also included for the same reason, but keep in mind that the number of particles that can be resolved at that size (about 0.5 ft in the long dimension) is greatly affected by the optical quality of the high-speed films.

Tables 27 and 28 show the screen sizes for the 80-, 50-, and 20-percent passing points from the particle size distributions of the Marriottsville and Downingtown blasts, respectively. Figures 54 and 55 are plots of the screen size at the 50% passing point versus relief between holes in a row for the two sites. At both quarries, a trend is suggested by the plots. Higher spacing relief corresponds to finer fragmentation. A best fit line through the Marriottsville data

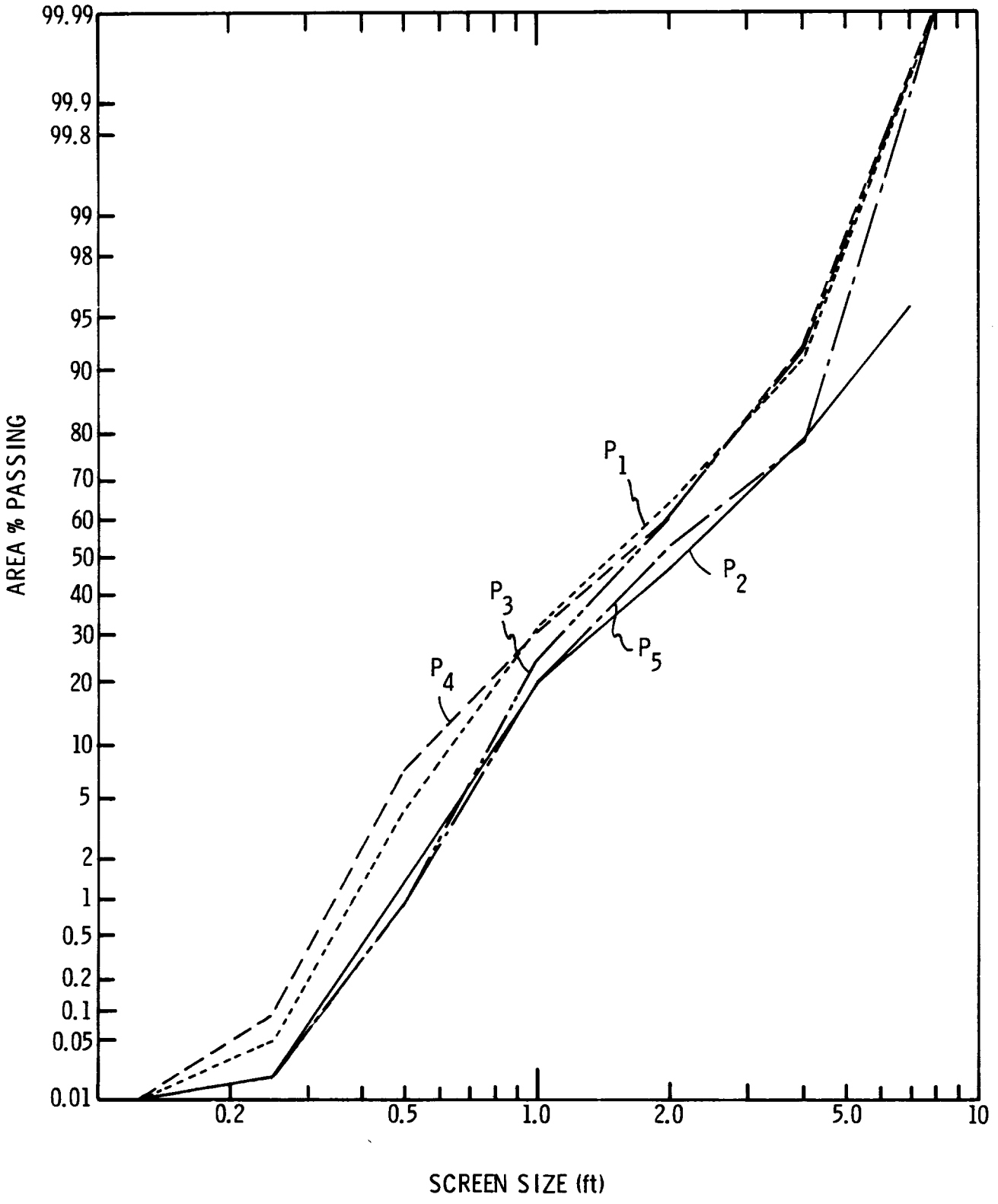

Figure 52. Fragment-size distribution, Marriottsville production shots.

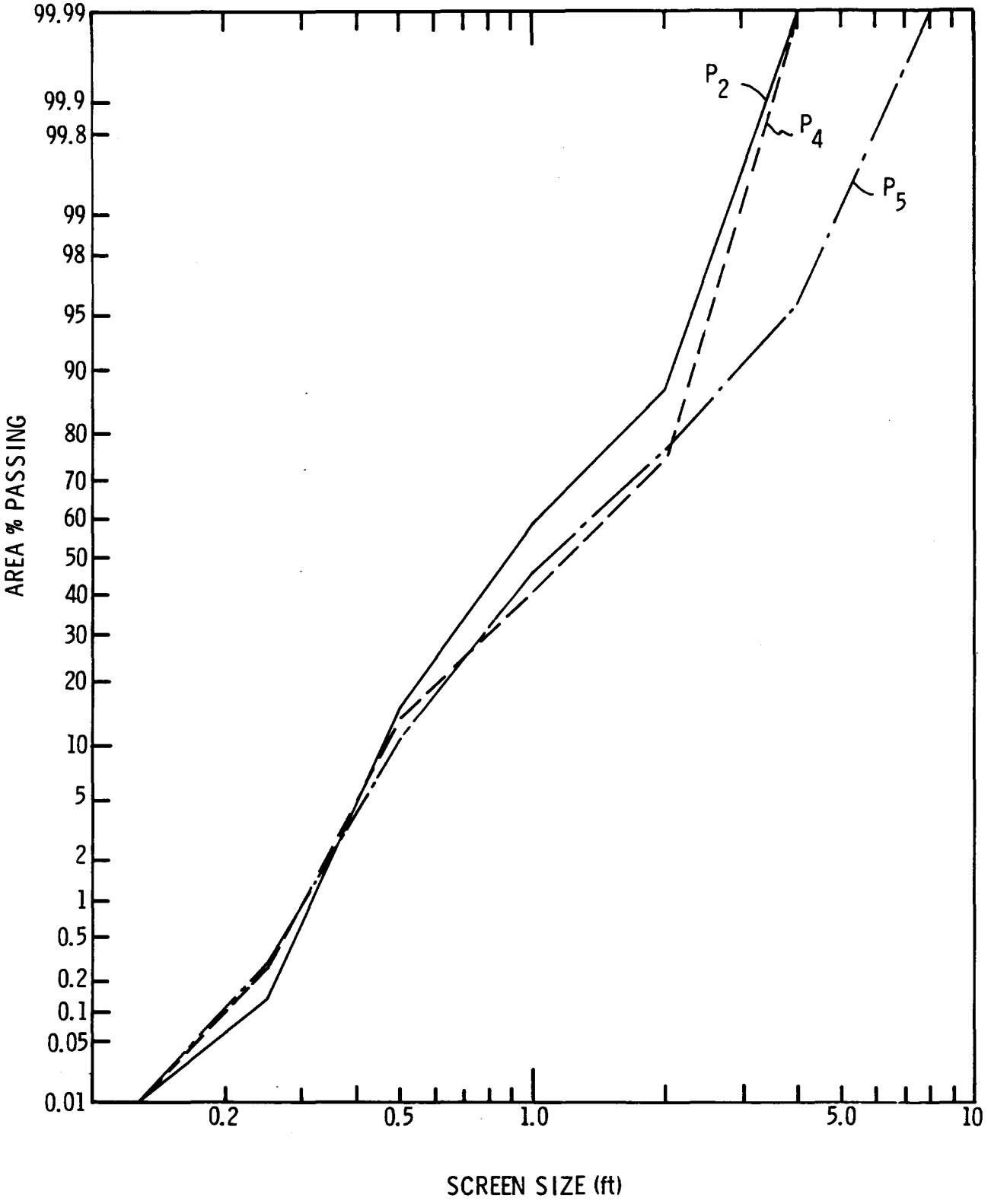

Figure 53. Fragment-size distribution, Downingtown production shots.

TABLE 27

FRAGMENTATION RESULTS

MARRIOTTSVILLE

Shot #	Screen Sizes (ft) 20% Passing	50% Passing	80% Passing
S1	0.8	1.5	2.2
S2	0.9	1.7	2.3
P1	0.8	1.5	2.8
P2	1.0	2.1	4.1
P3	0.9	1.7	2.8
P4	0.8	1.6	2.8
P5	1.0	1.9	4.1

TABLE 28

FRAGMENTATION RESULTS

DOWNINGTOWN

Shot #	Screen Sizes (ft) 20% Passing	50% Passing	80% Passing
S2	0.5	1.0	1.9
P2	0.6	0.9	1.6
P4	0.6	1.2	2.1
P5	0.6	1.1	2.2

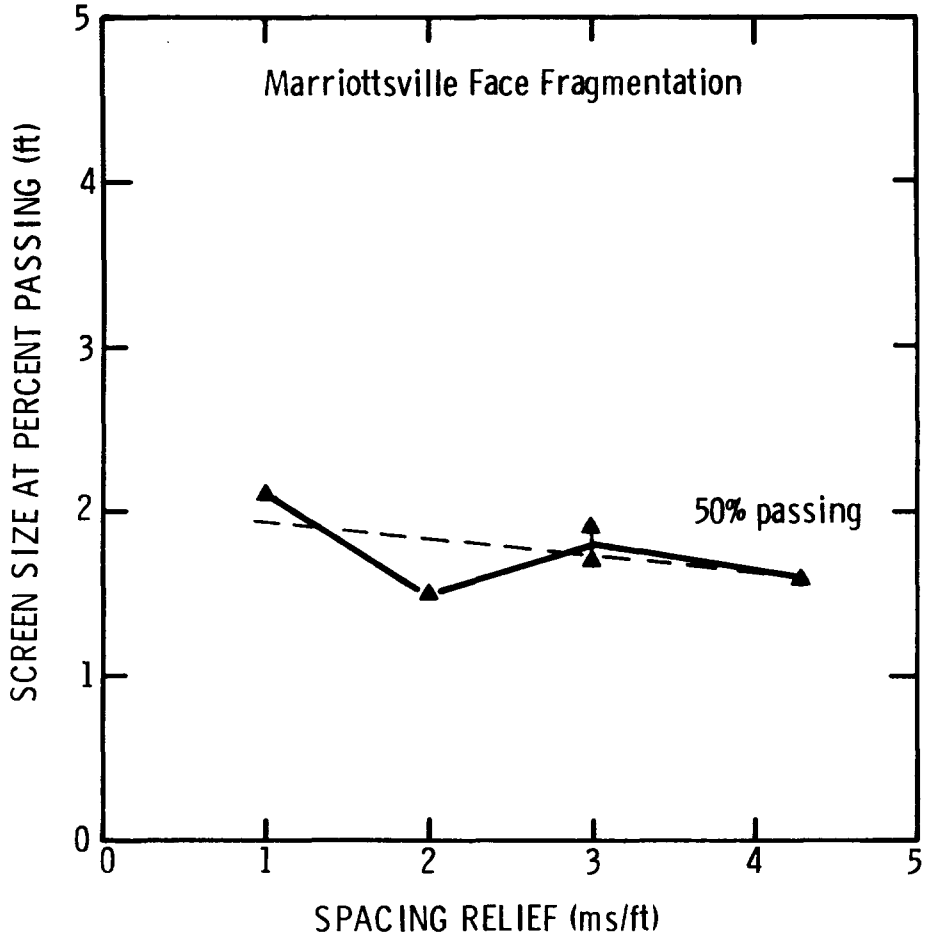

Figure 54. Screen size versus relief, Marriottsville.

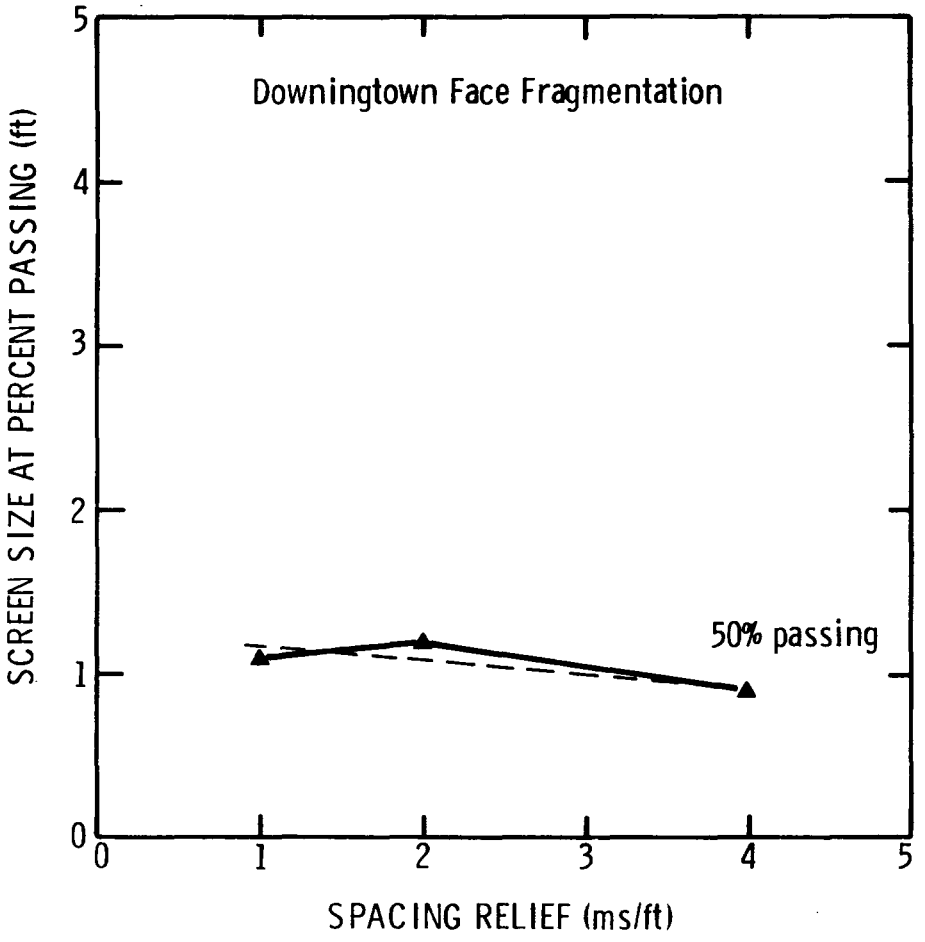

Figure 55. Screen size versus relief, Downingtown.

(Figure 54) shows a 20% particle size reduction for a spacing delay of 4.3 ms/ft as compared to one at 1 ms/ft (at 50% passing). A similar comparison for Downingtown indicates a 25% decrease in size.

The data from the single hole tests are also included in Tables 27 and 28. These data are not believed to be directly comparable to the production shot data because the distributions from the single-hole tests are more heavily weighted to the finer screen fractions. The single-hole shots were much smaller than the production ones; thus, the high-speed camera filming the face fragmentation had a much smaller field of view, and smaller fragments could be resolved. Based on previous work, we expect the fragmentation from the single-hole tests to be poorer than the production shots, although data from the Marriottsville and Downingtown shots do not confirm this.

Our data suffer from the lack of repeat tests at the same delays; however, we do have two tests that were duplicated, which help to establish confidence levels in our results. As discussed previously, the two single-hole tests at Marriottsville were compared and found to have similar particle size distributions except for one piece of "oversize" which greatly skewed the distribution of test S-2. The two particle size distributions calculated from the raw data from those tests had a range of 25% in the coarser fractions; however, recalculated distributions with the large piece excluded only varied by an average of 12%.

Two production blasts with 3 ms/ft of spacing relief were done at Marriottsville quarry, tests P-3 and P-5; however, those tests did have different between-row relief. P-3 had a relief of 7.5 ms/ft of burden

and P-5 had a between-row relief of 9 ms/ft. One of our initial assumptions for these fragmentation tests was that the face fragmentation would to first order, be affected only by the between-hole relief and not by the delay time between rows. Examination of Table 27 shows an 11% variation in the screen sizes at the 20- and 50-percent passing points of the particle size distributions of those two shots. The range seen in the median fractions of these two shots is comparable to that of the single-hole tests at Marriottsville. There is a 38% variation at the 80% passing point; however, for reasons stated above, the large variations in the coarse fractions are most likely attributable (or at least inseparable) to sampling errors of our analytical method. Based on the variation in data from the two sets of duplicated tests, we can have a confidence of approximately 11-12% in the median and fine fractions of the distributions, but much less confidence in the data in the coarser size fractions. The error bars in Figure 54 reflect the variation.

According to previous work on the effect of delay on face fragmentation done with two-hole production-scale blasts in granit, there is a critical delay at which optimum fragmentation is achieved. Too short delays give the poorest fragmentation; however, at spacing delays that have higher relief than optimum, fragmentation degrades. When considering the particle sizes of the 50% passing sizes at Marriottsville (Figure 54), an interesting trend is suggested. The finest fragmentation is determined for the shot that had 2 ms/ft of spacing relief. While our data suggest that there is a critical delay at Marriottsville, given the range in our data, we cannot conclusively determine if the particle size minimum at 2 ms/ft is real or not.

Earlier work in small limestone blocks, reduced-scale bench blasting, and two-hole production-scale blasting done at Martin Marietta Laboratories has indicated a delay effect on fragmentation (Winzer, et al., 1983).

In the small-Limestone block tests, fragmentation became finer as the spacing relief was increased. At very short delays, i.e., relief less than 1 ms/ft, the mean particle size was seen to be relatively large. At longer delays, reliefs up to 6 ms/ft, the average fragment size remained essentially constant. However, the size consist (the percentages of coarse rock versus fine rock) was seen to shift to finer size distributions as the spacing delay was increased.

The two-hole production-scale blasting tests, done in granite, showed that the best overall fragmentation was obtained using spacing reliefs of 2-4 ms/ft. Coarser fragmentation was noted for blasts with reliefs of 1 ms/ft and > 4 ms/ft. In these tests, an effect from the preblast fracture network was also noted. In sections of the faces that were relatively massive, optimum fragmentation was achieved at delays of 2 ms/ft, whereas in more highly fractured areas of the face, the best fragmentation was seen at 4 ms/ft.

The results of this research project are consistent with the findings of earlier work. Based on face fragmentation analyses of shots made in two different quarries, finer fragmentation is obtained as higher spacing reliefs are used. In comparing size distributions from shots at each site with spacing reliefs that were varied from 1 ms/ft to 4 ms/ft (4.3 ms/ft at Marriottsville), the finest fragmentation is seen in the

higher relief shots. At Marriottsville, where the rock is a "massive" dolomite, the finest fragmentation was obtained from a shot with 2 ms/ft of spacing relief. At Downingtown, where the rock is thinly bedded limestone, the best fragmentation was seen from a shot with 4 ms/ft spacing relief. While these results are consistent with the findings of the previous study in granite (discussed above) that indicated different optimum spacing relief for massive and highly fractured rock, the lack of repeat tests at the critical delays makes our data inconclusive.

Current blasting fragmentation theories emphasize the importance of the interaction of stress waves with flaws and discontinuities as a dominant mechanism by which cracks nucleate and propagate. We hypothesize that the fracture network that develops around a detonated borehole serves as additional nucleation sites for later firing holes. If the explosive columns are delayed so that the fracture network from previously fired holes is fully developed, but the majority of the cracks are closed (i.e., not gas-pressurized), fragmentation should be maximized. If the charges are detonated with too little delay, fewer nucleation sites will result in poorer fragmentation. Theoretically, If the delay between holes is too long, fragmentation should suffer because the open cracks will prevent the passage of the stress waves necessary to continue to fragment rock in that part of the bench.

The findings of this study are also consistent with possible effects of gas-pressurized crack extension. Stress-wave/flaw interaction blasting theories do not account for the effects of gas pressure in the fragmentation process. An alternate, and perhaps not mutually exclusive, hypothesis involving gas pressurization parallels the one outlined

above. If boreholes are detonated with too little delay between them, crack networks from flaws induced by the interaction of stress waves are not well developed enough to communicate gas pressure to all parts of the bench. Thus, potential crack extension is limited. If the boreholes are detonated with too great a delay between them, the amount that the cracks are open may relieve some of the gas pressure before it can work to drive cracks.

The findings of our study, while documenting a delay effect on fragmentation, do not allow either of the hypotheses presented above to be supported over the other.

The qualitative observations made as these blasting tests were carried out also provided some insights on the effect of delay on muckpile diggability. In shots using the shortest overall delays, i.e, a combination of the between-hole and between-row delays, the resulting muckpiles were piled high against the face and were very difficult to dig. Some of the rock in the back row, while highly fractured, had remained virtually in place. The greatest muckpile displacements were obtained using the highest relief shots; these shots were also generally easier to dig.

7 DISCUSSION OF RELATED ISSUES

At this point, we turn to issues which did not fit into previous discussions. We will describe 1) the possible influence of fragmentation on the resultant vibration, and 2) the possibility of using vibration as a measure of fragmentation efficiency. We will also discuss the implications of inaccuracy of initiator firing times on the predictability of ground vibration.

7.1 EFFECT OF FRAGMENTATION EFFICIENCY ON GROUND VIBRATION

As discussed in the introduction, it would appear reasonable that a blast in which the explosive energy to fragment rock is used most efficiently will generate the least possible ground vibration. We have used the single-hole ground vibration signatures as the starting point for our analyses. Conventional wisdom has it that the worst fragmentation is observed for opening holes on shots and for the final holes. The work on the delay effect on fragmentation is dependent on the assumption that there is some interaction between the action of individual boreholes in a multi-hole shot which improves fragmentation. The basic mechanisms for this interaction remain uncertain although we have alluded to various possibilities in the previous section. However, it appears that, in most cases, a single-hole shot has an unfavorable partition between the energy used for fragmentation and that wasted in ground vibration. Holes detonated subsequent to the first hole would then generate a ground vibration with low amplitude than the single-hole shot.

A synthetic seismogram generated by the linear superposition of single-hole waveforms should then predict a vibration somewhat higher than that

actually observed for a multiple-hole shot. We have compared the actual and predicted vibration for the shots in the test series. As will become apparent, a difficulty in this comparison is that some single criterion must be used as a scaling factor to compare the actual to the predicted waveforms.

Two forms of comparison were used to calculate a scaling factor. The first was a ratio of the measured peak particle velocity to the predicted peak particle velocity and the second was the average ratio of the predicted response spectra values to the measured response spectra values from 3 to 50 Hz. The peak particle velocity and response spectrum scaling factor for Marriottsville can be seen in Tables 29 and 30, respectively.

The scaling factors for the Marriottsville tests are summarized below:

Blast No.	PPV Scaling Factor	Response Spectrum Scaling Factor	Sum
1	0.73	0.89	1.62
2	0.89	1.28	2.17
3	0.71	0.77	1.48
4	0.54	0.76	1.30
5	0.74	0.99	1.73

According to the hypothesis that the larger the scaling factor the less efficient the blast, the blasts at Marriottsville are rated in terms of decreasing efficiency as:

TABLE 29

PEAK PARTICLE VELOCITY - SCALING FACTORS - MEASURED/PREDICTED

MARRIOTTSVILLE

Location	Blast No.					Mean	Standard Deviation
	1	2	3	4	5		
West Opposite	1.06	0.70	0.50	0.51	0.56	0.66	0.21
West Halfway	1.11	0.77	0.91	0.66	1.28	0.95	0.22
Lime/Fill*	0.64	1.00	0.48	0.59	0.74	0.69	0.18
Lime/Marr.*	0.88	1.27	1.24	0.44	1.14	0.99	0.31
Ward's Chapel*	0.61	0.47	0.45	0.52	0.48	0.52	0.08
Wash House*	0.80	0.81	0.68	0.62	0.58	0.70	0.09
East Halfway	0.48	0.62	0.75	0.36	0.54	0.55	0.13
East Opposite	0.74	0.45	0.32	0.36	0.61	0.83	0.12
Mean (all locations)	0.79	0.76	0.67	0.51	0.74	0.74	
Standard Deviation	0.22	0.27	0.30	0.11	0.30		
Mean using only locations behind blasting to eliminate shielding	0.73	0.89	0.71	0.54	0.74	0.73	
Standard Deviation	0.13	0.34	0.37	0.08	0.29		

TABLE 30

RESPONSE SPECTRUM - SCALING FACTORS - MEASURED/PREDICTED

MARRIOTTSVILLE

Location	Blast No. 1	2	3	4	5	Mean	Standard Deviation
West Opposite	1.03	1.29	0.67	0.78	0.98	0.95	0.24
West Halfway	1.09	2.26	1.72	1.44	2.42	1.78	0.56
Lime/Fill*	0.97	1.88	0.65	0.70	0.67	0.97	0.52
Lime/Marr.*	1.06	1.62	1.30	0.99	1.48	1.29	0.27
Ward's Chapel*	0.60	0.61	0.44	0.51	0.48	0.53	0.07
Wash House*	1.04	1.02	0.69	0.85	1.31	0.98	0.23
East Halfway	0.57	1.11	0.65	0.36	0.49	0.64	0.29
East Opposite	0.78	0.73	0.61	0.38	0.62	0.62	0.15
Mean	0.89	1.32	0.84	0.75	1.06	0.97	
Standard Deviation	0.21	0.57	0.43	0.36	0.67		
*Mean using only locations behind blasting to eliminate shielding	0.92	1.28	0.77	0.76	0.99	0.94	
Standard Deviation	0.21	0.58	0.37	0.21	0.48		

Blast	Average Scaling Factor
4	0.65
3	0.74
1	0.81
5	0.87
2	1.08

The corresponding values at Downingtown are shown in Tables 31 and 32.

The scaling factors for the Downingtown tests are summarized below:

Blast No.	PPV Scaling Factor	Response Spectrum Scaling Factor	Sum
1	1.06	2.56	3.62
2	0.89	1.45	2.34
3	0.83	1.34	2.17
4	0.82	1.80	2.62
5	0.92	1.89	2.81

Blast	Average Scaling Factor
3	1.09
2	1.17
4	1.31
5	1.41
1	1.81

TABLE 31

PEAK PARTICLE VELOCITY - SCALING FACTORS - MEASURED/PREDICTED

DOWNINGTOWN

Location	Blast No.				
	1	2	3	4	5
Close 1	0.83	0.84	0.71	0.70	—
Close 2	1.19	0.87	0.68	0.78	0.74
Close 3	0.73	0.87	9.71	0.71	1.39
Far 1	1.42	1.35	1.09	0.62	0.78
Far 2	0.87	0.83	1.10	0.96	0.60
Far 3	1.41	0.77	0.73	1.06	1.12
Far 4	0.80	0.63	0.57	0.91	0.84
Far 5	0.97	0.89	0.94	0.67	1.00
Mean (all locations except C-1)	1.06	0.89	0.83	0.82	0.92

TABLE 32

RESPONSE SPECTRA SCALING FACTORS -- MEASURED/PREDICTED

DOWNINGTOWN

	Blast No.				
Location	1	2	3	4	5
Close 1	1.23	1.28	0.67	1.15	--
Close 2	2.19	1.22	0.87	1.61	1.41
Close 3	1.65	1.19	0.95	1.21	1.66
Far 1	3.61	1.76	1.32	1.93	1.58
Far 2	1.69	1.15	1.00	1.77	1.44
Far 3	3.50	2.03	2.00	2.91	2.04
Far 4	2.09	1.15	0.98	1.47	1.78
Far 5	3.21	1.62	2.29	1.70	3.33
Mean (all locations except C-1)	2.56 0.85	1.45 0.35	1.34 0.57	1.80 0.54	1.89 0.67

It is apparent from comparing the scaling factors at Marriottsville with those at Downingtown, that the Marriottsville predicted levels are higher relative to the measured values than the Downingtown predicted values. Some screening of the Marriottsville data is required to remove the effects of shielding by face relief. The opposite and halfway locations are shielded by having an open face between the blast and seismograph on some blasts and not having one on others. Eliminating these locations from the Marriottsville data analysis will produce an average scaling factor for all shots of 0.83. The average scaling factor for Downingtown was 1.34 or approximately 62% higher.

This difference can be explained by the differences in relief on the single-hole shots at each quarry. At Marriottsville, there was only relief to the front and not to the side which would produce higher vibrations. A predictive waveform using a higher vibration-intensity single hole as the source would produce higher predictive levels. Therefore, the Marriottsville predicted waveforms were higher, which resulted in lower scaling factors since:

Scaling Factor = Measured Intensity/Predicted Intensity.

The scaling factors are compared with the observed 80% passing fragmentation for Marriottsville in Fig. 56 and Downingtown in Fig. 57. As may be seen, there is a good correlation of the scaling factor with the 80% passing fragmentation. There is a zero-offset of the scaling factor at Downingtown, which we cannot explain either. However, it does appear that this first attempt at correlating vibration with fragmentation is successful enough that the approach warrants further investigation.

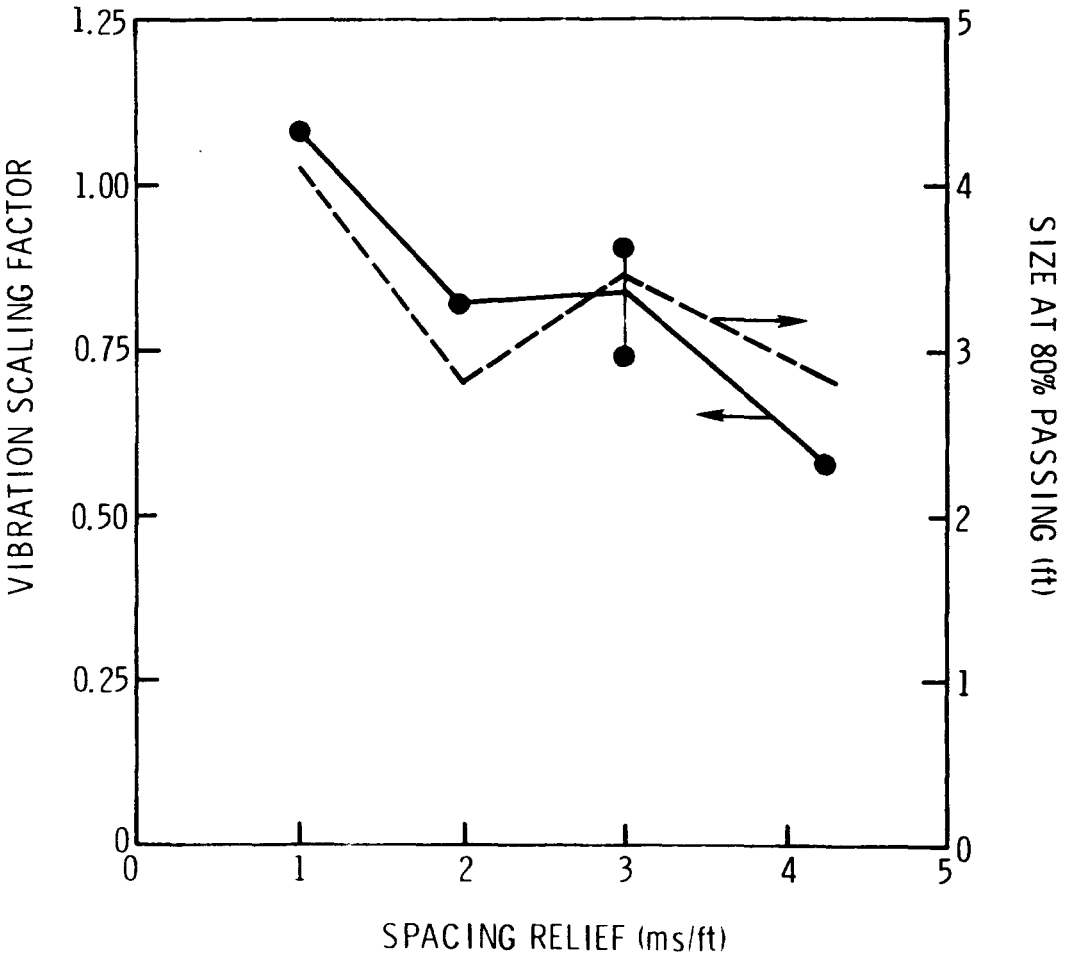

Figure 56. Vibration scaling factor and screen size versus relief, Marriottsville.

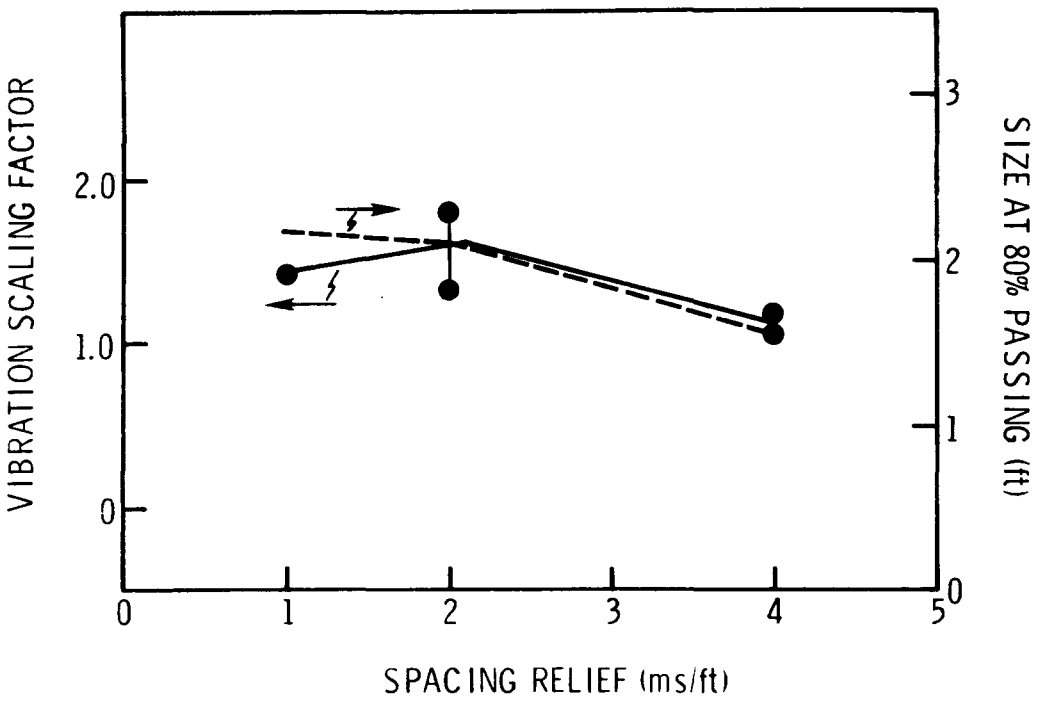

Figure 57. Vibration scaling factor and screen size versus relief, Downingtown.

7.2 INITIATOR ACCURACY -- EFFECT ON VIBRATION PREDICTABILITY

Commercial millisecond-delay initiators are known to have scatter, in which the actual firing time may differ from the nominal firing time, with standard deviations reaching 20 ms or more (Winzer, 1978). It should be noted that one standard deviation corresponds to a 65% confidence level that the time will be within that standard deviation; two standard deviations, double the number for one standard deviation, will increase the confidence level to 95%, but the level is double, so that 65% confidence at 20 ms will correspond to 95% confidence at 40 ms. It has been shown (Winzer, et al., 1979), that this level of scatter results in reversals and crowding of firing times, which will result in adverse fragmentation. We are here concerned with the effect of such scatter on the predictability of the ground vibration.

We have generated a set of synthetic firing times for two of the Downingtown shots which were discussed in detail earlier: the constructive interference shot with 72 ms between holes in a row and 153 ms between rows, and the destructive interference shot with 36 ms between holes in a row and 135 ms between rows. We will compare response spectra for synthetic seismograms constructed using scattered firing times for the Far 5 location.

We have assumed that the mean firing times are the same as the nominal. This is not a significant assumption, because if the mean firing times are known, those values, rather than the nominal, may be incorporated into the Fourmap program to generate the predictive plots. We are here concerned with the possible effect of the scatter on the predictability.

The scatter is incorporated by using a Gaussian distribution of a random number generator. For each standard deviation for the values 2, 5, 10, and 15 ms, synthetic seismograms were generated and the response spectra calculated to be compared with the response spectrum for the ideal cap times. Fifteen shot times were determined for each standard deviation, and the synthetic seismograms constructed for these.

Figures 58, 59, 60, and 61 show the response spectra generated for 2-, 5-, 10-, and 15-ms standard deviations, respectively, for the constructive interference shot. Figures 62, 63, 64, and 65 are the comparable plots for the destructive interference shots. There are three lines on each figure corresponding to the mean, and plus and minus one standard deviation for all the response spectra. Initially, we wish to know how the scatter will affect the response for destructive interference shots, where we would assume that deviations from this condition could appreciably worsen the vibration. It should be noted that the resonant frequency at this site was 15 Hz, and the blast times were designed to minimize vibration at this frequency.

The 2-ms standard deviation response spectra do not deviate very much from the response spectra for the ideal times. What is most important, there is no apparent amplification at 15 Hz. The 5-ms standard deviation shows some amplification at 15 Hz, and a greater scatter in the predictability. It should also be noted that the best case is no better than the ideal firing times. Scatter does not improve vibration when the appropriate delay sequence is chosen. The 10- and 15-ms standard deviation plots show significant degradation in the ability to predict the vibration, and the 15-Hz peak emerges for most of the records, as shown by the mean level. Even the best case contains the 15-Hz peak.

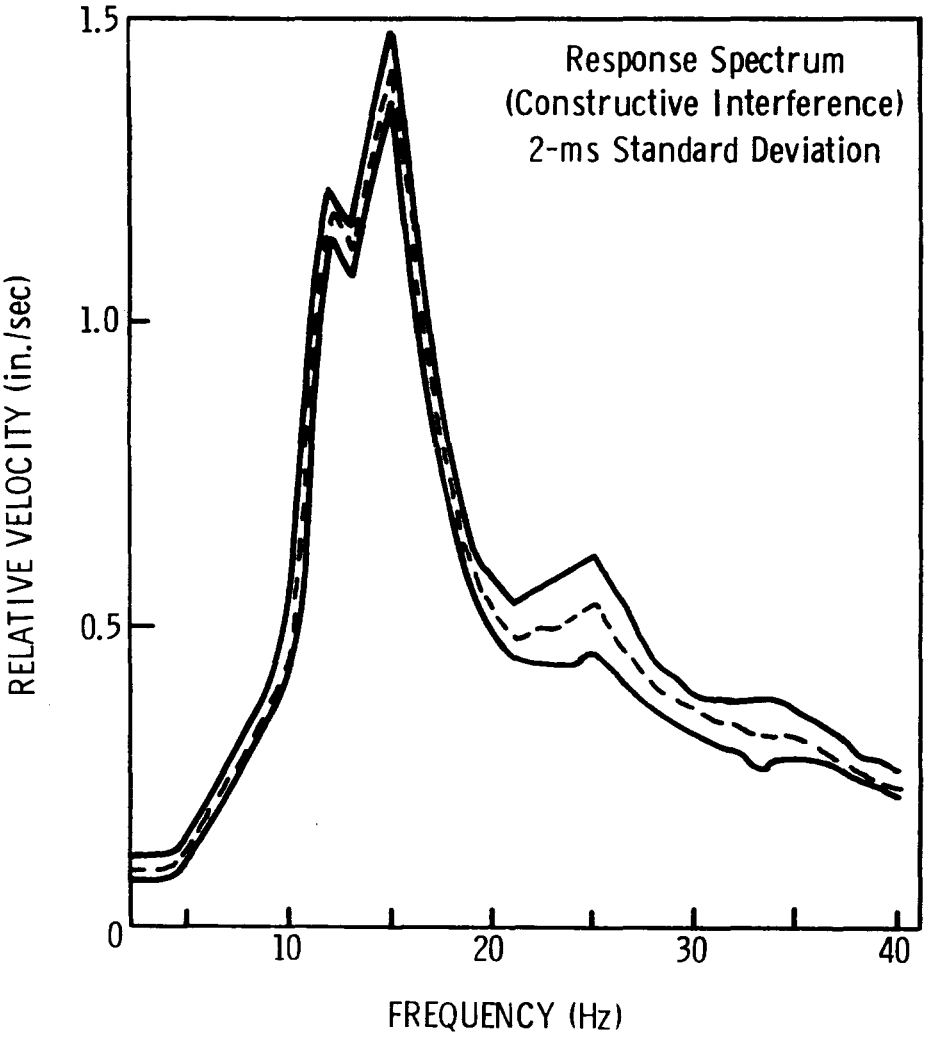

Figure 58. Response spectra calculated from ten synthetic seismograms, from constructive interference shot. Cap firing times varied in a Gaussian distribution around nominal on each seismogram by 2-ms standard deviation. Dashed line shows mean of ten response spectra; solid lines show one-standard-deviation limits. See text for discussion.

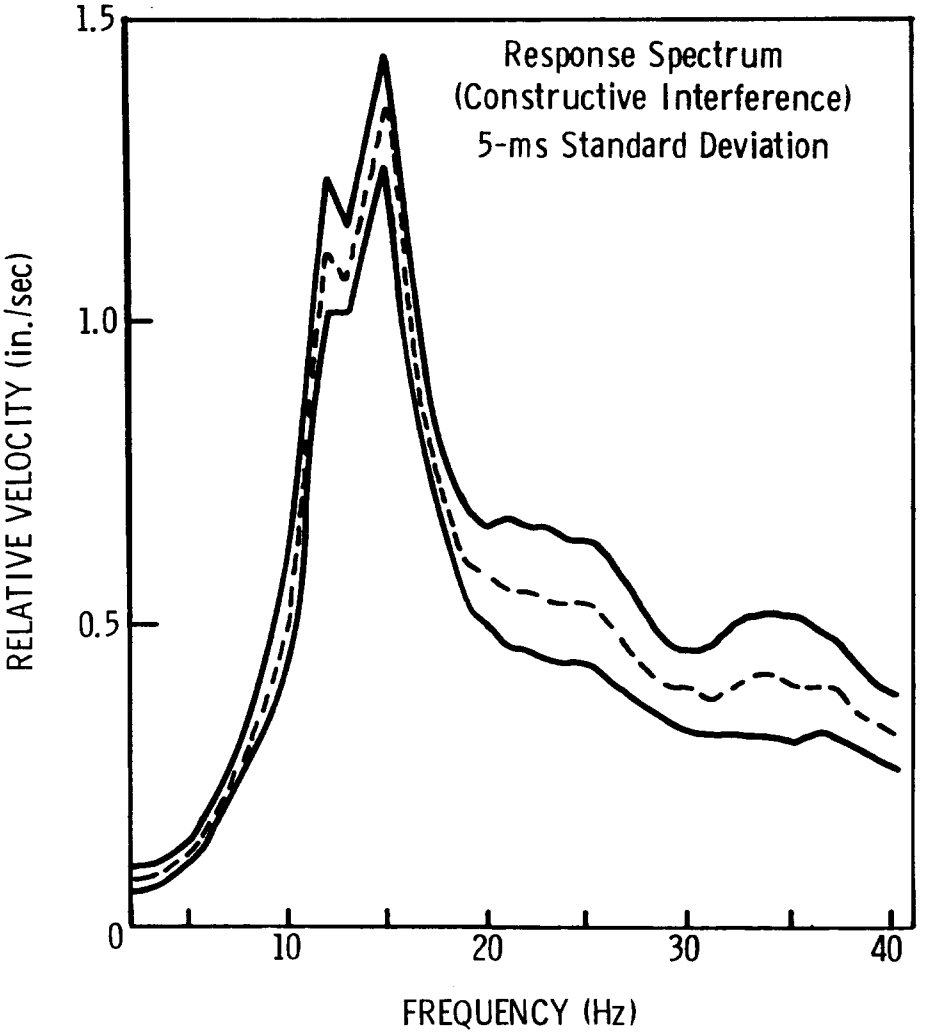

Figure 59. Same as Fig. 58, but with 5-ms standard deviation on caps.

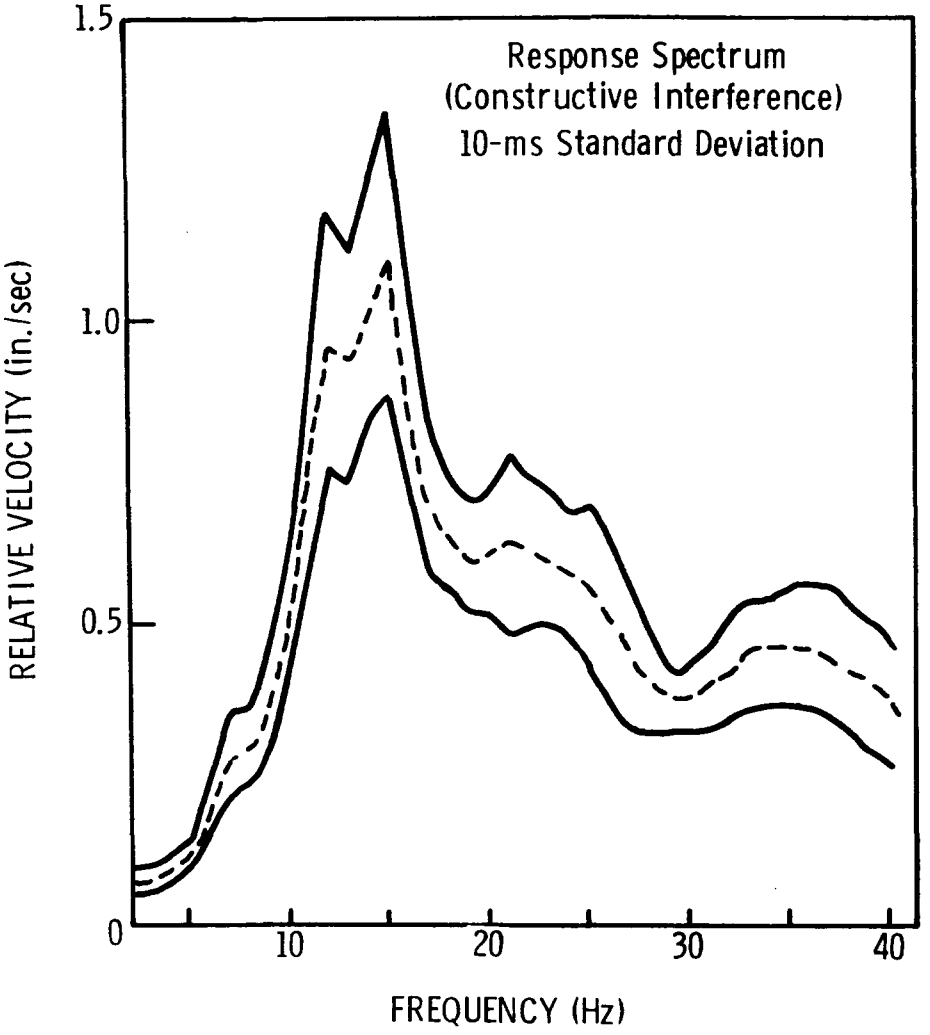

Figure 60. Same as Fig. 58, but with 10-ms standard deviation on caps.

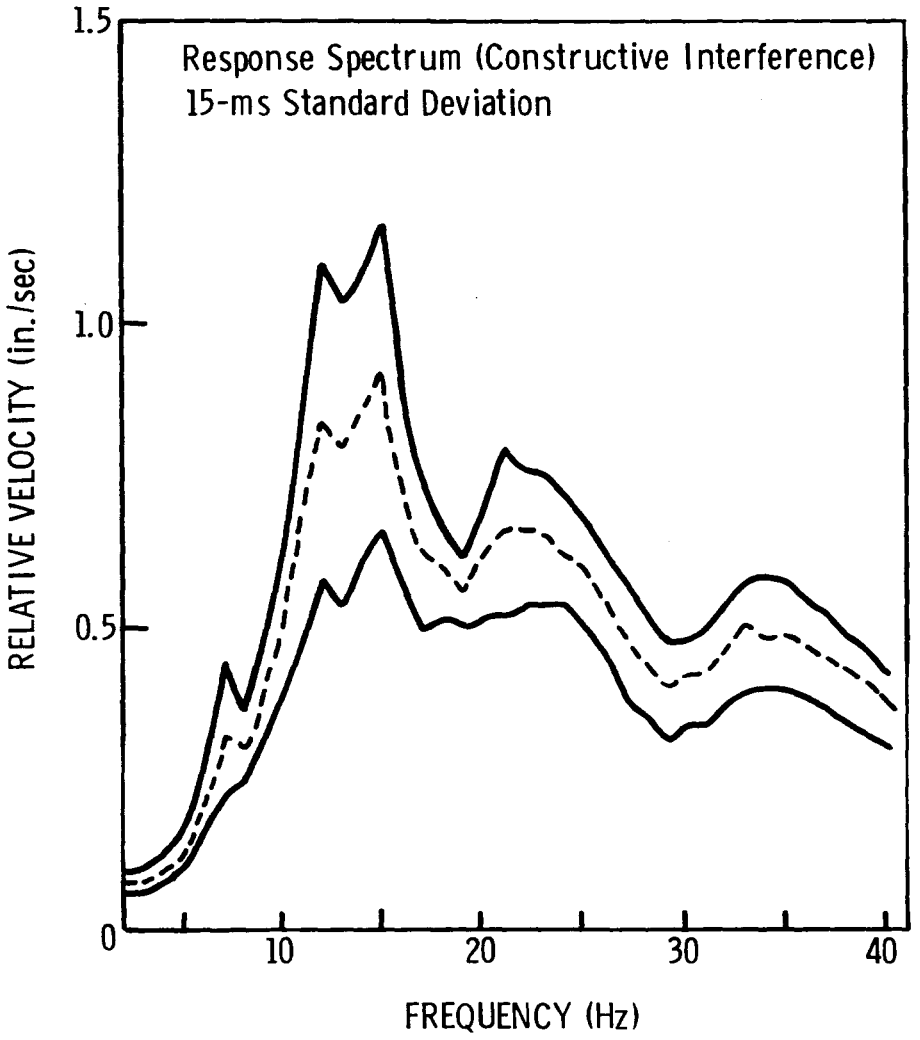

Figure 61. Same as Fig. 58, but with 15-ms standard deviation on caps.

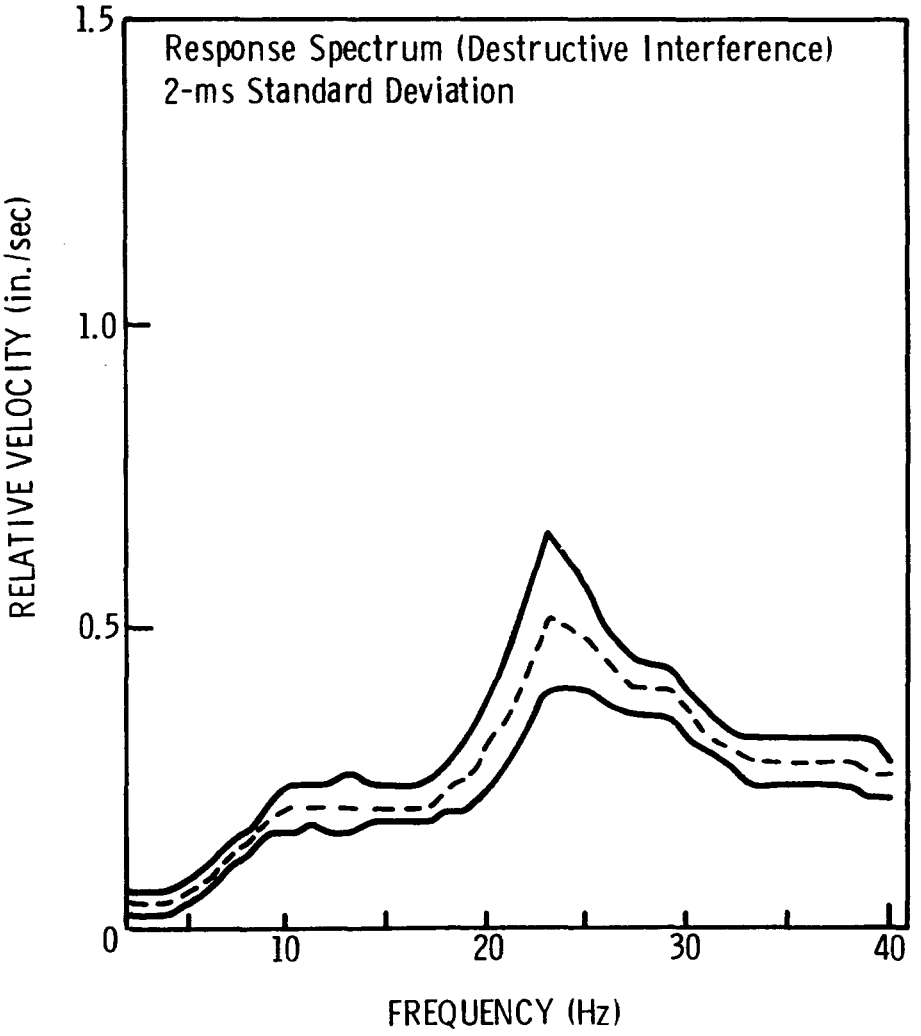

Figure 62. Same as Fig. 58, with 2-ms standard deviation on caps, but for destructive interference shot.

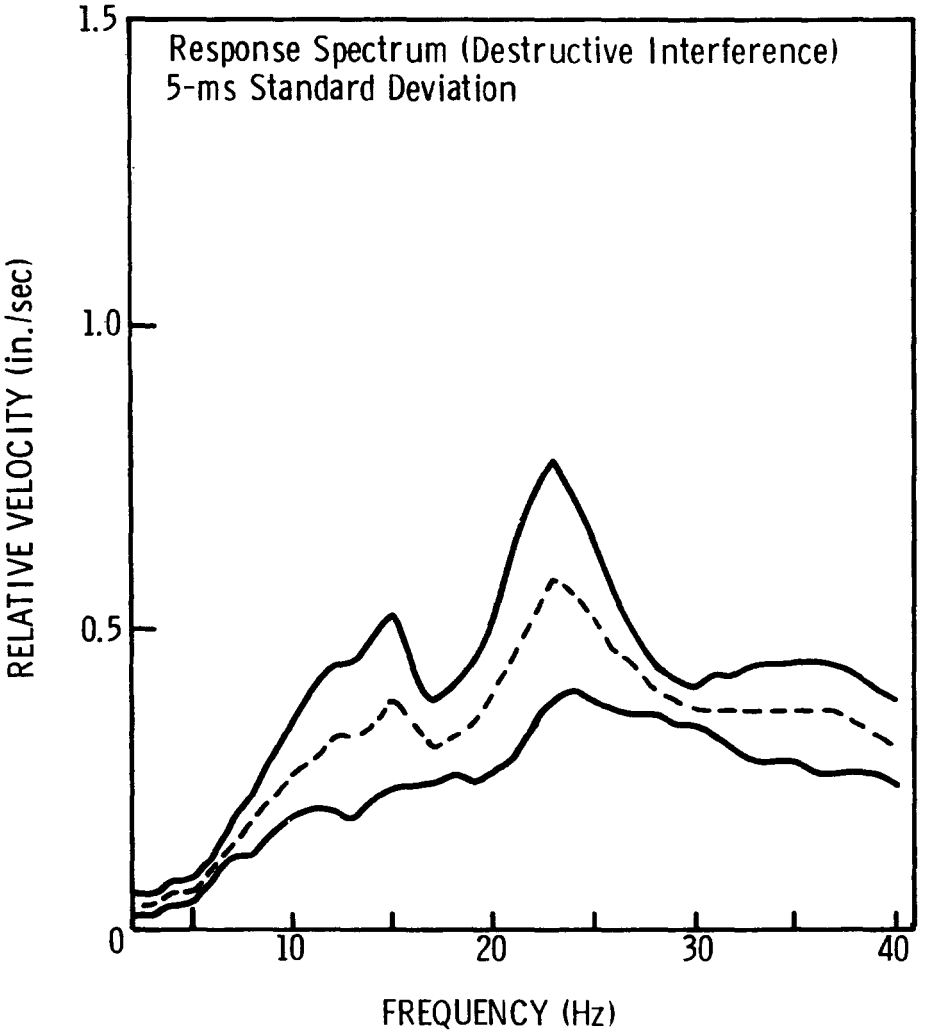

Figure 63. Same as Fig. 62, with 5-ms standard deviation on caps.

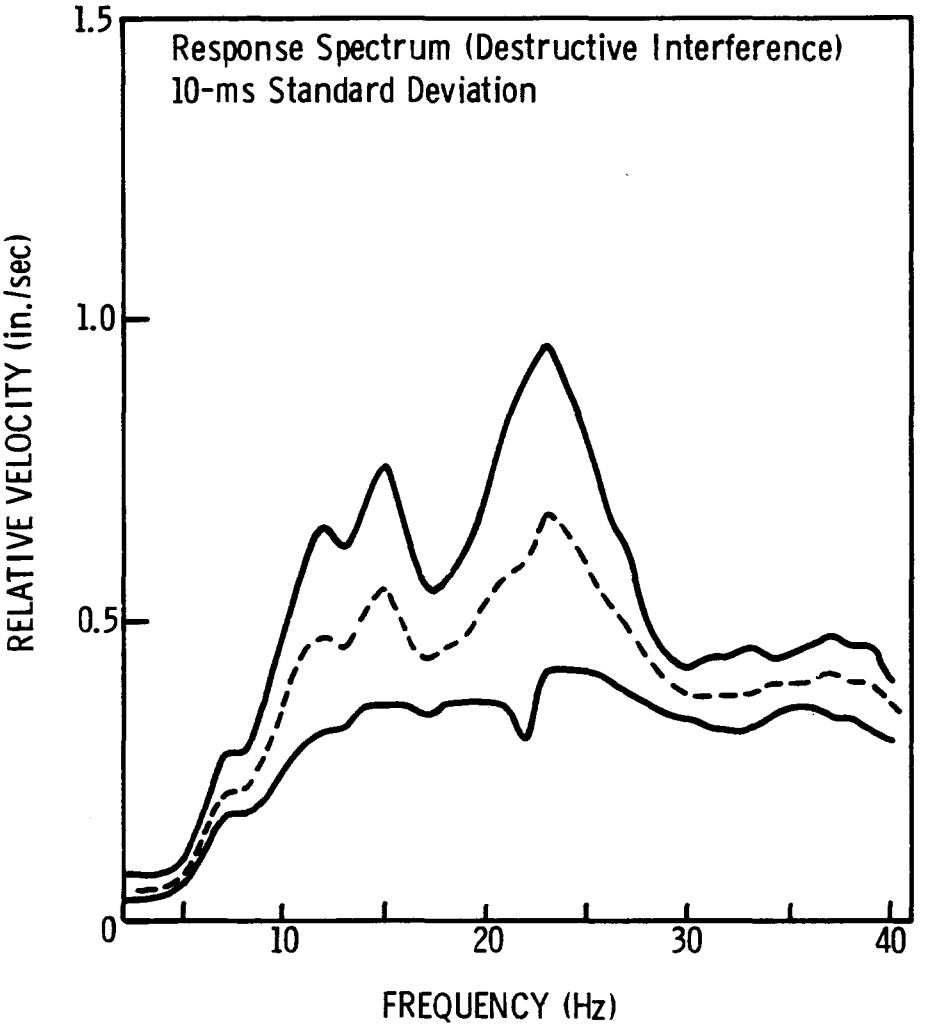

Figure 64. Same as Fig. 62, with 10-ms standard deviation on caps.

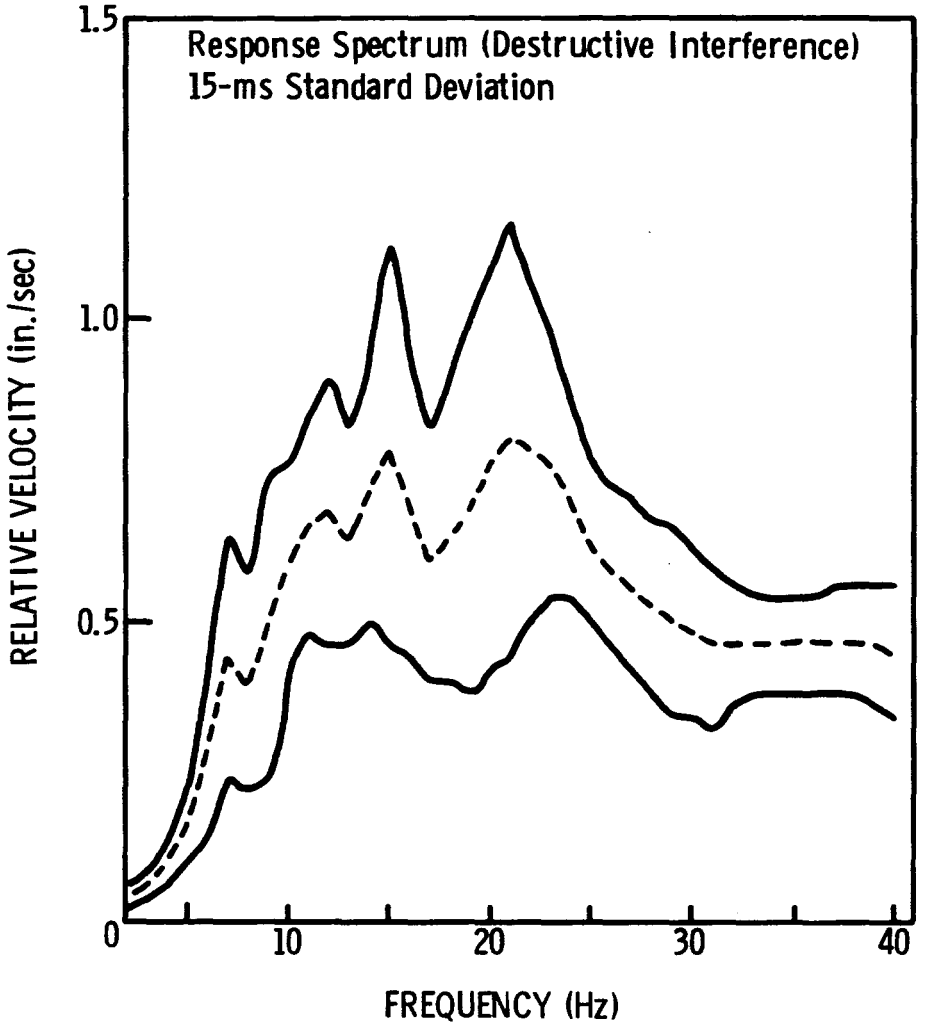

Figure 65. Same as Fig. 62, with 15-ms standard deviation on caps.

The constructive interference plots show that the vibration improves slightly as the standard deviation increases. The Langefors and Kihlstrom (1978) method of using the scatter to avoid constructive interference was meant to deal with this situation. It may be noticed that the vibration is worse than the vibration for the destructive interference pattern, even at the highest standard deviations. The Fourmap method should consistently improve vibration if the standard deviations are 5-ms or less. Of course, predictability and the ability to control vibration will improve proportionally to the accuracy of the initiators.

With accurate initiators, destructive interference can virtually eliminate the major natural resonance peak (e.g., Fig. 58). A small amount of scatter, 2-ms standard deviation, is tolerable, but with scatter of 5 ms and above, the resonant peak reappears. The strength of this peak is proportional to the scatter.

Nevertheless, a short note of caution is in order. If delays are chosen which produce the constructive interference, more accurate initiators will produce worse vibrations. If an operator obtains accurate initiators, he should use the appropriate blast design tools so that he does not design a blast that will create constructive interference.

8 CONCLUSIONS

We have conducted a well-controlled study to determine the effect of geology on low-frequency ground vibration, and tested means to predict and control that vibration based upon modifying blast design, while ensuring adequate fragmentation. First, we will discuss the effect of wave-guide-generated geology on resonant vibrations. We will then review briefly the hypotheses we tested and verified, and the means of implementing them.

The results of Gupta (1961), showing that a resonant vibration may be set up in a low-velocity surface layer, have been confirmed. The predominant resonant frequency can be quite accurately predicted if its thickness and wave velocity are known. Blasts may be designed by destructive interference using delays corresponding to half-periods of the fundamental frequency. This approach may be used if single-hole data are not available. Frequencies other than the predominant are also present, however, and knowledge of the geologic structure is usually not sufficient in itself for effective blast design.

To determine the complete frequency spectrum response, we have detonated single-hole shots at our study locations. We hypothesized that the seismic waveforms generated by single-hole shots measured at a given location are reproducible. We have demonstrated that this hypothesis is in fact verified, even when there are significant variations in the rock type at the bench. It is not yet clear what effects differences in explosive type, borehole diameter, or charge length may have on the vibration signature. Small charges may possibly be used to obtain the single-hole signature, using a scaling factor, but again that remains to be tested.

Time-lagged linear superposition of the single-hole waveform produces synthetic seismograms which are very similar to the actual vibration observed in precisely controlled test blasts. In many cases the predicted and actual waveforms are virtually indistinguishable. Peak particle velocities and response spectra obtained may vary due to changes in the blast design alone. The response spectra are even sensitive to the delay design when a particular delay is chosen which produced either constructive or destructive interference at the resonant frequencies of the local site.

Two methods, autocorrelation and Fourmap, have been used to choose the delay times to be used in shots at a particular location for destructive and constructive interference. Autocorrelation is computationally efficient and can give an operator a quick idea whether a particular delay sequence should be favorable or not. The Fourmap method graphically depicts the Fourier spectra as a function of delay so that the best delay time may be chosen for various frequency ranges for a range of sites. Both these methods have been shown to accurately predict good and bad vibration for blasts designed from them in this test series.

Delay time between holes in a row appears to affect fragmentation, supporting earlier work on a smaller scale, and for smaller shots. At the two locations we studied, the optimum time for relief between holes in a row appears to be 2 ms/ft. However, the limited nature of the data somewhat limits our confidence in these results. Further, because we do not have a complete understanding of the mechanisms involved in fragmentation, we still do not have a means of extending this work to other locations. Substantial further work in this area needs to be done.

We have tried to understand some of the behavior of the strain waves in the blast area. At distances more than 15 feet or so from the detonation, the strain pulse appears to be impulsive and of short (approximately 5 ms) duration. At short distances, the record is more complicated. Late arriving, broad, strong pulses are observed, which have marked shear components and do not propagate any significant distance. They may either be impeded from propagating across slightly open discontinuities or they may be absorbed in the creation of new discontinuities. We have attributed these pulses to reflections from the bench free-face, reflections from discontinuities generated during the blasting process, or gas pressurization of cracks. At this time, the data are insufficient to distinguish between these cases. Since the pulses are not always present, we suggest that they are related to localized propagation of gas-driven cracks. The relative propagation rates of strain-wave- and gas-driven cracks may be important in the effect of delay on fragmentation, noted above.

Predictability of the ground vibration is substantially enhanced by accuracy in the initiator firing times. A 2-ms standard deviation in firing times produces results comparable to exact firing times and acceptable results are obtained with a standard deviation of 5 ms, whereas standard deviations of 10 or 15 ms significantly degrade predictability. Site-specific resonant frequencies appear in shots with high initiator scatter, even where vibration at this frequency has been minimized by the blast design, using autocorrelation or Fourmap. However, even with 15-ms scatter, the shot designed for destructive interference will

produce better vibration than a shot designed for constructive interference with a similar scatter. If accurate initiators are used, they should be used with the appropriate design tools to avoid strong constructive interference at the resonant frequencies.

We believe that the approach of using a single-hole blast in order to characterize vibration and fragmentation at a mine is an important new tool which should allow some of the problems associated with mining to be solved. Although we believe that more work needs to be done in certain areas, particularly in understanding the factors affecting productivity, in many cases, ground vibration problems may either be solved or substantially alleviated by use of the methods described here.

9 REFERENCES

Achenbach, J.D., K.-I. Hirashima, and K. Ohno (1983), "Acoustic emission due to nucleation of a microcrack in the proximity of a macrocrack," J. Sound and Vibration, 89, 523-532.

Adams, T.F., R.B. Demuth, L.C. Margolin, and B.D. Nichols (1983), "Simulation of rock blasting with the SHALE code," in Proceedings of the First International Symposium on Rock Fragmentation by Blasting, Lulea, Sweden, 361-373.

Aki, K., and P.G. Richards (1980), Quantitative Seismology: Theory and Methods, San Francisco: W.H. Freeman and Co. Vol. 2, pp. 932.

Anderson, D.A., S.R. Winzer, and A.P. Ritter (1982), "Blast design for optimizing fragmentation while controlling frequency of ground vibration," in Proceedings of the Eighth Conference on Explosives and Blasting Technique, New Orleans, LA, 69-89.

Anderson, D.A., S.R. Winzer, and A.P. Ritter (1983), "Synthetic delay versus frequency plots for predicting ground vibration from blasting," in Proceedings of the Third International Symposium on Computer Aided Seismic Analysis and Discrimination, Washington, DC, 70-74.

Anderson, D.A., S.R. Winzer, and A.P. Ritter (1984), "Time-histories of principal strains generated in rock by cylindrical explosive charges," in Proceedings of the 25th U.S. Symposium on Rock Mechanics, Evanston, IL, 959-968.

Andrews, A.B. (1981), "Design criteria for sequential blasting," in Proceedings of the 7th Conference on Explosives and Blasting Techniques, Pheonix, AZ, 173-192.

Barker, D.B., W.L. Fourney, and D.C. Holloway (1979), "Photoelastic investigation of flaw initiated cracks and their contribution to the mechanisms of fragmentation," in Proceedings of the 20th U.S. Symposium on Rock Mechanics, Austin, TX, 119-126.

Bergmann, O.R., Wu, F.C., and Edl, J.W. (1974), "Model rock blasting measures effects of delays and hole patterns on rock fragmentation," Eng. Min. J., 175, 124-127.

Borcherdt, R.D. (1970), "Effects of local geology on ground motion near San Francisco Bay," Bull. Seismol. Soc. Am., 60, 29-61.

Dienes, J.K. (1981), "On the effect of anisotropy in explosive fragmentation," in Proceedings of the 22nd U.S. Symposium on Rock Mechanics, Cambridge, MA, 164-170.

Dowrick, D.J. (1977), Earthquake Resistant Design, A Manual for Engineers and Architects, New York: John Wiley & Sons.

Dravinski, M. (1982), "Influence of interface depth upon strong ground motion," Bull. Seismol. Soc. Am., 72, 597-614.

Favreau, R.F. (1969), "Generation of strain waves in rock by an explosion in a spherical cavity," J. Geophys. Res., 74, 4267-4280.

Fish, B.G. (1951), "Seismic vibrations from blasting," Mine and Quarry Eng., 17, 189.

Fourney, W.L., D.B. Barker, and D.C. Holloway (1983), "Fragmentation in jointed rock material," in Proceedings of the First International Symposium on Rock Fragmentation by Blasting, Lulea, Sweden, 505-531.

Frantti, G.E. (1963), "Spectral energy density for quarry explosions," Bull. Seismol. Soc. Am., 53, 989-996.

Fung, Y.C. (1965), Foundations of Solid Mechanics, New York: Prentice-Hall.

Greenhalgh, S. (1980), "Effects of delay shooting on the nature of P-wave seismograms," Bull. Seismol. Soc. Am., 70, 2037-2050.

Gupta, I.N. (1961), "Resonant oscillations of the overburden excited by seismic waves," Earthquake Notes, 32, 5-11.

Heelan, P.A. (1953), "Radiation from a cylindrical source of finite length," Geophysics, 18, 685-696.

Holloway, D.C., D.B. Barker, and W.L. Fourney (1980), "Dynamic crack propagation in rock plates," in Proceedings of the 21st U.S. Symposium on Rock Mechanics, Rolla, MO, 271-279.

Hudson, J.A. (1981), "Wave speeds and attenuation of elastic waves in material containing cracks," Geophys. J.R. Astr. Soc., 64, 133-150.

Jordan, D.W. (1962), "The stress wave from a finite, cylindrical explosive source," J. Math. Mech., 11, 503-552.

Joyner, W.B., and R.E. Warrick, and T.E. Fumal (1981), "The effect of quaternary alluvium on strong ground motion in the Coyote Lake, CA, earthquake of 1979," Bull. Seismol. Soc. Am., 71, 1333-1349.

Kikuchi, M. (1981), "Dispersion and attenuation of elastic waves due to multiple scattering from cracks," Phys. Earth Planet Int., 27, 100-105.

King, J.L., and J.N. Brune (1981), "Modeling the seismic response of sedimentary basins," Bull. Seismol. Soc. Am., 71, 1469-1487.

Langefors, U. and B. Kihlstrom (1978), The Modern Technique of Rock Blasting, New York: Halsted Press, 438 pp.

Linehan, P. and J.F. Wiss (1982), "Vibration and air blast noise from surface coal mine blasting," Min. Eng., 34, 391-395.

Medearis, K. (1977), "The development of rational damage criteria for low-rise structures subjected to blasting vibrations," in Proceedings of the 18th U.S. Symposium on Rock Mechanics, 1-16.

Murphy, J.R., A.H. Davis, and N.L. Weaver (1971), "Amplification of seismic body waves by low-velocity surface layers," Bull. Seismol. Soc. Am., 61, 109-145.

Nye, J.F. (1957), Physical Properties of Crystals: Their Representation by Tensors and Matrices, New York: Oxford University Press.

Plewman, R.P. and A.M. Starfield (1965), "The effects of finite velocities of detonation and propagation on the strain pulses induced in rock by linear charges," J. South African Inst. Min. Metall., 66, 77-96.

Pollack, H.N. (1963), "Effect of delay time and number of delays on the spectra of ripple-fired shots," Earthquake Notes, 34, 1-12.

Reed, R.P. (1979), "Triaxial measurement of stress waves in the free-field," Sandia Laboratories Report SAND-78-2123C.

Rice, J.R. (1980), "Elastic wave emission from damage processes," J. Non-destructive Evaluation, 1, 149-155.

Rinehart, J.S. (1975), Stress Transients in Solids, Hyperdynamics, Santa Fe, NM, 230 pp.

Rosenblueth, E. (1980), Design of Earthquake Resistant Structures, New York: Halstead Press, John Wiley and Sons.

Sharpe, J.A. (1942), "The production of elastic waves by explosion pressure," Geophysics, 7, 144.

Shoop, S.A. and J.J.K. Daemen (1983), "Ground and air vibrations caused by surface blasting, Volume II. Ground vibrations monitoring and assessment of conventional predictors," Final Technical Report to the U.S. Bureau of Mines, AZ MMRRI 80-MNG(2).

Siskind, D.E., M.S. Stagg, J.W. Kopp, and C.H. Dowding (1980), "Structure response and damage produced by ground vibration from surface mine blasting," U.S. Bureau of Mines RI 8507.

Starfield, A.M. and J.M. Pugliese (1968), "Compression waves generated in rock by cylindrical explosive charges: A comparison between a computer model and field measurements," Int. J. Rock Mech. Min. Sci., 5, 65-77.

Winzer, S.R. (1978), "The firing times of ms delay blasting caps and their effect on blasting performance," Report to the National Science Foundation, Contract DAR-77-05171.

Winzer, S.R. and A.P. Ritter (1980), "The role of stress waves and discontinuities in rock fragmentation: A study of fragmentation in large limestone blocks," in Proceedings of the 21st U.S. Symposium on Rock Mechanics, Rolla, MO, 362-371.

Winzer, S.R. and A.P. Ritter (1980), "Effect of delays on fragmentation in large limestone blocks," Martin Marietta Laboratories Technical Report 80-25.

Winzer, S.R., W. Furth, and A. Ritter (1979), "Initiator firing times and their relationship to blasting performance," in Proceedings of the 20th U.S. Symposium on Rock Mechanics, Austin, TX, 461-468.

Winzer, S.R., V.I. Montenyohl, and A. Ritter (1979), "High-speed cinematography of production blasting operations," Mining Congress J., 10, 46.

Winzer, S.R., V.I. Montenyohl, and A.P. Ritter (1979), "The science of blasting," in Proceedings of the 5th Conference on Explosives and Blasting Techniques, St. Louis, MO, 132-160.

Winzer, S.R., D.A. Anderson, and A.P. Ritter (1981), "Application of fragmentation research to blast design: Relationships between blast design for optimum fragmentation and frequency of resultant ground vibration," in Proceedings of the 20th U.S. Symposium on Rock Mechanics, Austin, TX, 237-242.

Winzer, S.R., D.A. Anderson, and A.P. Ritter (1983), "Rock fragmentation by explosives," in Proceedings of the First International Conference on Rock Fragmentation by Blasting, Lulea, Sweden, 225-251.